



5-2017

# ANGLE OF ATTACK DETERMINATION USING INERTIAL NAVIGATION SYSTEM DATA FROM FLIGHT TESTS

Jack Kevin Ly

*University of Tennessee, Knoxville, [jly@utsi.edu](mailto:jly@utsi.edu)*

---

## Recommended Citation

Ly, Jack Kevin, "ANGLE OF ATTACK DETERMINATION USING INERTIAL NAVIGATION SYSTEM DATA FROM FLIGHT TESTS." Master's Thesis, University of Tennessee, 2017.  
[https://trace.tennessee.edu/utk\\_gradthes/4757](https://trace.tennessee.edu/utk_gradthes/4757)

This Thesis is brought to you for free and open access by the Graduate School at Trace: Tennessee Research and Creative Exchange. It has been accepted for inclusion in Masters Theses by an authorized administrator of Trace: Tennessee Research and Creative Exchange. For more information, please contact [trace@utk.edu](mailto:trace@utk.edu).

To the Graduate Council:

I am submitting herewith a thesis written by Jack Kevin Ly entitled "ANGLE OF ATTACK DETERMINATION USING INERTIAL NAVIGATION SYSTEM DATA FROM FLIGHT TESTS." I have examined the final electronic copy of this thesis for form and content and recommend that it be accepted in partial fulfillment of the requirements for the degree of Master of Science, with a major in Engineering Science.

Steve Brooks, Major Professor

We have read this thesis and recommend its acceptance:

Peter Solies, Trevor Moeller

Accepted for the Council:

Dixie L. Thompson

Vice Provost and Dean of the Graduate School

(Original signatures are on file with official student records.)

---

# **ANGLE OF ATTACK DETERMINATION USING INERTIAL NAVIGATION SYSTEM DATA FROM FLIGHT TESTS**

A Thesis Presented for the  
Master of Science  
Degree  
The University of Tennessee, Knoxville

Jack Kevin Ly

May 2017

Copyright © 2017 by Jack Kevin Ly

All rights reserved.

# Dedication

---

To my family, my friends, and my love, Sonia Joshi.

# Acknowledgements

---

To everyone in the UTSI Flight Research Department, I would like to say thank you for your guidance, feedback, elbow grease, and humanity. Greg Heatherly, Jacob Bowman, and Jonathan Kolwyck for helping to prioritize my thesis over other work. Dr. Steve Brooks, Dr. Peter Solies, and Dr. Trevor Moeller for all your understanding, guidance, input, advice, and knowledge on flight testing, engineering, and academics. Thank you Dr. Borja Martos for providing me with the starting point to launch my thesis. To my mom and dad for always supporting me, even if you do not completely understand what I am doing or why I'm doing it. And with all my heart, to Sonia Joshi, for all your unrelenting support, I can say no more than thank you.

# Abstract

---

Engineers and pilots rely on mechanical flow angle vanes on air data probes to determine the angle of attack of the aircraft in flight. These probes, however, are costly, come with inherent measurement errors, affect the flight characteristics of the aircraft, and are potentially dangerous in envelope expansion flights. Advances in the accuracy, usability, and affordability of inertial navigation systems allow for angle of attack to be determined accurately without direct measurement of the airflow around the aircraft. Utilizing an algorithm developed from aircraft equations of motion, a post-flight data review is completed as the first step in proving the low cost feasibility of utilizing inertial navigation data for such analysis. Flight tests were conducted with the UTSI Cessna 210 research aircraft to calibrate an angle of attack flow angle vane and obtain inertial navigation data from a commercial INS system in typical flight scenarios. The results of the angle of attack algorithm are compared to the measured angle of attack flow angle vane. Discussed in this thesis are the feasibility and potential applications of angle of attack determination from inertial data.

# Table of Contents

---

<b>Chapter 1: Introduction</b> .....	1
Overview .....	1
Motivation/Purpose.....	2
Solution/Approach.....	3
Objectives .....	3
Scope/Out-of-scope .....	3
Assumptions.....	4
<b>Chapter 2: Theory</b> .....	5
Coordinate Reference Systems, Transformations, and Flow Angles Overview .....	5
Coordinate Reference Systems.....	5
Coordinate System Transformations .....	6
Flow Angles .....	7
Derivation of the Angle of Attack Algorithm from the Equations of Motion .....	10
Basic Force Equations .....	10
Stability Derivative Estimation.....	14
Air Data and Inertial Navigation System Data Reduction .....	19
In-Flight Calibrations – Air Data Flow Angle System.....	19
Drag Coefficient Determination.....	20
<b>Chapter 3: Platform, Equipment, and Instrumentation</b> .....	22
UTSI Cessna 210, N33UT .....	22
Air Data Boom Assembly (Truth Source) .....	23
Calibration of Air Data System (ADS) Boom Flow Angle Vane.....	23
Ellipse-N INS System .....	25
<b>Chapter 4: Flight Test</b> .....	27
Philosophy/Methodology .....	27
Flight Test Technique – Ellipse-N INS Calibration .....	27
Flight Test Technique – Power Speed (P <sub>iw</sub> -V <sub>iw</sub> ), Steady Level Trim Shots .....	27
Flight Test Technique – Level Acceleration and Deceleration .....	28
Flight Test Technique – Abrupt Pull up.....	28
Flight Test Technique – Windup Turn.....	28
Flight Conditions .....	29

<b>Chapter 5: Data Reduction and Results</b> .....	31
Flow Angle Alpha Vane Calibration.....	31
Trim Shot.....	33
Level Acceleration and Deceleration .....	35
Pull Up Maneuver .....	39
<b>Chapter 6: Conclusions and Recommendations</b> .....	41
<b>References</b> .....	43
<b>Appendices</b> .....	46
Appendix A – Computer Program .....	47
Appendix B – UTSI Cessna 210 Aircraft Description .....	53
Appendix C – Air Data System Boom Description.....	57
Appendix D – Ellipse-N Inertial Navigation System Unit.....	59
Appendix E – Sample Calculations + Flow Chart to Determine .....	61
Appendix F – Supporting Plots.....	69
Appendix G - Windup Turn Maneuver Addendum .....	75
Appendix H – Flight Test Cards .....	76
<b>Vita</b> .....	82

# List of Tables

---

<i>Table 1: Components in a body-fixed coordinate system [7].</i>	<i>6</i>
<i>Table 2: Summary of Aerodynamic Stability Derivatives for AOA algorithm.</i>	<i>13</i>
<i>Table 3: Angle of Attack and Pitch Angle Data acquired in Flight Tests.</i>	<i>31</i>
<i>Table 4: Cessna 210 Aircraft Geometry and Data.</i>	<i>55</i>
<i>Table 5: SpaceAge Control 100400 Mini Air Data Boom Specifications.</i>	<i>58</i>
<i>Table 6: Ellipse-N Data.</i>	<i>59</i>
<i>Table 7: Sensor Outputs.</i>	<i>60</i>

# List of Figures

Figure 1: NACA Air Data Boom Design with Flow Angle Vanes on the UTSI Cessna 210 right wingtip. ....	1
Figure 2: Inertial (North-East-Down) Coordinate System. Credit USAF TPS [6]. ....	5
Figure 3: Body-Fixed Coordinate System. Credit USAF TPS [6]. ....	6
Figure 4: Flow Angle Reference Frame. $u, v, w$ are the velocity vectors in the $x, y, z$ directions, respectively, on the body-fixed reference system. Credit NASA [9] .....	8
Figure 5: Angle of Attack, Pitch Angle, and Flight Path Angle view on X-Z axis. Credit Boeing Aero Magazine [11]. ...	9
Figure 6: Difference in Angle of Attack and Pitch Angle in varied situations [12]. ....	9
Figure 7: Varying angle of attack in level flight due to lift requirements [12]. ....	9
Figure 8: Method for Estimating Oswald's Efficiency Factor. Credit Roskam [15]. ....	16
Figure 9: Typical change in drag coefficient with change in Mach number. Credit Kroo [16]. ....	18
Figure 10: Upwash over airfoil in smoke wind tunnel test. Credit Babinsky [17]. ....	20
Figure 11: UTSI Cessna 210 N33UT Research Aircraft .....	22
Figure 12: Angle of Attack Reference Line for Cessna 210, aligned with DAS rack and ADS Boom. ....	24
Figure 13: Aircraft water level reference line. The ADS Boom aligned with this reference line; the INS unit has a $0.1^\circ$ offset from this reference line. ....	24
Figure 14: Angle of Attack Flow Angle Vane (Alpha Vane) Ground Calibration for Instrument Error Correction Determination. ....	25
Figure 15: Ellipse-N INS EFIS User Interface. ....	25
Figure 16: Ellipse-N INS Installed in Cessna 210 DAS Rack in Rear Seat Station. ....	26
Figure 17: Angle of Attack (Alpha Vane) Calibration Curve .....	32
Figure 18: Angle of Attack vs. Time for Steady Level Trim Shot. ....	34
Figure 19: Angle of Attack vs. Time for Level Acceleration and Deceleration. ....	36
Figure 20: Angle of Attack vs. Time for 2G Pull up Maneuver .....	40
Figure 21: Cessna 210 Aircraft Three-View. ....	53
Figure 22: Cessna 210 Aircraft 3D Model .....	54
Figure 23: Cessna 210 Engine Power Chart (TSIO-520-H). ....	56
Figure 24: Sample Cessna 210 Weight and Balance CG Spreadsheet. ....	56
Figure 25: SpaceAge Control 100400 Mini Air Data Boom 3D model. ....	57
Figure 26: SpaceAge Control 100400 Mini Air Data Boom Drawings and Dimensions. ....	57
Figure 27: SBG Ellipse-N INS Unit. ....	59
Figure 28: NACA64A215 Airfoil at $Re=4.0 \times 10^6$ [23]. ....	65
Figure 29: NACA64A412 Airfoil at $Re=3.0 \times 10^6$ .....	66
Figure 30: Drag Polar for Cessna 210 obtained through Power-Speed Flight Test Technique .....	69
Figure 31: Time history of Angle of Attack Algorithm for Level Acceleration/Deceleration with Pitch Rate .....	69
Figure 32: Level Acceleration and Deceleration: Inertial-to-Body Transformation Data Inputs .....	70
Figure 33: INS Data inputs ( $u, w, \theta, q$ ) utilized by Angle of Attack Algorithm - Level Accel/Decel. ....	71
Figure 34: Peak Value for first Deceleration - Level Acceleration and Deceleration. ....	72
Figure 35: Calibrated Alpha Vane change in angle of attack - first deceleration .....	72
Figure 36: Calculated Angle of Attack change in angle of attack - first deceleration. ....	73
Figure 37: 2G Pull Up: Inertial-to-Body Transformation Data Inputs .....	73
Figure 38: INS Data inputs ( $u, w, \vartheta, q$ ) utilized by Angle of Attack Algorithm - 2G Pull Up .....	74
Figure 39: Angle of Attack vs. Time - Windup Turn, Left Bank. ....	75

# Nomenclature

---

<u>Acronyms</u>	<u>Title/Description</u>
ADS	Air Data System
AHRS	Attitude Heading Reference System
AOA	Angle of Attack
CG	Center of Gravity
COTS	Commercial-off-the-shelf
DAS	Data Acquisition System
EFIS	Electronic Flight Interface System
EKF	Extended Kalman Filter/Filtering
FAA	Federal Aviation Administration
FAR	Federal Aviation Regulation
FTE	Flight Test Engineer
GNSS	Global Navigation Satellite System
GPS	Global Positioning System
INS	Inertial Navigation System
KIAS	Knots Indicated Airspeed
MAC	Mean Aerodynamic Chord
MAP	Manifold Pressure
NACA	National Advisory Committee for Aeronautics
NASA	National Aeronautics and Space Administration
NED	North, East, Down Axis Reference System
OML	Outer Mold Line
Piw-Viw	Power-Speed Method (indicated, weight corrected)
RPM	Rotations / Revolutions per minute
UTSI	University of Tennessee, Space Institute
YAPS	Yaw-Attack-Pitch-Sideslip

<u>Symbol</u>	<u>Title/Description</u>	<u>Units</u>
$\mathcal{A}$	Aspect Ratio	
$a$	Local Speed of Sound	ft/s
$a_{cg}$	Aircraft acceleration at center of gravity	ft/s <sup>2</sup>
$b$	Wing Span	ft
$B$	Compressibility Correction	
$c_r$	Chord length - root	ft
$c_t$	Chord length – tip	ft
$\bar{c}$	Chord length – mean aerodynamic chord	ft
$C_D$	Drag Coefficient – Reference Condition	
$C_{D_0}$	Zero-Lift Drag Coefficient	
$C_{D_\alpha}$	Change in Drag Coefficient with Angle of Attack	
$C_{D_u}$	Change in Drag Coefficient with Forward Speed	
$C_L$	Lift Coefficient – Reference Condition	

$C_{l\alpha}$	Change in Lift Coefficient - 2D Wing Section lift curve slope	
$C_{L_u}$	Change in Lift Coefficient with Forward Speed	
$C_{L\alpha}$	Change in Lift Coefficient with Angle of Attack	
$C_{L\alpha_H}$	Change of Lift Coefficient with Angle of Attack - Tail	
$C_{T_u}$	Change in Thrust Coefficient with Forward Speed	
$C_{Z\dot{\alpha}}$	Change in Downward Force Coefficient with time rate of change of Angle of Attack	
$C_{Zq}$	Coefficient of Change in Downward Force with Pitch Rate	
$e$	Oswald's Efficiency Factor	
$F$	Force	lbf
$F_X, F_Y, F_Z$	Force about the $X_b, Y_b, Z_b$ directions, respectively	lbf
$g$	Gravitational Acceleration on Surface of Earth (32.1740)	ft/s <sup>2</sup>
$h$	Altitude - Geometric	ft
$h_i$	Pressure Altitude - Indicated	ft
$h_p$	Pressure Altitude	ft
$i$	Initial data point from INS	
$j$	Sequential data point from INS	
$m$	Mass	slug
$M$	Mach Number	
MAP	Manifold pressure	inHg
$p_{SSL}$	Pressure – Standard Sea Level	lbf/ft <sup>2</sup>
$P_{i,w}$	Power - indicated weight corrected	hp
$P_{iwn}$	Power – indicated weight corrected, normalized	hp
$p, q, r$	Rotational Rates (angular velocity) about the $X_b, Y_b, Z_b$ directions, respectively	degree/s
$\dot{p}, \dot{q}, \dot{r}$	Rotational Accelerations about the $X_b, Y_b, Z_b$ directions, respectively	degree/s <sup>2</sup>
$q$	Dynamic Pressure	lbf/ft <sup>2</sup>
RPM	Rotations / Revolutions Per Minute	
$R$	Universal gas constant = 1716	ft lbf / slug °R
$S$	Wing Area	ft <sup>2</sup>
$S_H$	Wing Area – Horizontal Tail	ft <sup>2</sup>
$SHP$	Shaft Horse Power	hp
$t$	Time	s
$T$	Outside Air Temperature	°F or °R
$T_{i \rightarrow b}$	Transformation matrix – inertial to body	
$T_{SSL}$	Temperature – Standard Sea Level	°R
$u, v, w$	Velocity components in $X_b, Y_b, Z_b$ directions, respectively	ft/s
$\dot{u}, \dot{v}, \dot{w}$	Acceleration in the $X_b, Y_b, Z_b$ directions, respectively	ft/s <sup>2</sup>
$V_b$	Body Velocity	ft/s
$V_i$	Inertial Velocity	ft/s
$V_H$	Volume Ratio – Horizontal Tail	
$V$	Velocity	ft/s
$V_{cg}$	Aircraft Velocity at the center of gravity	ft/s
$V_i$	Airspeed - indicated	ft/s
$V_{i,w}$	Airspeed - indicated, weight corrected	ft/s
$V_{iwn}$	Airspeed - indicated, weight corrected, normalized	ft/s
$V_N, V_E, V_D$	North-East-Down inertial velocity components	ft/s or m/s

$V_t$	Airspeed - true	ft/s
$\mathcal{V}$	Fuel Volume	gal
$\mathcal{V}_0$	Takeoff Fuel Volume	gal
$W$	Weight – aircraft, test point	lbf
$W_{ref}$	Weight – aircraft reference (Max Gross Weight)	lbf
$W_{TO}$	Weight – aircraft takeoff	lbf
$X, Y, Z$	Longitudinal, Side, Downward Force	lbf
$\dot{X}, \dot{Y}, \dot{Z}$	Longitudinal, Side, Downward Force Change	lbf/s
$X_b, Y_b, Z_b$	X, Y, Z coordinate system, in the body-fixed reference system	
$X_i, Y_i, Z_i$	X, Y, Z coordinate system, in the inertial reference system	
$x_H$	Distance from wing quarter chord to horizontal tail quarter chord	ft
$X_u$	Change in X-force due to Forward Speed	1/s
$X_w$	Change in X-force due to Downward Speed	1/s
$Z_u$	Change in Z-force due to change in Forward Speed	1/s
$Z_w$	Change in Z-force due to change in Downward Speed	1/s
$Z_q$	Change in Z-force due to change in Pitch Rate	ft/s
$Z_{\dot{w}}$	Change in Z-force due to change in Downward Acceleration	
$\alpha$	Angle of Attack	degree
$\alpha_F$	Angle of Flank	degree
$\alpha_o$	Angle of Attack – Reference Condition	degree
$\alpha_{calc}$	Angle of Attack – Calculated from Algorithm	degree
$\alpha_{c,m}$	Angle of Attack – Calibrated measurement from alpha vane	degree
$\alpha_{i,j}$	Angle of Attack – Calculated angle of attack between INS data points	degree
$\alpha_m$	Angle of Attack – Measured	degree
$\beta$	Angle of sideslip	degree
$\gamma$	Ratio of Specific Heats for air = 1.4	
$\varepsilon$	Upwash Angle	degree
$\delta_{act}, \theta_{act}, \sigma_{act}$	Atmospheric Pressure, Temperature, and Density Ratio, respectively	
$\delta_e, \delta_a, \delta_r$	Change in Control Surface - elevator, aileron, rudder respectively	degree
$\delta_t$	Change in thrust	lbf
$\eta_p$	Propulsive Efficiency	
$\eta_H$	Horizontal Tail Efficiency	
$\kappa$	Ratio of average 2D wing section lift curve slope to $2\pi$	
$\lambda$	Taper Ratio	
$\rho_{SSL}$	Air Density – Standard Sea Level	slug/ft <sup>3</sup>
$\rho_{fuel}$	Fuel Density	lbf/gal
$\phi, \theta, \psi$	Roll, Pitch, Yaw Euler Angle about $X_i, Y_i, Z_i$ axes, respectively	degree
$\dot{\phi}, \dot{\theta}, \dot{\psi}$	Attitude Accelerations about $X_i, Y_i, Z_i$ axes, respectively	degree/s <sup>2</sup>
$\Lambda$	Sweep Angle	degree
$\Omega_{i \rightarrow b}$	Rotation Vector of body-fixed frame with respect to inertial frame	

<b><u>Symbol</u></b>	<b><u>Units</u></b>
bhp	Brake Horse Power
degree	Degree
ft	Foot
gal	Gallon
°F	Degree Fahrenheit
hp	Horse Power
h	Hour
Hz	Hertz
in	Inch
kts	Knots
lbf	Pound force
m	Meter
nm	Nautical Mile
radian	Radian
°R	Degree Rankin
rpm	Rotations/Revolutions Per Minute
lbf	Pound force
slug	Slug
s	Second
V	Volts

# Chapter 1: Introduction

---

## Overview

The orientation of an aircraft's flight path vector relative to the air mass surrounding it can be described by three angles: the angle of attack (alpha or  $\alpha$ ), the angle of flank ( $\alpha_f$ ), and the angle of sideslip (beta or  $\beta$ ). All aerodynamic forces and moments acting on the aircraft depend on these three flow angles. They are critical parameters for pilots and engineers in research and flight testing, as well as in military, commercial, and general aviation.

Angle of attack is critical during longitudinal maneuvers, most notably for low airspeed approach and landings, and therefore the pilot must continuously be aware of the angle of attack to prevent the aircraft from stalling. The angle of attack, however, is difficult to measure precisely. Traditionally, for flight testing, mechanical aerodynamic probes mounted in front of the nose or wing tip with alpha and beta vanes are relied upon by pilots and engineers to determine critical flow angles in the air mass around the vehicle (Figure 1). These devices exist to measure flow angles with varying levels of complexity, intrusiveness, accuracy, and cost.



*Figure 1: NACA Air Data Boom Design with Flow Angle Vanes on the UTSI Cessna 210 right wingtip.*

The desire to find a simple, unobtrusive, accurate, cost effective, and reliable method to measure angle of attack is of interest to many organizations.

## Motivation/Purpose

Two immediate reasons exist for the need to accurately determine angle of attack: the interest of the Federal Aviation Administration (FAA) and the demand of flight test and aerospace engineering organizations.

The FAA is looking for instrumentation to help pilots become more situationally aware of the angle of attack, as it is a critical safety parameter in preventing stall situations [1]. Currently, stall speed requirements are met by aircraft manufacturers per Federal Aviation Regulation FAR 23.49 and FAR 25.103.

However, stall is not a function of airspeed; stall is a function of the angle of attack. Certain situations, such as an accelerated stall, catch pilots by surprise because while the aircraft airspeed is above stall speed, the angle of attack has increased beyond the angle for which the aircraft can produce lift. If a pilot fails to recognize and correct a stall situation, loss of control of the aircraft can occur. Methods for angle of attack determination can help in this effort.

For engineering organizations, various types of mechanical air data probe and booms are customized and externally mounted for each individual aircraft to measure angle of attack and angle of sideslip. These probes and booms include flow angle vanes, null-seeking cones on the fuselage, yaw-attack-pitch-sideslip (YAPS) probes, and multi-port pressure-differential probes. To account for local flow effects (i.e. upwash, downwash, and sidewash) and their associated errors, these probes must be mounted far forward on the nose or wingtip of the aircraft to put the vanes into the freestream air flow. However, problems still exist with the use of these probes.

First, the existence of the probe and boom alters the outer mold line (OML) of the aircraft, thus affecting its performance, stability and control, and handling quality characteristics. Also, in the case of wingtip mounted probes, asymmetrical loading occurs because of the introduction of the probe on the aircraft. Second, the position of the externally mounted probes is away from the center of gravity (CG). This causes the probes to be subject to angular motion, which introduces errors that are associated with airspeed, trim, or maneuvering conditions [2]. Third, in flow-directional pitot static pressure probes, pressure lag is proportional to the length of tubing between the pressure transducer diaphragm and the airway opening; thus in systems with long tubing, the lag can be substantial [3]. Fourth, for all air data systems, the cost associated with design, manufacturing, installation, and testing of customized probes and booms for aircraft can be significant. And lastly, a safety risk is always present due to failure of a part, the whole, or the functionality of an air data boom assembly. Military aircraft have been lost due to failure of the angle of attack system, most notably F-16 and F-111 [4]. In the military scenarios, the

probe readings were required for advanced control system algorithms, which fed it erroneous high angle of attack data which triggered a stall inhibitor in an unwanted situation. But just as dangerous are failures of the physical assembly which could risk the test, the mission, the aircraft, or the safety of the crew.

## Solution/Approach

Common commercial-off-the-shelf (COTS) inertial navigation system (INS) units, with three-axis gyroscopes, three-axis accelerometers (inertial sensors), and magnetometers have become more compact, more accurate, and more cost effective since their inception in the 1940s. Using the INS position, velocity, angular rates, and acceleration data, the angle of attack can be determined with an algorithm, developed from the aircraft equations of motion.

The largest advantages of using the INS data for reconstruction is that the INS is not affected by the local flow or position error, the system is extremely accurate thus eliminating the need to calibrate raw probe data, the data output rate is on par or better than current flight test instrumentation ( $\geq 20\text{Hz}$ ), and the reliability and cost of the INS unit may translate to widespread use in commercial or private aviation with an installed attitude and heading reference system (AHRS) unit.

In situations where direct flow angle measurement devices are absolutely necessary, a post-flight derived angle of attack from the equations of motion can be used to readily verify and calibrate air data probes without lengthy flights or trim shots [5].

## Objectives

- 1) Calibrate flow angle vanes by using established angle of attack vane calibration techniques
- 2) Determine angle of attack in typical flight scenarios from INS data
- 3) Compare results to data retrieved from calibrated wingtip air data boom.

## Scope/Out-of-scope

The purpose of this thesis is to test and report a derived method for determining angle of attack using data readily collected and available from a COTS INS units. The results from the algorithm are compared to the data from the installed air data boom, which is considered the truth source. The objective of the post-flight algorithm is to determine to what level of accuracy and uncertainty the algorithm can provide to determining angle of attack.

The scope of the flight tests is within the operational limits of the aircraft. Out of scope for this thesis are high angles of attack ( $> 30$  degrees) and large angles of sideslip ( $>30$  degrees). The flow angle

vane potentiometers become oversaturated beyond 30 degrees, as per design. Typical flow angles for the operational limits of an aircraft range within -1 degrees and +25 degrees for angle of attack.

Also out of scope is different configurations of the aircraft. All comparisons are done with a clean configuration (gear up, flaps up, cowl flaps closed). The estimation of the stability derivatives in the algorithm depend on the particular configuration of the aircraft. The algorithm is readily available for different estimates of the necessary stability derivatives.

A distinct difference exists between a measured angle of attack and the true or absolute angle of attack of the aircraft. For many engineering applications, a correction must be made to a measured angle of attack to obtain the true angle of attack. The purpose of this thesis is to compare a calculated angle of attack to a measured angle of attack, both relative to the same reference line. No attempt is made to reconstruct the true angle of attack of the aircraft.

## Assumptions

To describe the flight dynamics of an aircraft, simplifying assumptions must be made in order to linearize the equations of motion:

- The curvature of the Earth does not affect the motion of the aircraft (i.e. "Flat Earth")
- Coriolis accelerations due to Earth's rotation do not affect the motion (non-rotating Earth)
- Aircraft mass during maneuvers is instantaneous and constant throughout maneuver
- Rigid aircraft (no elastic changes)
- Symmetric Aircraft
- Gyroscopic effects from rotating parts (propeller, engine shaft, et al) are neglected
- Constant, non-shearing wind (ignore turbulence and gusts)

# Chapter 2: Theory

## Coordinate Reference Systems, Transformations, and Flow Angles Overview

To describe the motion of an aircraft, it is necessary to define suitable coordinate systems for the formulation of the equations of motion. When using an INS unit, measurements are made in two coordinate systems. One coordinate system is fixed to the Earth, and is considered an inertial reference system. The other coordinate system is fixed to the aircraft and is referred to as a body-fixed reference system.

### Coordinate Reference Systems

The North-East-Down inertial coordinate reference system is a “flat Earth” inertial reference coordinate system. The subscript “i” is used to denote the inertial frame. The system is defined with the  $Z_i$ -axis aligned with the local gravity vector, pointing toward the center of the Earth, leaving the  $X_i$ -axis aligned toward true North and the  $Y_i$ -axis pointing East. The origin point is an arbitrary point on the surface. The North-East-Down system is a non-accelerating, non-rotating reference frame in which Newton’s second law is valid [6]. See Figure 2.

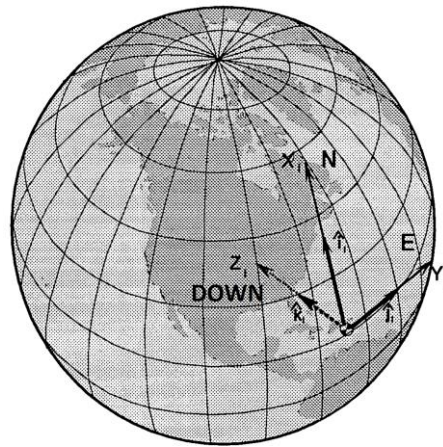


Figure 2: Inertial (North-East-Down) Coordinate System. Credit USAF TPS [6].

The body-fixed coordinate system is a reference frame with its origin fixed to the aircraft center of gravity. The subscript “b” is used to denote the body-fixed frame. The system is defined with the positive  $X_b$ -axis always pointing through the nose of the aircraft, the  $Y_b$ -axis out the right wing, and the positive  $Z_b$ -axis direction pointing straight down from the aircraft [6]. See Figure 3.

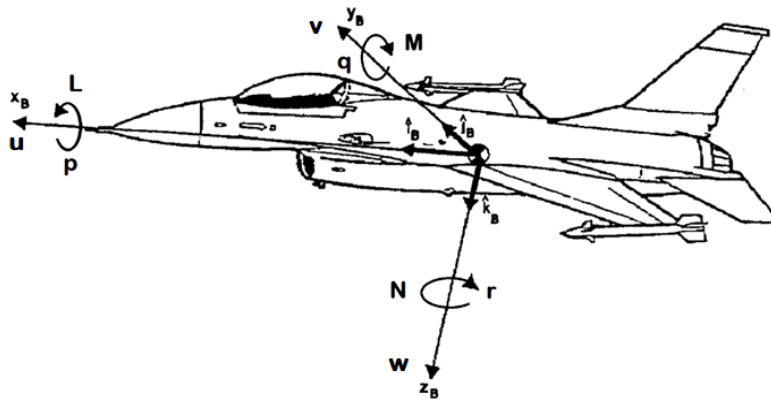


Figure 3: Body-Fixed Coordinate System. Credit USAF TPS [6].

The forces, velocities, and rotations of the aircraft can be resolved to components along the body-fixed coordinate system. Refer to Table 1 for the associated nomenclature for these components.

Table 1: Components in a body-fixed coordinate system [7].

	Roll Axis $X_b$	Pitch Axis $Y_b$	Yaw Axis $Z_b$
Angular velocities	$p$	$q$	$r$
Velocity components	$u$	$v$	$w$
Aerodynamic forces	$X$	$Y$	$Z$

### Coordinate System Transformations

It is necessary to be able to move between the inertial coordinate system and the body-fixed coordinate system. Positions, velocities (angular and translational), and accelerations (angular and translational) can be determined between the two reference systems in this manner. First, the inertial system must be rotated until it aligns with the body-fixed coordinate system. To accomplish this, Euler angles are utilized.

$\phi$  (roll Euler angle) is the rotation about the X-axis,  $\theta$  (pitch Euler angle) is the rotation about the Y-axis, and  $\psi$  (yaw Euler angle) is the rotation about the Z-axis. The order of rotations is important; changing the order of rotations yields entirely different results. To rotate from the inertial frame to the body-fixed frame ( $X_i-Y_i-Z_i \rightarrow X_b-Y_b-Z_b$ ):

- 1) Rotate the yaw Euler angle  $\psi$  about the Z-axis
- 2) Rotate the pitch Euler angle  $\theta$  about the Y-axis
- 3) Rotate the roll Euler angle  $\phi$  about the X-axis

This is denoted as [8]:

$$\begin{bmatrix} X \\ Y \\ Z \end{bmatrix}_b = [\phi][\theta][\psi] \begin{bmatrix} X \\ Y \\ Z \end{bmatrix}_i \quad (1)$$

The resulting inertial to body transformation matrix from the matrix multiplication of the rotations is [6]:

$$T_{i \rightarrow b} = [\phi][\theta][\psi] = \begin{bmatrix} \cos\theta\cos\psi & \cos\theta\sin\psi & -\sin\theta \\ \sin\phi\sin\theta\cos\psi - \cos\phi\sin\psi & \sin\phi\sin\theta\sin\psi + \cos\phi\cos\psi & \sin\phi\cos\theta \\ \cos\phi\sin\theta\cos\psi + \sin\phi\sin\psi & \cos\phi\sin\theta\sin\psi - \sin\phi\cos\psi & \cos\phi\cos\theta \end{bmatrix} \quad (2)$$

When analyzing an aircraft from the inertial reference frame, it can be thought of as a point mass; all forces go through the center of gravity (CG) of the aircraft. However, the motion on a three-dimensional aircraft from the body-fixed frame requires knowing the movement of the CG, as well as any rotations and translations of the parts of the aircraft. This vector relation is described by:

$$\left. \frac{dV_i}{dt} \right|_i = \left. \frac{dV_b}{dt} \right|_b + \Omega_{i \rightarrow b} \times V_b \quad (3)$$

$\Omega_{i \rightarrow b}$  is the rotation vector of the body-fixed frame with respect to the inertial frame. This relation holds true for every vector, including position, velocity, and acceleration, which is important for the algorithm derivation.

### Flow Angles

Three relative angles are formed between a moving aircraft and the air mass. Angle of attack (alpha or  $\alpha$ ) is the angle between the oncoming air or relative wind and a longitudinal reference line on the aircraft or wing. The body-fixed  $X_b$ -axis is a useful reference line. Utilizing the body-fixed reference system, and the associated velocity components, the angle of attack is defined as:

$$\alpha = \arctan\left(\frac{w}{u}\right) \quad (4)$$

Continuing the use of the body-fixed reference system, the Flank angle of attack (flank or  $\alpha_F$ ) is defined by:

$$\alpha_F = \arctan\left(\frac{v}{u}\right) \quad (5)$$

Angle of sideslip (beta or  $\beta$ ) is the angle between the velocity vector and the longitudinal axis of the aircraft. It is defined as:

$$\beta = \arcsin\left(\frac{v}{V_t}\right) \quad (6)$$

Figure 4 demonstrates the relationship between the flow angles on the aircraft and the oncoming air mass. The vectors  $u$ ,  $v$ ,  $w$  are the velocity components on the body-axis frame:  $u$  points in the positive  $X_b$ -direction,  $v$  points in the positive  $Y_b$ -direction, and  $w$  points in the positive  $Z_b$ -direction.  $V_t$  is the true airspeed vector and denotes the true speed and direction of motion of the aircraft relative to the air mass (equation 7). In the situation where the angle of sideslip is steady and does not contain a downward velocity component in  $w$ , then  $\alpha_F = \beta$  [9].

$$V_t = \sqrt{u^2 + v^2 + w^2} \quad (7)$$

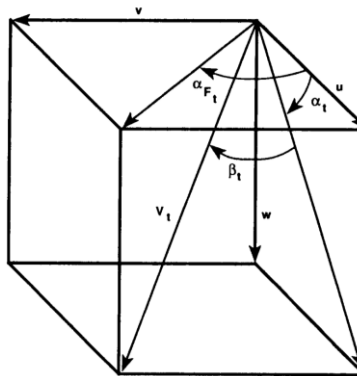


Figure 4: Flow Angle Reference Frame.  $u, v, w$  are the velocity vectors in the  $x, y, z$  directions, respectively, on the body-fixed reference system. Credit NASA [9]

It is important to note the difference between the angle of attack, the pitch attitude, and flight path angle of the aircraft. The angle of attack, as already defined, is the angle between the oncoming air mass and a longitudinal reference line on the aircraft. The pitch attitude angle is an angle between the same longitudinal reference line and the horizon, which on an inertial reference frame is also the pitch Euler angle. Flight path angle is the angle between the flight path vector (where the aircraft is going) and

the horizon. Angle of attack is the difference between the pitch angle and flight path angle when the flight path angle is referenced to the horizon. Because of the relationship of angle of attack, pitch angle, and flight path angle, and aircraft can reach very high angles of attack, even with the nose below the horizon, if the flight path angle is a steep descent. This important relation allows for proper calibration of alpha (angle of attack) vanes, because in steady level flight, the angle of attack and the pitch angle experienced by the aircraft are equal ( $\alpha = \theta$ ) [10]. Refer to Figure 5, Figure 6, Figure 7.

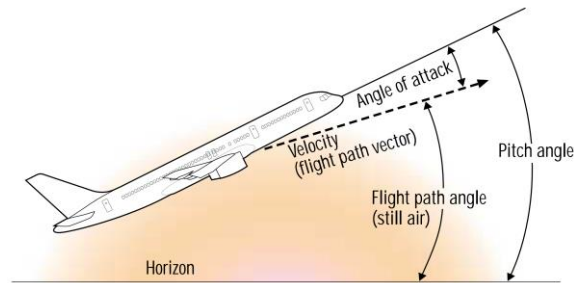


Figure 5: Angle of Attack, Pitch Angle, and Flight Path Angle view on X-Z axis. Credit Boeing Aero Magazine [11].

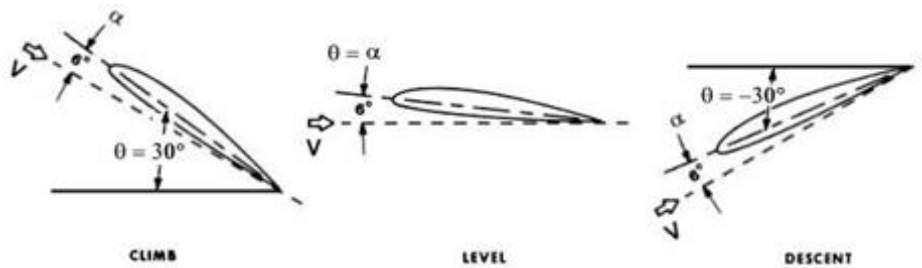


Figure 6: Difference in Angle of Attack and Pitch Angle in varied situations [12].

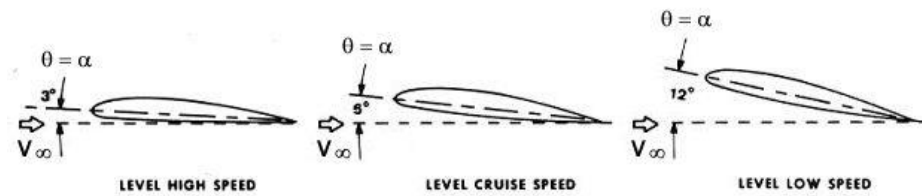


Figure 7: Varying angle of attack in level flight due to lift requirements [12].

## Derivation of the Angle of Attack Algorithm from the Equations of Motion

Rigid-body aircraft equations of motion are derived from Newton's second law. The developed angle of attack algorithm utilizes linear, time-invariant equations of motion, and this is done through small perturbation theory and Taylor series expansion. This method follows the same derivation as a similar algorithm for angle of sideslip described by Heller [13].

### Basic Force Equations

Newton's second law, when applied to an aircraft, only holds true in an inertial reference frame; the aircraft body-fixed system is not suitable because it is not an inertial reference frame, but the North-East-Down Earth-fixed is an inertial reference frame.

Newton's second law states:

$$F = m \left( \frac{d}{dt} \right) V_{CG} = ma_{CG} \quad (8)$$

This relation states that only the magnitude and direction of the forces determine the acceleration of the CG of the aircraft, and not how the forces are distributed along the aircraft. As a simplification, from the point of view of the inertial frame, the aircraft can be treated as a point-mass.

Understanding the equations of motion requires understanding the position, velocities, and accelerations in the body-fixed frame. Utilizing equation 3 with equation 8, the forces on the aircraft in the body-fixed reference system can be described by:

$$F = m \left( \frac{d}{dt} \right) V_{CG} = m \left. \frac{dV_b}{dt} \right]_b + m(\Omega_{i \rightarrow b} \times V_b) \Rightarrow \quad (9)$$

$$\begin{bmatrix} F_x \\ F_y \\ F_z \end{bmatrix} = m \begin{bmatrix} \dot{u} + qw - rv \\ \dot{v} + ru - pw \\ \dot{w} + pv - qu \end{bmatrix}$$

- $\dot{u}, \dot{v}, \dot{w}$  is the acceleration of the aircraft in the  $X_b, Y_b, Z_b$  directions, respectively.
- $u, v, w$  are the velocity components in the  $X_b, Y_b, Z_b$  directions, respectively.
- $p, q, r$  are the angular velocities about the  $X_b, Y_b, Z_b$  axes, respectively.

The velocity components  $u, v, w$  are not directly provided by the inertial navigation system. These components must be computed from the inertial North-East-Down velocities, which are provided. To accomplish this, the transformation matrix in equation 2 is utilized to convert inertial North-East-Down velocities to body-fixed velocities.

The external forces which act on the aircraft can be broken down into gravitational, aerodynamic, and thrust forces. As the aircraft can be in any orientation relative to the inertial frame, the component of gravitational acceleration (which is defined as positive in the Z-axis) must be rotated to align with the body-fixed frame. Aerodynamic and thrust forces can be generalized as  $X, Y, Z$  forces, which is expanded upon later. The resulting equation set is:

$$mg \begin{bmatrix} -\sin\theta \\ \sin\phi\cos\theta \\ \cos\phi\cos\theta \end{bmatrix} + \begin{bmatrix} X \\ Y \\ Z \end{bmatrix} = m \begin{bmatrix} \dot{u} + qw - rv \\ \dot{v} + ru - pw \\ \dot{w} + pv - qu \end{bmatrix} \quad (10)$$

This set of equations is non-linear for real aircraft motions. To linearize the system, small perturbation theory is used. Small perturbation theory assumes that the motion of the airplane consists of small deviations about a steady flight condition [7]. Each variable within the equation is replaced by the steady flight reference value and a perturbation. The right hand side of equation 10, when applying small perturbation theory, is depicted as:

$$m \begin{bmatrix} (\dot{u} + \Delta\dot{u}) + (q + \Delta q)(w + \Delta w) - (r + \Delta r)(v + \Delta v) \\ (\dot{v} + \Delta\dot{v}) + (r + \Delta r)(u + \Delta u) - (p + \Delta p)(w + \Delta w) \\ (\dot{w} + \Delta\dot{w}) + (p + \Delta p)(v + \Delta v) - (q + \Delta q)(u + \Delta u) \end{bmatrix} \quad (11)$$

The left hand side of the equation is more difficult to linearize, as the forces  $X, Y, Z$  are not part of the state of the aircraft; instead they depend on the current state and entire history of states of the aircraft [14]. For example, a change in angle of attack could create disturbances at the wing, which later results in forces acting on the tail of the aircraft. Through experience and assumptions, higher order terms are ignored as they do not significantly contribute to the force [7] [14] [15]. These assumptions make use of steady and symmetric flight, thus:

- no initial accelerations ( $\dot{u} = \dot{v} = \dot{w} = 0$ )
- no initial angular velocity ( $p = q = r = 0$ )
- no angular acceleration ( $\dot{p} = \dot{q} = \dot{r} = 0$ )
- no attitude accelerations ( $\dot{\phi} = \dot{\theta} = \dot{\psi} = 0$ )
- no force changes ( $\dot{X} = \dot{Y} = \dot{Z} = 0$ )
- symmetry ( $v = \phi = Y = 0$ ).

These assumptions apply to the entire system (both left and right hand side). The resulting equations are shown as:

$$\begin{aligned}
 F_X &= -mg\cos(\theta)\Delta\theta + \frac{\partial X}{\partial u}\Delta u + \frac{\partial X}{\partial w}\Delta w + \frac{\partial X}{\partial q}\Delta q + \frac{\partial X}{\partial \delta_e}\Delta\delta_e + \frac{\partial X}{\partial \delta_t}\Delta\delta_t \\
 F_Y &= mg\cos(\theta)\Delta\phi + \frac{\partial Y}{\partial v}\Delta v + \frac{\partial Y}{\partial \dot{v}}\Delta\dot{v} + \frac{\partial Y}{\partial p}\Delta p + \frac{\partial Y}{\partial r}\Delta r + \frac{\partial Y}{\partial \delta_a}\Delta\delta_a + \frac{\partial Y}{\partial \delta_r}\Delta\delta_r \\
 F_Z &= -mg\sin(\theta)\Delta\theta + \frac{\partial Z}{\partial u}\Delta u + \frac{\partial Z}{\partial w}\Delta w + \frac{\partial Z}{\partial \dot{w}}\Delta\dot{w} + \frac{\partial Z}{\partial q}\Delta q + \frac{\partial Z}{\partial \delta_e}\Delta\delta_e + \frac{\partial Z}{\partial \delta_t}\Delta\delta_t
 \end{aligned} \tag{12}$$

At this point, it is necessary to return to the purpose for the derivation of an angle of attack algorithm using inertial navigation data. First, commercial off-the-shelf inertial navigation systems cannot provide data regarding the change in control surfaces ( $\delta_e$ ,  $\delta_a$ ,  $\delta_r$ ) or change in thrust ( $\delta_t$ ). It is thus, necessary to exclude those parameters from future use in the algorithm. Second, in reviewing the angle of attack definition from equation 4, it can be seen that the force in the Y component does not contribute as the angle of attack is only a function of longitudinal motion, normal motion, and pitching motion. Moving forward, analysis of the forces is only conducted in the  $X_b$  and  $Z_b$  directions.

To make further simplifications, Nelson and Roskam state that the effects of changes in pitch rate to longitudinal forces ( $\frac{\partial X}{\partial q}$ ) are usually negligible for the subsonic Mach range, and thus is not a factor moving forward [7] [15]. For the normal force equations, Nelson notes that in practical applications, the downward acceleration term ( $\frac{\partial Z}{\partial \dot{w}}$ ) is typically neglected as it contributes little to aircraft response [7]. This component is kept in the derivation, to test the assertion of Nelson. The longitudinal and normal force equations for small perturbations from steady symmetric flight are [7]:

$$\begin{aligned}
 -mg\cos(\theta)\Delta\theta + \frac{\partial X}{\partial u}\Delta u + \frac{\partial X}{\partial w}\Delta w &= m\Delta\dot{u} \\
 -mg\sin(\theta)\Delta\theta + \frac{\partial Z}{\partial u}\Delta u + \frac{\partial Z}{\partial w}\Delta w + \frac{\partial Z}{\partial \dot{w}}\Delta\dot{w} + \frac{\partial Z}{\partial q}\Delta q &= m(\Delta\dot{w} + u\Delta q)
 \end{aligned} \tag{13}$$

Dividing through both sides by the mass  $m$  and solving for the perturbed acceleration components  $\Delta\dot{u}$  and  $\Delta\dot{w}$  yields:

$$\begin{aligned}
& -g\cos(\theta)\Delta\theta + \frac{\left(\frac{\partial X}{\partial u}\right)}{m}\Delta u + \frac{\left(\frac{\partial X}{\partial w}\right)}{m}\Delta w = \Delta\dot{u} \\
\left(\begin{array}{c} 1 \\ 1 - \frac{\left(\frac{\partial Z}{\partial w}\right)}{m} \end{array}\right) & \left[ -g\sin(\theta)\Delta\theta + \frac{\left(\frac{\partial Z}{\partial u}\right)}{m}\Delta u + \frac{\left(\frac{\partial Z}{\partial w}\right)}{m}\Delta w + \left(\frac{\frac{\partial Z}{\partial q}}{m} - u\right)\Delta q \right] = \Delta\dot{w} \quad (14)
\end{aligned}$$

Ultimately, the two equations are Newton's second law in the form of  $\frac{F}{m} = a$ , with the acceleration component (or change in the perturbed speed) on the right and the force and mass components on the left. The partial-derivative-divided-by-mass terms are called aerodynamic stability derivatives. Descriptions of each stability derivative are noted in Table 2.

Table 2: Summary of Aerodynamic Stability Derivatives for AOA algorithm

Derivative	Symbol	Summary	Description
$\frac{\left(\frac{\partial Z}{\partial u}\right)}{m}$	$Z_u$	$-(C_{L_u} + 2C_L)\frac{qS}{mu}$	Change in Z-force due to change in Forward speed
$\frac{\left(\frac{\partial Z}{\partial w}\right)}{m}$	$Z_w$	$-(C_{L_\alpha} + C_D)\frac{qS}{mu}$	Change in Z-force due to change in Downward speed
$\frac{\left(\frac{\partial Z}{\partial q}\right)}{m}$	$Z_q$	$-(C_{Z_q}\frac{\bar{c}}{2})\frac{qS}{mu}$	Change in Z-force due to change in pitch rate
$\frac{\left(\frac{\partial Z}{\partial \dot{w}}\right)}{m}$	$Z_{\dot{w}}$	$-(C_{Z_{\dot{\alpha}}}\frac{\bar{c}}{2u})\frac{qS}{mu}$	Change in Z-force due to change in Downward acceleration
$\frac{\left(\frac{\partial X}{\partial u}\right)}{m}$	$X_u$	$-((C_{D_u} + 2C_D) + C_{T_u})\frac{qS}{mu}$	Change in X-force due to Forward speed
$\frac{\left(\frac{\partial X}{\partial w}\right)}{m}$	$X_w$	$-(C_{D_\alpha} + 2C_L)\frac{qS}{mu}$	Change in X-force due to Downward speed

It is noted that for each stability derivative term, there are more coefficients that need to be defined. These coefficients and their solutions are briefly discussed in the next section.

Reexamining equation 14, the perturbed-acceleration value can now be determined for the longitudinal and normal equations. Given the data collection rate of the inertial navigation system, the resulting accelerations can be integrated between each point to yield the resulting velocity vectors:

$$\begin{aligned}
u_{i,j} &= \int_i^j \Delta \dot{u} dt \\
w_{i,j} &= \int_i^j \Delta \dot{w} dt
\end{aligned}
\tag{15}$$

The points  $i$  and  $j$  are the individual points taken by the inertial navigation system. At 20Hz,  $dt$  is given at 0.05s. These velocity vectors are used in equation 4 to give the resulting angle of attack ( $\alpha_{i,j}$ ). The reference angle of attack ( $\alpha_o$ ), at the trim condition, is also calculated with the same equation 4. Equation 4 is reiterated here:

$$\alpha = \arctan\left(\frac{w}{u}\right)
\tag{4}$$

The complete time history of the calculated angle of attack can be built up in post-flight, as such:

$$\alpha_{calc} = \alpha_o + \alpha_{i,j}
\tag{16}$$

Each calculation of angle of attack is from the steady state reference condition, thus each new angle of attack is always added to the initial steady state angle of attack.

### Stability Derivative Estimation

The stability derivatives outlined in Table 2 are required to calculate the perturbed acceleration values for the angle of attack algorithm. A discussion of each reveals the effects and applicability of each component on the motion of the aircraft. All of the stability derivatives are calculated at the initial steady level flight condition.

#### *Change in the downward force (Z-force) with respect to forward speed ( $Z_u$ ) – “Lift Damping”*

The coefficient  $C_{L_u}$  is the change in the lift coefficient with the change in forward speed, and can be estimated as:

$$C_{L_u} = \frac{\partial C_L}{\partial M} = \frac{M^2}{1 - M^2} C_{L_\alpha}
\tag{17}$$

The forward speed is expressed as a function of the Mach number ( $M$ ), as defined by:

$$M = \frac{V_t}{a} = \frac{V_t}{\sqrt{\gamma RT}}
\tag{18}$$

Where:

- $a$  is the local speed of sound
- $\gamma$  is the ratio of specific heat, and is 1.4 for air on Earth
- $R$  is the universal gas constant, and is 1716 ft lbf / slug °R.
- and  $T$  is the outside air temperature.

The entire term holds true for Mach numbers  $M \leq 0.8$ . The term utilizes the Prandtl-Glauert rule, which corrects for compressibility effects to yield the incompressible lift coefficient [7].

Lastly, the three-dimensional lift coefficient ( $C_{L\alpha}$ ) is estimated by the lifting-line theory, finite wing, subsonic lift curve slope formula [15]:

$$C_{L\alpha} = \frac{\partial C_L}{\partial \alpha} = \frac{2\pi\mathcal{A}}{2 + \sqrt{\frac{\mathcal{A}^2\mathcal{B}^2}{\kappa^2} \left(1 + \frac{\tan^2\Lambda}{\mathcal{B}^2}\right) + 4}} \quad (19)$$

Where:

- $\mathcal{A}$  is the aspect ratio of the wing, which is equal to  $\frac{b^2}{S}$
- $\mathcal{B}$  is the compressibility correction, where  $\mathcal{B} = \sqrt{1 - M^2}$
- $\kappa$  is the ratio of average 2D wing section lift curve slope to  $2\pi$ , where  $\kappa = \frac{C_{l\alpha}}{2\pi}$
- $\Lambda$  is the sweep angle of the wing

Lastly, the steady-state lift coefficient is required for the “lift damping” ( $Z_u$ ) term, and is as described by the equilibrium lift equation:

$$C_L = \frac{W}{qS} \quad (20)$$

#### *Change in the downward force (Z-force) with respect to downward speed ( $Z_w$ )*

Within the  $Z_w$  stability derivative are the three-dimensional lift curve slope and drag curve slope. These estimates hold true for low, subsonic Mach numbers. Both values are taken at the reference condition, thus are analyzed at a specific angle of attack.

Estimates of the three-dimensional lift coefficient utilizes the same lift coefficient in equation 19, from the lift damping  $Z_u$  stability derivative.

The reference drag polar, assumed to fit the parabolic approximation, can be written as:

$$C_D = C_{D_o} + \frac{C_L^2}{\pi\mathcal{A}e} \quad (21)$$

The zero-lift drag coefficient ( $C_{D_0}$ ) must be estimated for each aircraft. A flight test technique, covered in a later section, takes advantage of the steady level flight assumption that thrust equals drag, to accurately compute this value.  $e$  is the Oswald's efficiency factor, which is estimated from Figure 8.

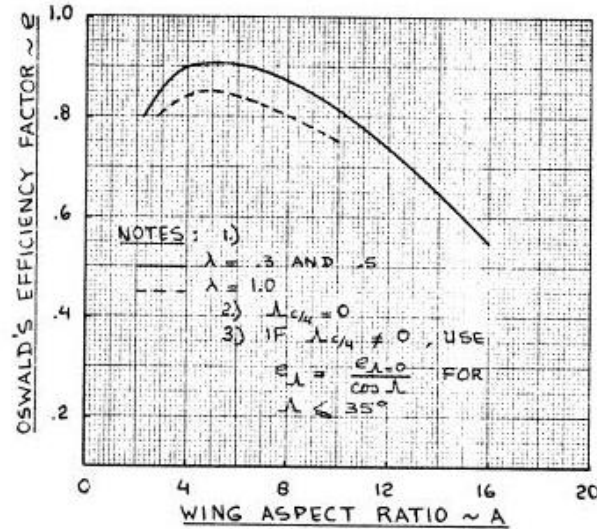


Figure 3.2 Method for Estimating Oswald's Efficiency Factor

Figure 8: Method for Estimating Oswald's Efficiency Factor. Credit Roskam [15].

#### Change in the downward force (Z-force) with respect to pitch rate ( $Z_q$ )

Aerodynamically, any changes in pitch to the aircraft from a trim condition changes the contribution of the forces from the wing and the horizontal tail. The contribution of the wing is smaller than the contribution of the tail, thus a common practice is to compute the tail contribution and multiply by 1.1 (an increase of 10 percent) to account for the wing [7].

The pitch rate causes a change in the angle of attack on the horizontal tail, and thus a change in the lift from the tail. The wing + tail contribution is noted as:

$$C_{Z_q} = 1.1(-2C_{L_{\alpha_H}} \eta_H V_H) \quad (22)$$

$C_{L_{\alpha_H}}$  is the three-dimensional lift curve slope for the tail, which is estimated in the same way as equation 18, which was for the wing of the aircraft.  $\eta_H$  is the horizontal tail efficiency factor, which is the ratio of the dynamic pressure experienced by the tail to that of the freestream. Typical values for the tail efficiency factor is 0.9.  $V_H$  is the horizontal tail volume ratio as, defined as:

$$V_H = \frac{x_H S_H}{\bar{c} S} \quad (23)$$

Typically,  $x_H$  is the distance from the airplane center of gravity to the horizontal tail aerodynamic center. As the CG changes in flight, it is often acceptable to use the distance from the quarter mean geometric chord of the wing to the quarter mean geometric chord of the horizontal tail as an initial guess [15]. Lastly,  $S_H$  is the horizontal tail area.

*Change in the downward force (Z-force) with respect to downward acceleration ( $Z_w$ )*

According to Nelson and Roskam, for pure pitching motion, this term can be neglected because “it contributed very little to aircraft response” [7]. However, within the stability derivative is a time rate of change of angle of attack term. This term contributes to the angle of attack determination in non-longitudinal (or out of plane-of-symmetry) motion or in accelerated motion with changing load factor.

The Z-force coefficient  $C_{Z\dot{\alpha}}$  necessarily details the time rate of change of angle of attack, and is expressed as:

$$C_{Z\dot{\alpha}} = -2C_{L\alpha_H} \eta_H V_H \frac{2C_{L\alpha}}{\pi \mathcal{A}} \quad (24)$$

This expression is very similar to the pitch rate coefficient, except for the last term.  $\frac{2C_{L\alpha}}{\pi \mathcal{A}}$  is the estimate for the rate of change of the downwash angle with respect to the angle of attack. In other words, for a given angle of attack, there is a given downwash due to the airflow circulation around the wing; when this angle of attack changes, the downwash changes.

*Change in the forward force (X-force) with respect to forward speed ( $X_u$ ) – “Speed Damping”*

$C_{D_u}$  and  $C_{T_u}$  are the changes in the drag and thrust coefficients with forward speed. Typically for low subsonic Mach numbers, the variation of the drag coefficient is negligible, as demonstrated by Figure 9. The drag coefficient remains constant with change in speed until near the transonic range ( $M > 0.8$ ). The formal estimate is given by:

$$C_{D_u} = M \frac{\partial C_D}{\partial M} \quad (25)$$

As the flight condition does not approach transonic or supersonic, there is no drag divergence due to change in Mach number. Assuming the change is small, and the reality that the Mach number is already small for low subsonic flight  $M < 0.2$ , the change in drag coefficient due to forward speed can be ignored ( $C_{D_u} = 0$ ).

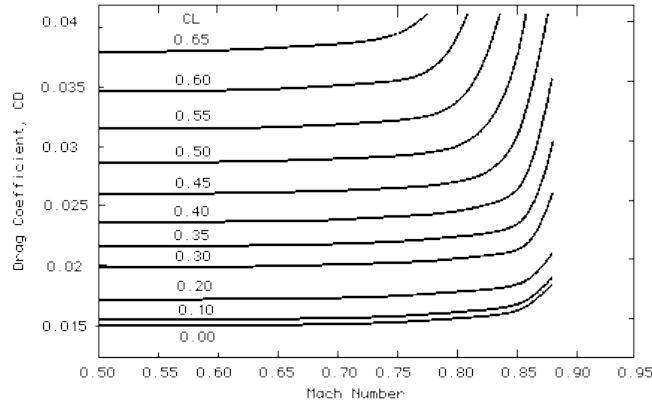


Figure 9: Typical change in drag coefficient with change in Mach number. Credit Kroo [16].

Estimates of the reference drag coefficient utilizes the same drag coefficient in equation 21. The thrust term  $C_{T_u}$ , for piston engine power plant and variable pitch propeller aircraft, is estimated as equaling the opposite value of the reference drag coefficient, as defined in equation 20 [7].

$$C_{T_u} = -C_D \quad (26)$$

Thus, the resulting “speed damping” derivative is shown simply as:

$$X_u = -(C_D) \frac{qS}{mu} \quad (27)$$

*Change in the forward force (X-force) with respect to downward speed ( $X_w$ )*

Taking the derivative of the parabolic drag polar (equation 21) yields the local fit to the actual drag polar:

$$C_{D_\alpha} = \frac{\partial C_{D_o}}{\partial \alpha} + \frac{2C_L}{\pi \mathcal{A} e} C_{L_\alpha} \quad (28)$$

The drag curve slope ( $C_{D_\alpha}$ ) is dependent on the lift curve slope, as defined by equation 19, as well as the steady state lift coefficient, defined in equation 20. Roskam details that the  $\frac{\partial C_{D_o}}{\partial \alpha}$  represents the change in profile drag with angle of attack, and the contribution is often very small, and is thus acceptable to consider  $\frac{\partial C_{D_o}}{\partial \alpha} = 0$  [15].

## Air Data and Inertial Navigation System Data Reduction

Data from the Cessna 210 production system and the inertial navigation unit are utilized for the data reduction of the angle of attack algorithm. The air data system (ADS) boom allows for data collection of indicated airspeed and altitude, but because the purpose of this report is to utilize only INS and shipboard data, the ADS data was not utilized.

Inertial North-East-Down airspeeds ( $V_N, V_E, V_D$ ) signals were readily obtained from the INS unit. Conversion to obtain body-fixed airspeed ( $u, v, w$ ) utilizes equations 1 and 2, and then the true airspeed  $V_t$  is obtained through equation 7.

Altitude signals ( $h$ ) were readily available from the INS unit. Air density was calculated through the standard exponential atmosphere equations for input into the stability derivatives and algorithm. The atmospheric pressure ratio ( $\delta$ ), temperature ratio ( $\theta$ ), and density ratio ( $\sigma$ ), can be determined from:

$$\delta_{act} = (1 - 6.8756 \times 10^{-6} \times h_p)^{5.2559} \quad (29)$$

$$\theta_{act} = \frac{T_{act}}{T_{SSL}} \quad (30)$$

$$\sigma_{act} = \delta_{act} / \theta_{act} \quad (31)$$

For the temperature ratio ( $\theta_{act}$ ), the observed temperature ( $T_{act}$ ) is considered accurate. This observed temperature was recorded from the Cessna 210 onboard thermometer located on the windshield. The resulting pressure ratio ( $\delta_{act}$ ) and temperature ratio ( $\theta_{act}$ ) was utilized to determine the density ratio, which is used in calculations of the subsonic dynamic pressure:

$$q = \frac{1}{2} \rho V_t^2 = \frac{1}{2} \sigma_{act} \rho_{ssl} V_t^2 \quad (32)$$

## In-Flight Calibrations – Air Data Flow Angle System

In-flight calibration for the angle of attack flow angle vane, from this point forward referred to as “alpha vane”, is required. The alpha vane measures the flow direction at its mounted position. Errors in the reading for the measured angle of attack due to the location of the vane is called the angle of attack position error. Deviations of the aircraft angle of attack from the angle of attack measured from the alpha vane may be a result of upwash due to the flow around the leading edge of the wing and/or

elasticity in the air data boom and wing. The relationship between measured angle of attack and the corresponding freestream value needed to be established.

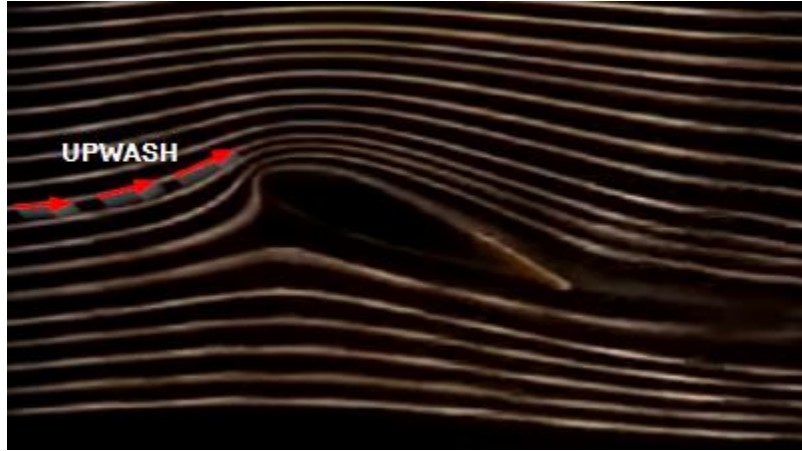


Figure 10: Upwash over airfoil in smoke wind tunnel test. Credit Babinsky [17].

In constant speed, zero-sideslip, steady level flight, the angle of attack and pitch angle are theoretically equal ( $\alpha = \theta$ ) (Figure 6). Deviations in steady level flight are described by a climb or descent angle [5]. Thus the calibration, utilizing the pitch angles, is:

$$\alpha = \theta - \arcsin\left(\frac{\left(\frac{dh}{dt}\right)}{V_t}\right) \quad (33)$$

Where  $\alpha$  is the angle of attack of the aircraft with respect to a reference line,  $\theta$  is the pitch Euler angle relative to the horizon,  $\frac{dh}{dt}$  is the rate of climb, and  $V_t$  being the true airspeed. Once the relationship is established for the full range of flow angles experienced by the aircraft, the measured angle of attack can be corrected. The description of the flight test technique is described in a later section.

### Drag Coefficient Determination

As a consequence of having to calibrate the alpha vane, an established method of determining the drag polar can be accomplished simultaneously. The Power-Speed (Piw-Viw) flight test technique was utilized. A description of the technique is in the Flight Test Technique section.

The theory behind the method utilizes steady, equilibrium flight to equate thrust and drag forces equaling to one another, thus remain balanced. Thus, with the ability to determine thrust through

measurements of power at a given level flight speed, drag can be determined at that given speed. This method is described by Kimberlin [18]. To summarize, weight standardized, indicated engine power is obtained from:

$$P_{iw} = \frac{(SHP)\sqrt{\sigma}}{\left(W_{ref}/W\right)^{3/2}} [hp] \quad (34)$$

Shaft horse power is taken from the manufacturer engine power chart (Figure 23). Both the indicated power and indicated speed are weight normalized, and the relationship is linearized with [18]:

$$V_{iwn} = \left( \left( \frac{V_{iw}^4}{10^7} \right)_n \times 10^7 \right)^{1/4} [kts] \quad (35)$$

$$P_{iwn} = \frac{\left( \frac{P_{iw} \times V_{iw}}{10^3} \right)_n \times 10^3}{V_{iwn}} [hp] \quad (36)$$

The resulting drag coefficient and lift coefficient are calculated as [18]:

$$C_D = \frac{2 * 550 * P_{iwn} \eta_p}{\rho_0 * (1.687 * V_{iwn})^3 * S} = \frac{2 * 550 * [hp]}{\left[ \frac{slug}{ft^3} \right] * (1.687 * [kts])^3 * [ft^2]} \quad (37)$$

$$C_L = \sqrt{\left( \frac{2 * W_{ref}}{\rho_0 * (1.687 * V_{iwn})^2 * S} \right)^2} = \sqrt{\left( \frac{2 * [lbf]}{\left[ \frac{slug}{ft^3} \right] * (1.687 * [kts])^2 * [ft^2]} \right)^2} \quad (38)$$

This relationship can then be plotted. The total drag, in subsonic flight, is a combination of the zero-lift (parasitic) drag and the lift induced drag. When  $C_L = 0$ , then the zero-lift drag coefficient can be determined. It is also noted that the numerical formulas for equation 37 and 38 are only valid with the listed units.

## Chapter 3: Platform, Equipment, and Instrumentation

---

### UTSI Cessna 210, N33UT

Flight testing was accomplished using a Cessna 210 Centurion research aircraft, tail number N33UT, registered to the University of Tennessee, Space Institute. The modified Cessna 210 Centurion had a Continental TSIO-520-C engine, fixed gear, a three blade propeller, and modified seating for four. A commercial stall kit was also installed on the wings.

Research modifications required the removal of two rear seats; mounted in their place was an installed rack with an expandable data acquisition system (DAS) and instrument power control system. The aircraft has also been equipped with an instrument video system, upward and downward facing radiometer sensors, a pyrometer system, and laser altimeter. The aircraft is modified with a wingtip boom on the right wing provides inflight readings for pitot-static pressures, angle of attack, and angle of sideslip. The aircraft with all the extra added modifications and equipment is utilized by the University for flight testing and atmospheric research.

Weight was available through production fuel sensors on board the aircraft which measure fuel remaining in each tank to the accuracy of 0.1 gal. The weight of the aircraft is calculated by knowing the empty weight, max gross reference weight, and the weight immediately prior to flight. For each maneuver, the weight and mass of the aircraft is considered instantaneous and constant through the maneuver, and thus is only noted immediately prior to the test points.



*Figure 11: UTSI Cessna 210 N33UT Research Aircraft*

Full details on the standard Cessna 210 are listed in Appendix B – UTSI Cessna 210 Aircraft Description.

## Air Data Boom Assembly (Truth Source)

The wingtip air data boom assembly is installed on the underside of the right wing tip. The tip of the boom assembly is the Space Age Control Mini Boom, which collects pitot-static pressures from pressure transducers and flow angles from mechanical alpha and beta flow angle vanes. Data provided from the boom includes total pressure, static pressure, altitude, air speed, angle of attack, and angle of sideslip. For the purposes of the thesis, the measurements from the alpha vane is considered the truth source after calibration. The operating speeds and altitude of the Cessna 210 allows for incompressible airflow assumptions to be maintained for engineering analysis.

Full details on the SpaceAge Control Air Data System Boom are listed in Appendix C – Air Data System Boom Description.

## Calibration of Air Data System (ADS) Boom Flow Angle Vane

The Space Age Control air data system flow angle alpha vane required calibration. As previously discussed, upwash is present in flight due to the air mass being disturbed by the leading edge of the wing. The boom-tip is placed one chord length ahead of the leading edge, at the wing tip, in an attempt to acquire freestream data of the angle of attack and mitigate errors due to this disturbance [19].

## *Angle of Attack Reference Line*

Measurements of the angle of attack do not necessarily reveal the true angle of attack of the aircraft. Typically, the measured angle is a geometric angle of attack and a correction must be made to retrieve the true angle of attack, which is the angle between the aircraft zero lift line and the freestream velocity [20]. The purpose of this thesis attempts to determine the angle of attack through INS data then compared to flow angle data as seen by the alpha vane of the boom; attempts to determine true angle of attack of the aircraft are out of scope.

For the UTSI Cessna 210, all measurements are relative to a common reference line. A concerted attempt was made to align the reference line of the aircraft, the alpha vane, and the horizontal plane of the inertial navigation system. The longitudinal reference line of the aircraft is the deck level (or waterline) of the aircraft when placed on jacks, as designed by the manufacturer (two bolts on the aft fuselage, when lined up and leveled denote this line). The ADS boom was designed and mounted level with this line ( $0^\circ$  offset). The inertial navigation system was also placed on the DAS rack in a level position with the longitudinal aircraft reference line. However, for the actual mounting of the rack, a  $0.1^\circ$  noseup-offset was recorded. This angle was accounted for in the data reduction. Refer to Figure 12 and Figure 13 for measurements.

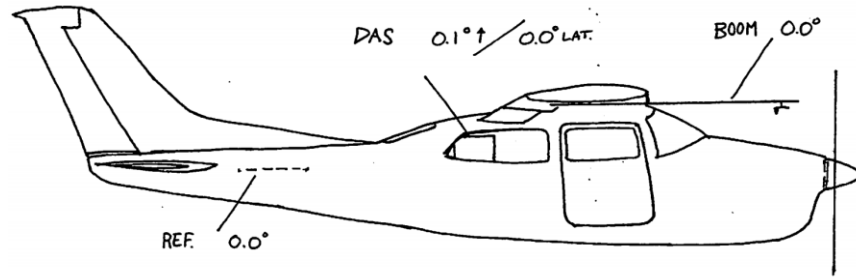


Figure 12: Angle of Attack Reference Line for Cessna 210, aligned with DAS rack and ADS Boom.



Figure 13: Aircraft water level reference line. The ADS Boom aligned with this reference line; the INS unit has a 0.1° offset from this reference line.

### Ground Calibrations

Ground calibrations are done for the alpha vane potentiometers. This effort identifies errors due to instrumentation readings and signals. A protractor device is used to calibrate the flow angle vanes (Figure 14). A calibration curve is generated between the values produced by the potentiometers on the DAS and the protractor angles, and the vane instrument correction is applied to readings through the DAS.



Figure 14: Angle of Attack Flow Angle Vane (Alpha Vane) Ground Calibration for Instrument Error Correction Determination

## Ellipse-N INS System

The inertial navigation system installed on the aircraft is an Ellipse-N miniature INS/GPS unit developed by SBG, inc. The microelectromechanical system is an inertial navigation system (INS) with integrated GPS navigation. The Ellipse-N provided full inertial data (angles, rates, and accelerations), GPS position, and inertial-derived North, East, Down velocities. The unit uses an Extended Kalman Filter (EKF) to fuse inertial data with GPS, GNSS, and odometer information to provide orientation and navigation data. This results in accuracies in pitch and roll on the order of  $<0.1$  degree, heading on the order of  $<0.8$  degree, and angular rate resolution of  $< 0.02$  degree/s.

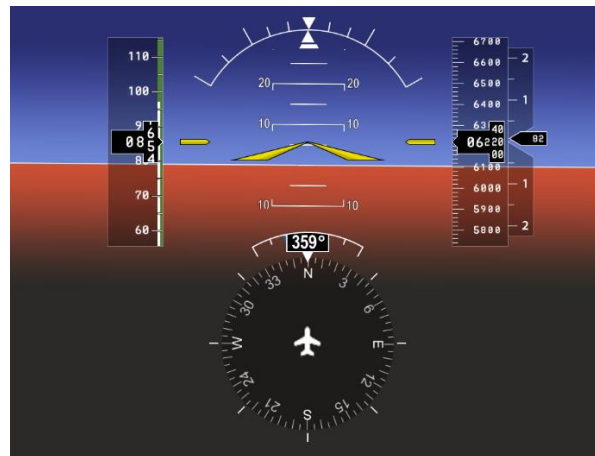


Figure 15: Ellipse-N INS EFIS User Interface

The Ellipse-N INS system was not fully integrated into the UTSI Cessna 210 Data Acquisition System; it was a standalone unit that was operated from a separate laptop. The data was timestamped with GPS-time, which was matched with the data from the DAS with the same GPS-time in post-flight. As

noted in the inertial coordinate reference system section, the origin point for all inertial data is an arbitrary point on the ground. The origin point for the Ellipse-N INS unit mounted in the Cessna 210 is the UTSI Aviation Systems Flight Research Hanger at the Tullahoma Regional Airport – GPS Coordinates 35.3801°N, 86.2479°W.

The Ellipse-N INS was mounted on the DAS rack in the Cessna 210, which is the location of the rear most seats, which was 101.0in aft of datum (Figure 16). It is removed from the CG of the aircraft, and thus a correction for the lever arms was required. Since the CG position changes in flight, the average of the CG position at the start of the flight and the estimated ending CG position are calculated from the standard Cessna 210 weight and balance. For both flights the starting CG was 42.18in aft of datum, and the estimated landing CG was 43.57in, thus the average CG was 42.88in. The resulting lever arm in the  $X_b$ -axis direction for the Ellipse-N was 58.12in aft of the CG location. Corrections for  $Y_b$  and  $Z_b$  axis were not made, and were left at zero in the Ellipse-N interface. Changes of weight in flight were not expected to severely affect measurements.



*Figure 16: Ellipse-N INS Installed in Cessna 210 DAS Rack in Rear Seat Station*

For the purposes of this thesis, the Ellipse-N is a commercial off-the-shelf inertial reference system which provides high accuracy, resolution, and bandwidth for reasonable cost. The full list of parameters, accuracies, and resolution outputs are listed in Appendix D – Ellipse-N Inertial Navigation System Unit.

# Chapter 4: Flight Test

---

## Philosophy/Methodology

The purpose of the flight test was to ensure proper operation of the post flight angle of attack algorithm using actual flight data. The goal was to utilize the measured angle of attack from the alpha vane and onboard aircraft instrumentation to correlate against the calculated angle of attack from INS data.

The flight test campaign consisted of two flight phases. The initial flight phase involved calibrating the Ellipse-N INS unit, calibrating the alpha vane, and determining the drag characteristics of the Cessna 210. The second phase involved gathering longitudinal data to validate the angle of attack algorithm.

### Flight Test Technique – Ellipse-N INS Calibration

For the first phase, because the Ellipse-N INS unit was a standalone INS unit, calibration was required. Following the procedures provided by the manufacturer, the test plan included flying figure 8's, high bank turns, high pitch ups and high pitch down maneuvers. The calibration was required for the INS unit to identify the hard and soft magnetic fields in the aircraft to allow for the magnetometers to compensate. This allowed for accurate heading data collection, which is required for the angle of attack algorithm. Following the calibration, to ensure accurate data and measurements, a GPS 4-leg technique was flown at a constant altitude and airspeed, at four headings for each leg.

### Flight Test Technique – Power Speed (P<sub>iw</sub>-V<sub>iw</sub>), Steady Level Trim Shots

As part of the angle of attack algorithm, the stability derivatives require input of the zero-lift drag coefficient ( $C_{D_0}$ ), which requires determining the drag polar of the aircraft. The method used for determining the drag polar of the aircraft was the power-speed (P<sub>iw</sub>-V<sub>iw</sub>) method [18]. The outcome captured the power required for level flight at various speeds and altitudes for a given aircraft configuration. This method implies constant propeller efficiency of the aircraft, assumed to be 85% ( $\eta_p = .85$ ). The aircraft was trim and stabilized in steady level flight at two separate altitudes, for three separate speeds. With the goal of capturing the parabolic drag polar, the speeds chosen were max allowable, one speed on the front side of the power require curve, and one speed on the back side of the power curve. Once trimmed and stabilized, airspeed, outside air temperature, altitude, RPM, manifold pressure, fuel quantity, and fuel burn was recorded.

The dual purpose of the steady level flight trim shots at various altitudes and speeds was the calibration of the alpha vane. The angle of attack measured by the alpha vane ( $\alpha_m$ ), and pitch angle ( $\theta$ )

measured by the INS unit, was collected during the steady flight condition. Utilizing equation 33, the climb angle term ( $\arcsin\left(\frac{dh}{dt}\right)$ ) is zero in steady level flight, thus leaving  $\alpha = \theta$ .

#### Flight Test Technique – Level Acceleration and Deceleration

The most efficient flight test technique for stable longitudinal flight with a full range of varying angle of attack was determined to be the level acceleration and deceleration maneuver. Throughout the level acceleration and deceleration maneuver, the aircraft maintained constant altitude and heading. The aircraft first stabilized and trimmed in a steady flight condition. To make the stabilization process less variable, an airspeed on the front side of the power required curve was chosen to minimize the input required from the pilot. Once stable, the pilot reduced the power to idle. This required the pilot to pull back on the yoke to pitch the aircraft up to a nose-high attitude, ultimately increasing the angle of attack. When the aircraft reached a predetermined indicated airspeed near the stall speed, the pilot input full power. The pilot is required to push the yoke forward to pitch the aircraft down continuously as power increases and the aircraft accelerates, which required a constant reduction in angle of attack throughout. Once the aircraft accelerated to the max indicated level airspeed, the pilot again reduced power, while pitching up and reducing airspeed until stall. The end of the level acceleration and deceleration maneuver was a recovery from the stall.

#### Flight Test Technique – Abrupt Pull up

The next logical step in the evaluation of the algorithm was to introduce abruptness and changes in load factor, while maintaining longitudinal maneuvers within the plane of symmetry. The purpose is to test the ability of the algorithm to determine the angle of attack in highly non-linear motion (changing load factor). The wings-level, abrupt pull up maneuver was attempted. The load factor in steady level flight is 1, thus the test limit are banded by a load factor difference from level flight of +/- 1.5. In the maneuver, the aircraft is trimmed at constant altitude, airspeed, and heading. The pilot then continually pulled up for a significant load factor greater than 1, aiming for a load factor of 2, before recovering. The pilot, ultimately, was responsible to not exceed the limits or damage the aircraft.

#### Flight Test Technique – Windup Turn

The final stage of the quantitative flight test evaluation of the angle of attack algorithm is the examination of out-of-plane-of-symmetry maneuvers. The motivation is to attempt to move the gravity vector from the longitudinal plane of the aircraft and evaluate the effects of load factor and banked flight. The windup turn was judged to be the best flight test technique to accomplish this dynamic flight condition. The pilot maintained constant airspeed with increasing bank angle and load factor by

sacrificing altitude. The aircraft was trimmed at constant airspeed and altitude. The pilot then climbs +500ft, without changing power settings, so as to start at the top of the prescribed altitude band. The aircraft was banked while maintaining constant airspeed, and then stabilized at 60° bank, resulting in a load factor of 2, before recovering to level flight.

## Flight Conditions

The first flight was on March 3, 2017. The flight included the Ellipse-N INS calibration, a GPS 4-Leg technique, and a level acceleration and deceleration. The flights took place in the immediate area of Tullahoma Regional airport (KTHA) in the UTSI Cessna 210 aircraft. The forecasted winds aloft at the closest class C airport (KHSV) were 360@28 at 3000ft and 330@29 at 6000ft. Takeoff time was 1442 Zulu with 86.3 gal of fuel, with a gross weight of 3635.6 lbs and a CG position of 42.82 in aft of the datum (firewall). Two flight test engineers and one test pilot were on board; all had attended the briefings and were familiar with the flight plan.

Upon reaching the test altitude of 5000ft, pressure altitude, slight chop and turbulence was detected, thus the decision was made to climb to 6000ft, where the air was more stable. The calibration procedure was flown, and after two attempts and adjustments for greater magnitude bank and pitch angles, the Ellipse-N was satisfactorily calibrated. An airspeed of 110KIAS was chosen for the GPS 4-Leg trim shots, as it would be on the front side of the power required curve and was a middle airspeed between stall and max airspeed for the Cessna 210. Cardinal headings (360°-270°-180°-90°) were flown at a constant airspeed of 110KIAS at 6000ft pressure altitude to check that the Ellipse-N INS parameters matched and were functioning. Once its functionality was verified, the level acceleration and deceleration maneuver was flown at 6000ft from 110KIAS trim airspeed. The UTSI Cessna 210 is limited to 168KIAS by the air data boom, thus the max airspeed attained, by pilot discretion, was 160KIAS. After completion, the mission concluded by returning to base, landing time of 1545 Zulu and 68.4 gal of fuel remaining.

The second flight was on March 9, 2017. The flight included the power-speed (P<sub>w</sub>-V<sub>w</sub>) method for drag determination and alpha vane calibration, the abrupt pitching maneuvers, and the windup turn. The flights took place in the immediate area of Tullahoma Regional airport (KTHA) in the UTSI Cessna 210 aircraft. The forecasted winds aloft at the closest class C airport (KHSV) were 290@22 at 6000ft and 270@21 at 9000ft. Takeoff time was 1451 Zulu with 65.7 gal of fuel, with a gross weight of 3503.6 lbs and a CG position of 42.18 in aft of the datum (firewall). Two flight test engineers and one test pilot were on board; all had attended the briefings and were familiar with the flight plan.

Again, upon reaching the test altitude of 5000ft, pressure altitude, slight chop and turbulence was detected, thus the decision was made to climb to 6000ft, where the air was more stable. The three airspeeds chosen for the method were 160, 110, and 70KIAS, which would adequately capture the parabolic power required curve and resulting drag polar. The second altitude flown was 10000ft. Upon completing the 10000ft trim shots, the aircraft descended back to 6000ft to attempt the pull up maneuver. Loose items within the aircraft were secured as the aircraft was trimmed at 6000ft at 110KIAS. Limits on the test were 3000ft MSL, 150KIAS and -0.5 load factor for pitch down, and 70KIAS and +2.5 load factor for pitch up. Once on condition, the pilot counted down from 3, then proceeded to continually pitch the aircraft up by pulling the yoke back, with a limit of 70KIAS, and then recovering to the trim conditions.

Following the pitching maneuvers, the Cessna 210 was retrimmed for the windup turns. The air data boom on the Cessna 210 is located on the right wing, thus windup turns were completed to both the left and right to allow for comparisons of angle of attack. The maneuver is accomplished within a 1000ft altitude band (+/-500ft) and load factor limits of +2.5/-0.5, with a load factor tolerance of +/- 0.3. The +/- 0.3 load factor tolerance allowed the pilot to stabilize at 55°.

For the Cessna 210, a g-meter was not installed on the onboard instrumentation, thus the maneuver was completed twice with feedback in between from the flight test engineers of the load factor shown by the INS unit. After completion, the mission concluded by returning to base, with a landing time of 1545 Zulu and 68.4 gal of fuel remaining.

Day-of-flight flight test cards are included in Appendix H – Flight Test Cards.

# Chapter 5: Data Reduction and Results

## Flow Angle Alpha Vane Calibration

The data taken for the calibration of the ADS boom angle of attack flow angle vane (alpha vane) is shown in Table 3. Pitch angle ( $\theta$ ) and measured angle of attack from the alpha vane ( $\alpha_m$ ) was taken at each steady level trim shot. The uncertainty for the pitch angle measurement is the accuracy value from the manufacturer of the Ellipse-N. The uncertainty for the measured angle of attack from the alpha vane is the standard deviation taken from the duration of the trim shot. This includes data at 10000ft, with indicated airspeeds of 160, 110, and 70KIAS, and data at 6000ft, with indicated airspeeds of 160, 110, and 70KIAS. This data is shown in Table 3. In Figure 17, the pitch angle is plotted on the Y-axis and the measured angle of attack is on the X-axis. The orange line is the ideal relationship, in which  $\alpha = \theta$ . The horizontal difference, depicted in green, from the orange line to the blue calibration curve is the upwash angle ( $\varepsilon$ ).

Table 3: Angle of Attack and Pitch Angle Data acquired in Flight Tests

Airspeed (KIAS)	Altitude (ft)	Pitch Angle $\theta$ (degree)	Pitch Angle Uncertainty	Measure AOA $\alpha_m$ (degree)	Measure AOA Uncertainty
70	6000	12.5	+/-0.1	16.81	+/-0.28
110	6000	4.9	+/-0.1	7.00	+/-0.29
160	6000	1.7	+/-0.1	3.02	+/-0.28
70	10000	12.8	+/-0.1	16.61	+/-0.28
110	10000	4.5	+/-0.1	7.12	+/-0.25
160	10000	1.8	+/-0.1	3.21	+/-0.28

As expected in Figure 17, the high speeds resulted in lower angle of attack and lower speeds resulted in higher angles of attack (refer to Figure 7). At the two altitudes, it appears that the angles of attack at the three different speeds are very nearly the same. It is also interesting to note that at slower airspeeds, there is a larger difference between the pitch angle and the measured angle of attack. This suggests that at slower speeds, the upwash at the alpha vane location is more significant than at high speeds. At 70KIAS, the difference in angle of attack and pitch angle averages to 4.05 degrees at both altitudes, while at 160KIAS, the difference averages to 1.35degrees.

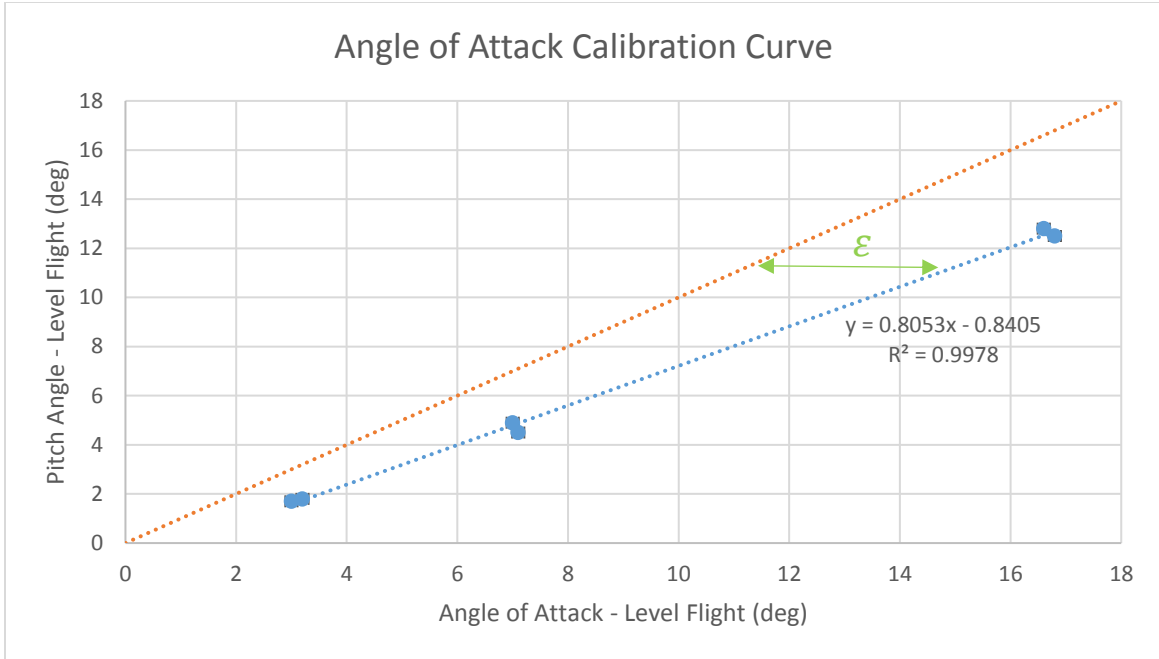


Figure 17: Angle of Attack (Alpha Vane) Calibration Curve

The established relationship is linear, defined by the upwash angle:

$$\varepsilon = \frac{2C_L}{\pi\mathcal{A}} = \frac{2C_{L\alpha}}{\pi\mathcal{A}}\alpha \quad (39)$$

In the linear regime of the relationship between the coefficient of lift and angle of attack (see example in Figure 28), the lift-curve slope ( $C_{L\alpha}$ ) is constant until the max lift coefficient, which yields the highest attainable angle of attack. Per equation 39, the upwash angle relates to the angle of attack linearly (i.e.  $\frac{2C_{L\alpha}}{\pi\mathcal{A}}$  is constant). The resulting calibration curve is utilized by taking the measured angle of attack from the alpha vane ( $\alpha_m$ ) as the x variable in order to determine a calibrated alpha vane ( $\alpha_{c,m}$ ) angle of attack. The calibration curve holds for the respective altitude and airspeeds. The maneuvers attempted for this thesis have angles of attack that fall within this range, and at the same altitudes and airspeeds. Only stall angles of attack are not obtained, as it would not be feasible to adequately trim the aircraft at the stall airspeed.

## Trim Shot

Figure 18 shows the result of the algorithm during a trim airspeed of 110KIAS at 6000ft. The data is presented as three angle of attack time-histories. The first is the calculated angle of attack (blue) from the algorithm. The second is the calibrated alpha vane (green). The third is the raw data from the alpha vane (red). Accompanying the angle of attack traces are load factor, altitude, and airspeed data for the duration of the maneuver. The magnitude of the changes in indicated airspeed and load factor is relatively miniscule, as indicated by the y-axis scale. The x-axis is time, in seconds; the negative time is due to establishing a time equal zero at some point prior to the next maneuver (the level acceleration and deceleration). This trim shot is taken prior to that zero point; the scale of time is still valid in that this trim shot took 3.94 seconds  $((-282.1)-(-286.04)=3.94$  seconds).

The calibrated alpha vane ( $\alpha_{c,m}$ ) differs from the raw data by 2.381degrees during the trim shot. There is noise within the alpha vane data: the mean for the calibrated alpha vane is 4.758degrees, with a standard deviation of 0.282degrees. The mean for the calculated angle of attack is 4.726degrees, with a standard deviation of 0.1degrees. The calculate angle of attack ( $\alpha_{calc}$ ) tracks well with the calibrated angle of attack throughout the trim shot, as expected. Minor perturbations always exist from trim, and the algorithm picks up those perturbations. Thus there are slight deviations in the calculated angle of attack ( $\alpha_{calc}$ ), but not significant. The indicated airspeed tracks around 105ft/s, and does not deviate more than 1 ft/s for the duration of the trim shot. The indicated altitude tracks around 5940 ft, and does not deviate more than 5ft. The load factor tracks around 1, with sporadic deviations less than 0.05, which is typical for inflight measurements due to the engine and the typical nature of flight. Overall, this trim shot allows the algorithm to track with the calibrated, measured alpha vane throughout.

Alpha Vane and Angle of Attack vs. Time - Trim Shot

Aircraft: Cessna 210 N33UT  
 Altitude: 6000 ft  
 Configuration: Clean: Flaps Up, Gear Up, Cowl Flaps Closed

Weight: 3532.4 lbf  
 CG: 42.88 in

Date: March 2, 2017  
 Airspeed: 110 KIAS (Trim)  
 Manuever: Trim Shot

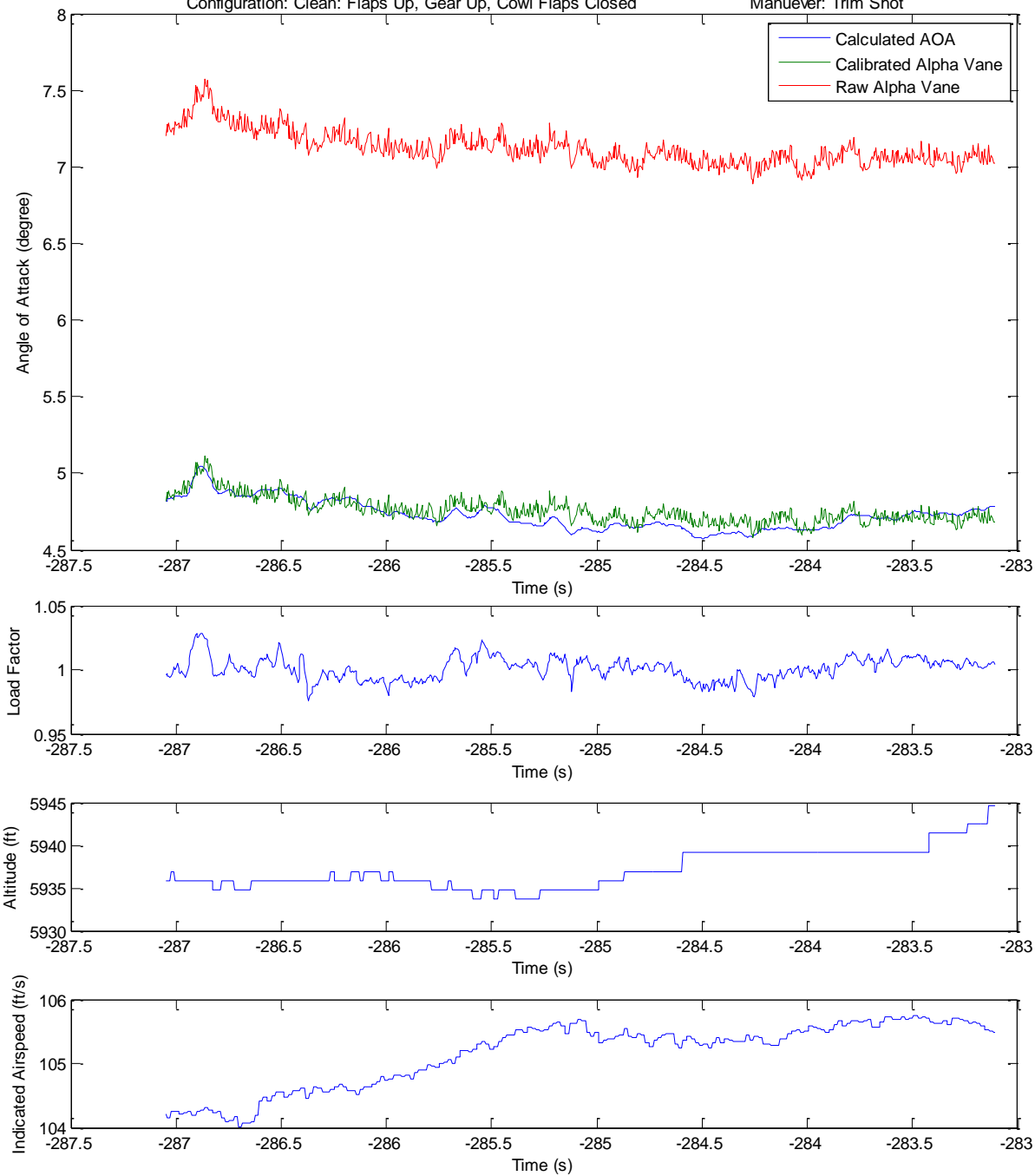


Figure 18: Angle of Attack vs. Time for Steady Level Trim Shot

## Level Acceleration and Deceleration

The results of the level acceleration and deceleration flight test are depicted in Figure 19. The maneuver started from a steady level trim airspeed of 110KIAS at 6000ft. The acceleration was from 70 to 150KIAS while maintaining the altitude at 6000ft. The data are presented as three angle of attack time-histories. The first is the calculated angle of attack (blue) from the algorithm. The second is the calibrated alpha vane (green). The third is the raw data from the alpha vane (red). Accompanying the angle of attack traces are load factor, altitude, and airspeed data for the duration of the maneuver. In Appendix F – Supporting Plots, individual data inputs utilized by the algorithm are provided and will be referred to in this discussion. Figure 32 and Figure 33 show the data inputs for the algorithm from the INS unit. Results are discussed moving from left to right in time.

At the beginning of the maneuver, the calibrated alpha vane and the calculated angle of attack produces roughly the same angle of attack ( $\alpha_{c,m} = \alpha_{calc} = 4.56 \text{ degrees}$ ). As the maneuver progresses (the pilot pulls the throttle back) there is an initial decrease in the calculated angle of attack. Examining equation 4, this can occur in two ways: vertical velocity ( $w$ ) gets smaller or forward velocity ( $u$ ) get larger. The pilot pulls the throttle to idle and thrust is no longer generated, so the forward velocity cannot increase unless altitude is lost. Examining the altitude and velocity plots, it can be seen that there is no initial speed loss, but a very slight altitude increase, which also explains why the vertical velocity ( $w$ ) gets smaller. However, the calibrated alpha vane soon after begins to increase while the calculated angle of attack continues to decrease.

The calculated angle of attack deviates from the alpha vane measurement because the effect of the downward velocity ( $w$ ) component (refer to Figure 33) dominates equation 4. The perturbed value deviates from the trim value faster than the other data inputs (from 23.20ft/s to 14.43ft/s), and thus the resulting calculated angle of attack continued to decrease. The forward velocity component continues to decrease at a more constant rate until it reaches a minimum of 72.27ft/s, at which point the pilot puts in full power. At the beginning of the deceleration, the calculated angle of attack is 3.138 degrees, while the calibrated alpha vane reads 4.607 degrees. The effect of the pitch angle, forward velocity steadily decreasing, and the downward velocity being steady contributes to the increase in calculated angle of attack. The discrepancy between the calculated angle of attack and the calibrated alpha vane is a serious limitation of the algorithm; the angle of attack is nearly identical in trim, but the algorithm under-predicts the actual angle of attack during deceleration.

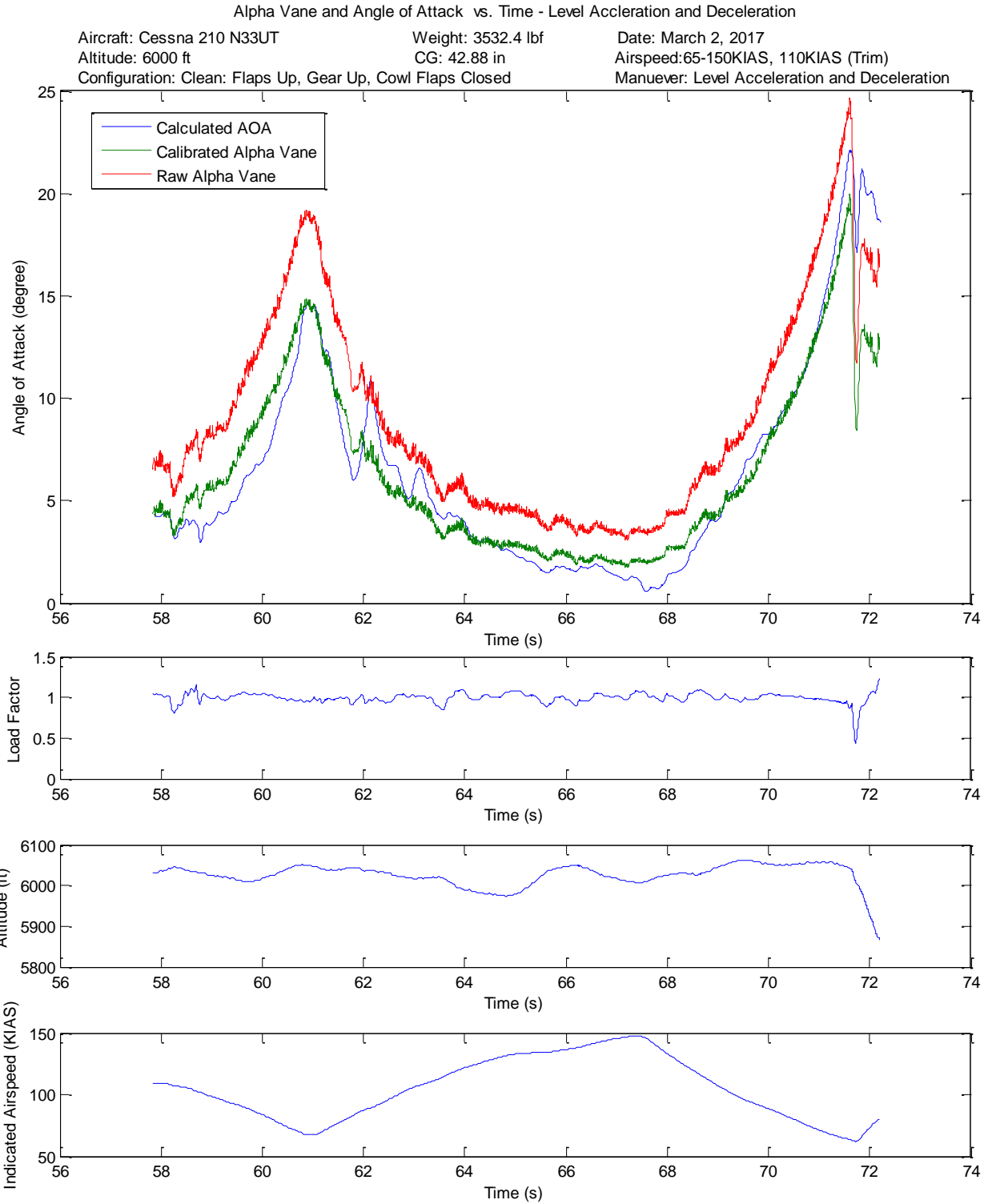


Figure 19: Angle of Attack vs. Time for Level Acceleration and Deceleration

The change in angle of attack during the first deceleration is 2.4 degree/second for the calculated and is 3.5 degree/second for the calibrated vane (refer to Figure 35, Figure 36). The peak of both calculated angle of attack and calibrated alpha vane is 14.85 degrees, within the uncertainty at trim of both the calculated angle of attack (+/- 0.1degree) and the calibrated alpha vane (+/- 0.28 degree).

The acceleration phase (when the pilot puts in full throttle, and puts the nose down) was a highly dynamic maneuver. The calibrated alpha vane gradually decreases in angle of attack, from a peak of 14.85 degrees to a steady 1.89 degrees at max indicated airspeed. The calculated angle of attack, however, is more chaotic. The initial acceleration causes the angle of attack to decrease quickly, but at 61.82seconds, the calculated angle of attack quickly reverses and reaches a max value of 11.13 degrees. This aberration can be explained by the inertial-to-body transformation (equation 2). The transformation requires input from INS angles and velocities; examining Figure 32, the yaw angle oscillates at this time. The dynamic maneuver required full throttle from the idle power setting, which induced a large P-factor on the propeller, causing the aircraft to yaw to the left. The pilot fought this motion to bring the aircraft heading back in line, thus the dual peaks at 61.82 seconds and 62.14 seconds. The aberration can be seen in the calibrated alpha vane as well; at 61.79 seconds, the angle of attack slightly increases before continuing to reduce as the aircraft accelerates.

As the aircraft accelerates toward max speed, the calibrated alpha vane and the calculated angle of attack converge, as desired. Slight variations occur, and at 64.67 seconds, the calculated angle of attack switches from estimating a larger angle of attack to estimating a smaller angle of attack. This occurs because the increase in forward airspeed ( $u$ ) becomes more shallow at that time, while the downward airspeed ( $w$ ) continues a gradual decrease (Figure 33).

At 67.22 seconds, the pilot pulls the throttle back. The forward airspeed peaks, and as seen in the first deceleration, the downward airspeed drops. This, again as in the first deceleration, causes the algorithm to underestimate the calculated angle of attack between 67.31 seconds and 68.82 seconds. However, unlike the first deceleration, between 69.19 seconds and 70.10 seconds, the algorithm overestimates the calculated angle of attack. The difference is approximately 1degree during that time period. Continuing the deceleration, the calculated angle of attack and calibrated alpha vane match closely, until the calculated angle of attack overestimates the calibrated alpha vane starting at 71.05 seconds. This deviation grows wider between the two angles. At the point of stall at 71.61 seconds, the calculated angle of attack is 22.32 degrees while the calibrated alpha vane is 19.96 degree, a difference of 2.36 degrees.

It is far worse for the calculated angle of attack to under predict the actual angle of attack, as in the first deceleration. If used as a stall indicator in the future, when under prediction occurs, the aircraft can stall before any indication is provided. Over prediction, however, is also not desirable if auto-pilots are involved. As discussed, military aircraft autopilots have been documented to react adversely to incorrect angle of attack measurement. If an over-predicted angle of attack is provided to a stall inhibitor, the aircraft will pitch down undesirably.

The recovery from the stall is another highly dynamic maneuver, where small perturbation theory cannot accurately or adequately determine the angle of attack. The drop in angle of attack from the calibrated alpha vane is from 19.96 degrees at stall to 8.394 degrees; while the calculated angle of attack calculates a maximum of 22.31 degrees at stall and only drops to 17.36 degrees at the bottom of the recovery. Every input parameter ( $u, w, q, \theta$ ) changes from the steady trim reference condition rapidly, as indicated by the reduction in load factor.

Throughout the whole maneuver, the effect of pitch rate and downward acceleration on the equation contributed more to noise, rather than any significant determination of the angle of attack; pitch rate and downward acceleration was removed from the calculation of results. See Figure 31, included in Appendix F – Supporting Plots for full results.

Due to the additive nature of integration, there is a time lag in between each individual data point. Since each data point is taken at 20Hz, which is one sample every 0.05seconds, the data is shifted by 0.25seconds, and is most apparent in the peaks. For the purpose of this thesis, it does not affect the analysis, but for real-time-in-flight implementation, an implementation of an Extended Kalman Filter would be recommended. The EKF would estimate a solution for the angle of attack utilizing the state-history of the system (airspeed, altitude, attitude, Euler angles, et al), the current state of the system, to calculate a perturbed-future angle of attack from the current state. New measurements are then taken, and the system is recursively refined to attempt to predict the state of the system, and a more accurate angle of attack can be attained.

Overall, the calculated angle of attack tracks with the calibrated alpha vane in the level acceleration and deceleration maneuver from the trim condition. Of concern is the effects of lateral motion during the acceleration portion. Lateral motion does affect the downward component of velocity, as seen in the data, and this would need to be explored. Also, both the under and over prediction of the angle of attack during the deceleration portions are suspect, as it does not appear to be consistent for the same type of maneuver.

## Pull Up Maneuver

The results of the pull up flight test are depicted in Figure 20. The maneuver started from a steady level trim airspeed of 110KIAS at 6000ft. The data are presented as three angle of attack time-histories. The first is the calculated angle of attack (blue) from the algorithm. The second is the calibrated alpha vane (green). The third is the raw data from the alpha vane (red). Accompanying the angle of attack traces are load factor, altitude, and airspeed data for the duration of the maneuver. In Appendix F – Supporting Plots, individual data inputs utilized by the algorithm are provided. Figure 37 and Figure 38 show the data inputs for the algorithm from the INS unit.

At the steady level flight trim condition, the calculated angle of attack and calibrated alpha vane track together very closely. Prior to the maneuver, there is a nominal offset of 0.262degrees which is caused by small variation in data and typical flight conditions. At 73.53seconds, the pilot abruptly pulled on the yoke to reach a load factor of 2, and then returned to trim. The entire maneuver lasted 0.44seconds. Load factor is not an input into the algorithm, but the result of changing load factor from a level steady trim condition is large changes in airspeed components, as demonstrated in Figure 38. The calculated angle of attack tracks very closely to the calibrated alpha vane for the entire maneuver. At the peak, the calibrated alpha vane was 11.45degrees and the calculated angle of attack was 10.92degrees; a difference of 0.53degrees. If the original offset of 0.262 degrees is considered, the peak difference is 0.27degrees.

Overall, the algorithm appears to work for longitudinal maneuvers with changes in load factor, which bodes well for predicting accelerated stalls. However, because the algorithm again under predicts the measured angle of attack, it can cause problems. More accurate modeling of the effect of change in pitch angle on the downward force ( $Z_q$ ) may yield a more representative peak reading of angle of attack. This assumption is made by examining the pitch angle data in Figure 38, and seeing the more pronounced peak.

Alpha Vane and Angle of Attack vs. Time - Pull Up Maneuver

Aircraft: Cessna 210 N33UT

Weight: 3361.4 lbf

Date: March 9, 2017

Altitude: 6000 ft

CG: 42.88 in

Airspeed: 110 KIAS (Trim)

Configuration: Clean: Flaps Up, Gear Up, Cowl Flaps Closed

Maneuver: Abrupt 2G Pull Up

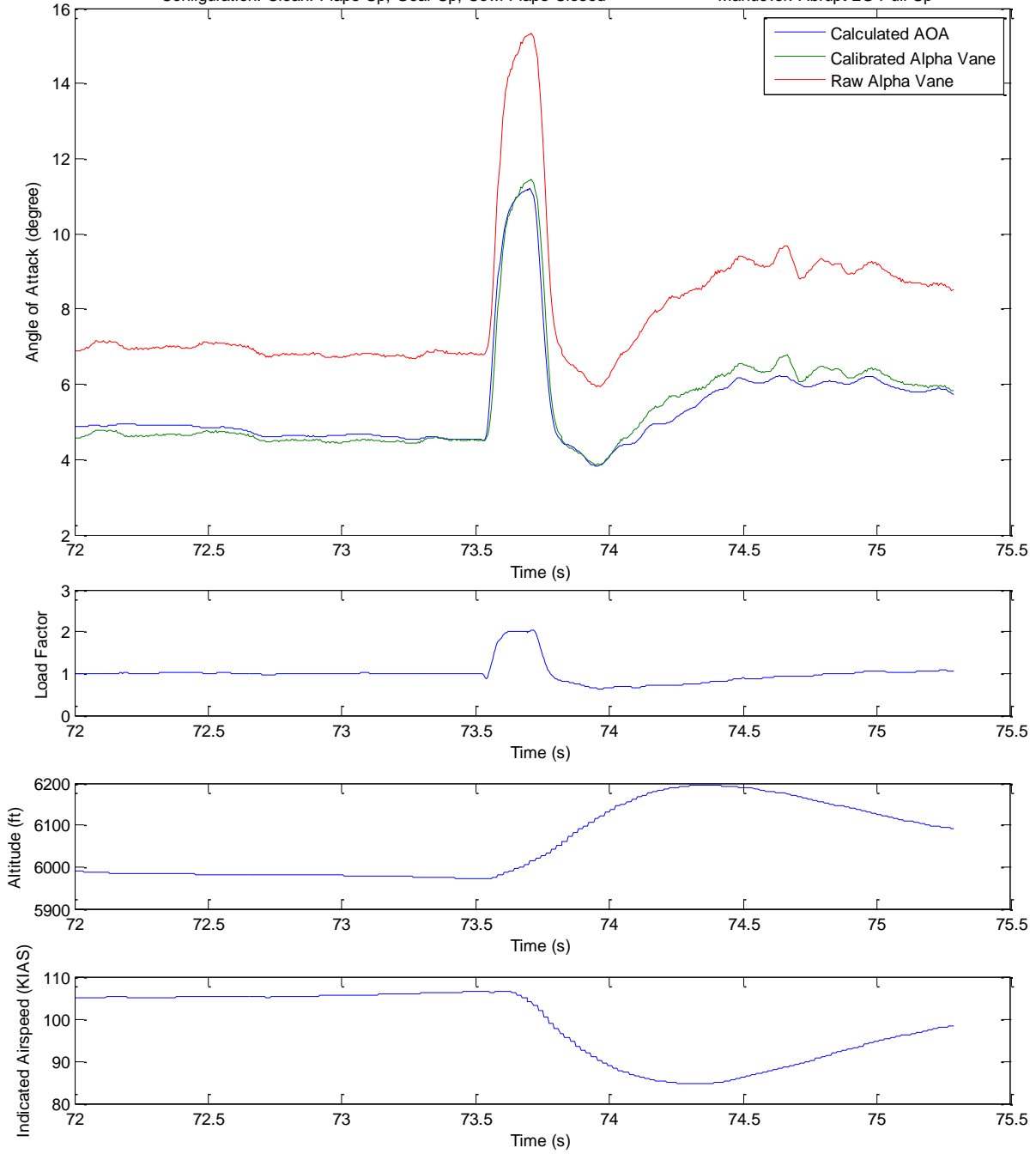


Figure 20: Angle of Attack vs. Time for 2G Pull up Maneuver

## Chapter 6: Conclusions and Recommendations

---

Upon reviewing the objectives of this thesis, the feasibility of utilizing only INS measurements to determine angle of attack is achievable.

To verify if the algorithm reproduces the angle of attack accurately, the alpha vane was used as the truth source. To reduce uncertainty in the measurements of angle of attack, calibrations were completed. The alpha vane and the INS unit are mounted relative to the Cessna 210 water level line, which acts as the reference line for establishing the angle of attack of the aircraft. Ground calibrations allowed for the instrumentation errors to be accounted for in the data analysis. In-flight calibration procedures, using steady level trim shots, allowed for the position error of the vane to be determined. The result was a non-linear calibration curve that is utilized to correct the alpha vane measurements.

Sole reliance on the INS unit for angle of attack determination cannot provide all state measurements of the aircraft. Control surface deflections and thrust settings must be neglected from the equations of motion, which is the basis of the angle of attack algorithm. The algorithm itself is condensed to determining the forward and downward accelerations of the aircraft from a trim condition. The forward and downward velocity components can then be determined from those accelerations through integration. The angle of attack is the ratio of those two velocity components.

The main test for the algorithm was putting it through the full range of typical angles seen by the aircraft, and the level acceleration and deceleration technique best accomplished this. The calculated angle of attack tracked with the angle of attack from the calibrated alpha vane throughout the entire maneuver, deviating +10.6% at stall (22.09 degrees calculated vs. 19.96 degrees measured). However, points of concern include: 1) the susceptibility of the algorithm to lateral motion 2) the inconsistency of prediction of the angle of attack during deceleration, and 3) bias errors when the initial condition is inaccurate. This would need to be a point of further investigation. In situations where there are changes in load factor and in pure pitching motion, the algorithm performed very well in determining angle of attack, predicting the measured angle of attack to within 2.1% (11.20 degrees calculated vs. 11.45 degrees measured).

A limiting factor in utilizing the linearized aircraft equations of motion is the need for a trim condition from which there can be a perturbation. Real-time parameter estimation of stability derivatives and coefficients is an area of continuing research for flight dynamics and could eliminate the requirement for known trimmed conditions. The first recommendation for future work would be to

utilize real-time parameter estimation to eliminate the requirement for known trim conditions to be able to determine angle of attack real-time.

To address the small-scale measurement errors from the INS sensors, it is recommended that modeling be completed in the frequency domain. Outlier data in the frequency domain can be removed so as to not contribute to noise, such as with the pitch rate [21]. To address susceptibility of the algorithm to lateral motion and potential time lag due to the additive effects of integration, an Extended Kalman Filter can be used to predict the angle of attack without lag, as well as weight and account for changes due to lateral motion. Repeating the level acceleration and deceleration maneuver to attempt to minimize the effects of the lateral motions would help with validating the algorithm for pure longitudinal motion. Out-of-plane-of-symmetry research should also be investigated further.

The post-flight algorithm is useful for engineers, but not for pilots. A second recommendation would be to work on refining and utilizing the algorithm for an in-flight indicator and warning system. Currently, COTS INS systems with similar capabilities to the Ellipse-N INS cost between \$1000-4500 USD (2017). Developing an accurate, real-time, low-cost system that can be easily integrated onto an aircraft and a user interface application for handheld tablets or smartphones with an EFIS is reasonable for general aviation usage.

In conclusion, the need to understand flow angles, either post flight or real-time, in an accurate and cost-effective manner is highly desired. Research on angle of attack is a challenging, nuanced field with lots of opportunity for further advancement. With computational power continually getting faster and cheaper, the ability to utilize the latest technologies for both research and safety applications of angle of attack determination is widely accessible. While the benefits of knowing angle of attack in real time is apparent, due to stall consideration for pilots, a wide open arena of research for angle of sideslip is also a necessity. The development of more advanced control laws and autopilots require the very accurate measurement of both angle of attack and angle of sideslip. Future research is readily available for angle of attack and angle of sideslip determination.

## References

---

- [1] B. E. Jackson, K. D. Hoffler, D. G. Sizoo and W. Ryan, "Experience with Sense and Derived Angle-of-Attack Estimation Systems on a General Aviation Airplane," in *AIAA SciTech*, Grapevine, TX, 2017.
- [2] T. Thacker, "Use of State Estimation to Calculate Angle of Attack Position Error from Flight Test Data," Air Force Institute of Technology, Wright-Patterson Air Force Base, Ohio, 1985.
- [3] J. J. Lamb, "The Influence of Geometry Parameters Upon Lag Error in Airborne Pressure Measuring Systems," Air Research and Development Command, Wright-Patterson Air Force Base, Ohio, 1957.
- [4] J. E. J. Zeis, "Angle of Attack and sideslip Estimation using an Inertial Reference Platform," Air Force Institute of Technology, Wright-Patterson Air Force Base, Ohio, 1988.
- [5] J. Lawford and K. Nippres, "Calibration of Air-Data Systems and Flow Direction Sensors," North Atlantic Treaty Organization, Loughton, Essex, UK, 1984.
- [6] G. L. Beeker, R. L. Bennet and J. M. Payne, "Equations of Motion I & II," in *Performance Flight Testing*, Edwards Air Force Base, CA, USAF Test Pilot School, 1993, pp. 13.1-13.26.
- [7] R. C. Nelson, *Flight Stability and Automatic Control*, Michigan: McGraw Hill, 1998.
- [8] M.-M. Siu, B. Martos and J. V. and Foster, "Flight Test Results of an Angle of Attack and Angle of Sideslip Calibration Method Using Output-Error Optimization," AIAA Atmospheric Flight Mechanics Conference, Tullahoma, TN, 2013.
- [9] E. A. J. Haering, "Airdata calibration of a high-performance aircraft for measuring atmospheric wind profiles," NASA Technical Reports Server, Edwards Air Force Base, CA, 1990.
- [10] W. Gracey, "Summary of Methods of Measuring Angle of Attack on Aircraft," National Advisory Committee for Aeronautics (NACA), Langley Field, VA, 1958.
- [11] J. E. Cashman, B. D. Kelly, B. N. Nield and J. Langer, "What is Angle of Attack?," Boeing Aero Magazine Issue 12, Seattle, WA, 2000.
- [12] J. Scott, "Angle of Attack and Pitch Angle," aerospaceweb, 29 February 2004. [Online]. Available: <http://www.aerospaceweb.org/question/aerodynamics/q0165.shtml>. [Accessed 23 February 2017].
- [13] M. Heller, S. Myschik, F. Holzapfel and G. Sachs, "Low-Cost Approach Based on Navigation Data for Determining Angles of Attack and Sideslip for Small Aircraft," in *AIAA Guidance, Navigation, and Control*, Austin, TX, 2003.
- [14] aerostudents.com, "Flight Dynamics," TU Delft, 1 September 2006. [Online]. Available: <http://www.aerostudents.com/thirdyear/flightDynamics.php>. [Accessed 31 January 2017].
- [15] J. Roskam, *Method for Estimating Stability and Control Derivatives of Conventional Subsonic Airplanes*, Lawrence, KS: University of Kansas, 1973, pp. 121-122.

- [16] I. Kroo, *Compressibility Drag: Introduction*, Stanford, CA: Standord University: Department of Aero/Astro, 2017.
- [17] H. Babinsky, "Flow Over Aerofoils," Cambridge University Department of Engineering, Cambridge, UK, 2003.
- [18] R. D. Kimberlin, *Flight Testing of Fixed-Wing Aircraft*, Reston, VA: AIAA Education Series, 2003.
- [19] K. N. Oegema, "Design, Testing, and Calibration of a Custom Air Data Boom to Obtain Flight Data for the UTSI Cessna-T210J (N33UT)," University of Tennessee, Knoxville, TN, 2015.
- [20] D. F. Rogers, "Absolute Angle of Attack," NAR-Associates, 2013.
- [21] E. A. Morelli, "Real-Time Aerodynamic Parameter Estimation without Air Flow Angle Measurements," AIAA, Hampton, VA, 2012.
- [22] D. Andrisani, "Stability and Control Derivatives, AAE421 MATLAB Code to Compute," Purdue University, West Lafayette, IN, 2001.
- [23] airfoiltools.com, "NACA64a21 Airfoil Polars," airfoiltools.com, 2017. [Online]. Available: <http://airfoiltools.com/airfoil/details?airfoil=naca64a210-il#polars>. [Accessed 15 March 2017].

# Appendices

---

## Appendix A – Computer Program

```

%DATA INPUTS FILE
filename = 'DAS+ELLIPSE.xlsx';

time = xlsread(filename,'A:A');
q_bar = xlsread(filename,'C:C');
V_i = xlsread(filename,'D:D');
p_s = xlsread(filename,'E:E');
h = xlsread(filename,'F:F');
a_x_nav = xlsread(filename,'M:M');
a_y_nav = xlsread(filename,'N:N');
a_z_nav = xlsread(filename,'O:O');
N_v_nav = xlsread(filename,'P:P');
E_v_nav = xlsread(filename,'Q:Q');
D_v_nav = xlsread(filename,'R:R');
GPS_alt_nav = xlsread(filename,'V:V');
GPS_lat_nav = xlsread(filename,'W:W');
GPS_long_nav = xlsread(filename,'X:X');
GPS_track = xlsread(filename,'Y:Y');
GPS_gs = xlsread(filename,'Z:Z');
alpha_vanes = xlsread(filename,'AY:AY');
beta_vanes = xlsread(filename,'AZ:AZ');
fuel = xlsread(filename,'BC:BC');
Counter = xlsread(filename,'BD:BD');
S_wing = xlsread(filename,'BE:BE');
OAT = xlsread(filename,'BF:BF');
RPM = xlsread(filename,'BG:BG');
MAP = xlsread(filename,'BH:BH');
Wref = xlsread(filename,'BI:BI');
Wstart = xlsread(filename,'BJ:BJ');
W = xlsread(filename,'BK:BK');
Theta_temp = xlsread(filename,'BL:BL');
Delta_pres = xlsread(filename,'BM:BM');
Sigma_density = xlsread(filename,'BN:BN');
V_iw = xlsread(filename,'BO:BO');
Del_V_pcw = xlsread(filename,'BP:BP');
Correction
Del_V_pc = xlsread(filename,'BQ:BQ');
V_c = xlsread(filename,'BR:BR');
V_true_aero = xlsread(filename,'BT:BT');
GPS_time_e = xlsread(filename,'CG:CG');
roll = xlsread(filename,'CG:CG');
pitch = xlsread(filename,'BX:BX');
yaw = xlsread(filename,'BY:BY');
N_ellipse = xlsread(filename,'BZ:BZ');
E_ellipse = xlsread(filename,'CA:CA');
D_ellipse = xlsread(filename,'CB:CB');
X_v_ellipse = xlsread(filename,'CC:CC');
Y_v_ellipse = xlsread(filename,'CD:CD');
Z_v_ellipse = xlsread(filename,'CE:CE');
GPS_lat_ell = xlsread(filename,'CF:CF');
GPS_long_ell = xlsread(filename,'CG:CG');
Az = xlsread(filename,'CJ:CJ');
rollrate = xlsread(filename,'CM:CM');
pitchrate = xlsread(filename,'CN:CN');
yawrate = xlsread(filename,'CO:CO');

%Time
%Dynamic pressure
%Indicated airspeed
%Static pressure
%Altitude
%Longitudinal Accel
%Lateral Accel
%Normal Accel
%North Velocity
%East Velocity
%Down Velocity
%GPS Altitude
%GPS Latitude
%GPS Longitude
%GPS Track
%GPS groundspeed
%AOA vane - wingtip boom
%AOS vane - wingtip boom
%Fuel
%Manuever Counter
%Wing Reference Area
%Outside Air Temperature
%RPM
%Manifold Pressure
%Reference Weight = 3800lbs
%Weight Start = 3637.6lbs
%Weight - Test
%Temperature Ratio
%Pressure Ratio
%Density Ratio
%Weight Corrected, Indicated Airspeed
%Weight Corrected Velocity Position Error
%Velocity Position Error Correction
%Corrected Airspeed
%True Airspeed, Aerodynamically calculated
%GPS Time - Ellipse
%Roll - Ellipse
%Pitch - Ellipse
%Yaw -Ellipse
%North Velocity - Ellipse
%East Velocity - Ellipse
%Down Velocity - Ellipse
%X Velocity - Ellipse
%Y Velocity - Ellipse
%Z Velocity - Ellipse
%GPS Latitude
%GPS Longitude
%Accelerometer Z
%Gyroscope X - Ellipse
%Gyroscope Y - Ellipse
%Gyroscope Z - Ellipse

mainData = repmat(emptyChunk,max(Counter)+1,1);
for m=0:max(Counter)
    mainData(m+1).event=m;
    while Counter(row)==m
        mainData(m+1).time = [mainData(m+1).time; time(row)];
        mainData(m+1).q_bar = [mainData(m+1).q_bar; q_bar(row)];
        mainData(m+1).V_i = [mainData(m+1).V_i; V_i(row)];
        mainData(m+1).p_s = [mainData(m+1).p_s; p_s(row)];
        mainData(m+1).h = [mainData(m+1).h; h(row)];
        mainData(m+1).a_x_nav = [mainData(m+1).a_x_nav; a_x_nav(row)];
        mainData(m+1).a_y_nav = [mainData(m+1).a_y_nav; a_y_nav(row)];
        mainData(m+1).a_z_nav = [mainData(m+1).a_z_nav; a_z_nav(row)];
    end
end

```

```

mainData(m+1).GPS_alt_nav = [mainData(m+1).GPS_alt_nav; GPS_alt_nav(row)];
mainData(m+1).GPS_lat_nav = [mainData(m+1).GPS_lat_nav; GPS_lat_nav(row)];
mainData(m+1).GPS_long_nav = [mainData(m+1).GPS_long_nav; GPS_long_nav(row)];
mainData(m+1).GPS_track = [mainData(m+1).GPS_track; GPS_track(row)];
mainData(m+1).GPS_gs = [mainData(m+1).GPS_gs; GPS_gs(row)];
mainData(m+1).alpha_vanes = [mainData(m+1).alpha_vanes; alpha_vanes(row)];
mainData(m+1).beta_vanes = [mainData(m+1).beta_vanes; beta_vanes(row)];
mainData(m+1).fuel = [mainData(m+1).fuel; fuel(row)];
mainData(m+1).S_wing = [mainData(m+1).S_wing; S_wing(row)];
mainData(m+1).OAT = [mainData(m+1).OAT; OAT(row)];
mainData(m+1).RPM = [mainData(m+1).RPM; RPM(row)];
mainData(m+1).MAP = [mainData(m+1).MAP; MAP(row)];
mainData(m+1).W = [mainData(m+1).W; W(row)];
mainData(m+1).Theta_temp = [mainData(m+1).Theta_temp; Theta_temp(row)];
mainData(m+1).Delta_pres = [mainData(m+1).Delta_pres; Delta_pres(row)];
mainData(m+1).Sigma_density = [mainData(m+1).Sigma_density; Sigma_density(row)];
mainData(m+1).V_iw = [mainData(m+1).V_iw; V_iw(row)];
mainData(m+1).Del_V_pcw = [mainData(m+1).Del_V_pcw; Del_V_pcw(row)];
mainData(m+1).Del_V_pc = [mainData(m+1).Del_V_pc; Del_V_pc(row)];
mainData(m+1).V_c = [mainData(m+1).V_c; V_c(row)];
mainData(m+1).V_true_aero = [mainData(m+1).V_true_aero; V_true_aero(row)];
mainData(m+1).GPS_time_e = [mainData(m+1).GPS_time_e; GPS_time_e(row)];
mainData(m+1).roll = [mainData(m+1).roll; roll(row)];
mainData(m+1).pitch = [mainData(m+1).pitch; pitch(row)];
mainData(m+1).yaw = [mainData(m+1).yaw; yaw(row)];
mainData(m+1).N_ellipse = [mainData(m+1).N_ellipse; N_ellipse(row)];
mainData(m+1).E_ellipse = [mainData(m+1).E_ellipse; E_ellipse(row)];
mainData(m+1).D_ellipse = [mainData(m+1).D_ellipse; D_ellipse(row)];
mainData(m+1).X_v_ellipse = [mainData(m+1).X_v_ellipse; X_v_ellipse(row)];
mainData(m+1).Y_v_ellipse = [mainData(m+1).Y_v_ellipse; Y_v_ellipse(row)];
mainData(m+1).Z_v_ellipse = [mainData(m+1).Z_v_ellipse; Z_v_ellipse(row)];
mainData(m+1).GPS_lat_ell = [mainData(m+1).GPS_lat_ell; GPS_lat_ell(row)];
mainData(m+1).GPS_long_ell = [mainData(m+1).GPS_long_ell; GPS_long_ell(row)];
mainData(m+1).Az = [mainData(m+1).Az; Az(row)];
mainData(m+1).rollrate = [mainData(m+1).rollrate; rollrate(row)];
mainData(m+1).pitchrate = [mainData(m+1).pitchrate; pitchrate(row)];
mainData(m+1).yawrate = [mainData(m+1).yawrate; yawrate(row)];
row = row+1;
end
end

save('DAS+ELLIPSE')

%True Velocity Vector
V_true = sqrt((V_x.^2)+(V_y.^2)+(V_z.^2));

%NED Velocity to Body Velocity Transformation Matrix
V_XYZ=[];
for n=1:length(mainData(x).N_v)
    NED = [mainData(x).N_v(n);mainData(x).E_v(n);mainData(x).D_v(n)];
    NED2Body=(cosd(mainData(x).pitch(n))*cosd(mainData(x).yaw(n))
    (cosd(mainData(x).pitch(n))*sind(mainData(x).yaw(n))
    (-sind(mainData(x).pitch(n))));...
    (sind(mainData(x).roll(n))*sind(mainData(x).pitch(n))*cosd(mainData(x).yaw(n)) -
    cosd(mainData(x).roll(n))*sind(mainData(x).yaw(n))
    (sind(mainData(x).roll(n))*sind(mainData(x).pitch(n))*sind(mainData(x).yaw(n))+cosd(mainData(x).roll(n))*cosd(mainData(x).yaw(n))
    (sind(mainData(x).roll(n))*cosd(mainData(x).pitch(n))));...

    (cosd(mainData(x).roll(n))*sind(mainData(x).pitch(n))*cosd(mainData(x).yaw(n))+sind(mainData(x).roll(n))*sind(mainData(x).yaw(n))
    (cosd(mainData(x).roll(n))*sind(mainData(x).pitch(n))*sind(mainData(x).yaw(n)) -
    sind(mainData(x).roll(n))*cosd(mainData(x).yaw(n))
    (cosd(mainData(x).roll(n))*cosd(mainData(x).pitch(n))]);
    V_xyz = NED2Body*NED;
    V_XYZ = [V_XYZ V_xyz];
end

%Calibrate Alpha Vane
for i = 1:length(mainData)

```

```

mainData(i).alpha_vanes_calibrated = 0.8053*(mainData(i).alpha_vanes)-0.8405;
end

% *****
% BasicConstants_Cessna210
% Template from AE421 Fall 2001 Purdue University
% Prof D. Andrisani [22]
%
% *****

aircraft='Cessna210, cruise configuration';

adelf = 0;           %% Two dimensional lift effectiveness parameter Ref.(2), Equ(8.7)
alpha = 0;          %% Angle of attack [deg]
alpha_0 = -.2;      %% Airfoil zero-lift AOA [deg] [NACA64A215]
AR_h = 3.45;        %% Aspect ratio of the horizontal tail
AR_wing = 7.72;     %% Aspect ratio of the wing
b_h = 13.00;        %% Span of the horizontal tail [ft]
b_wing = 36.75;     %% Span of the wing [ft]
C_bar_D_o = .02778; %% Parasite drag
Cd_0 = 0.02778;    %% Drag coefficient at zero lift (parasite drag)
c_h = 6.3;         %% Mean aerodynamic chord of the horizontal tail [ft]
CL = 0.307;        %% Lift coefficient (3-D)
CL_hb=.307;        %% Lift coefficient of the horizontal tail/body
CL_wb=.307;        %% Lift coefficient of the wing/body
Cl_alpha_h = 2*pi; %% 2-D Lift curve slope of wing
Cl_alpha_v = 2*pi; %% 2-D Lift curve slope of vertical tail
Cl_alpha = 6;      %% Two-dimensional lift curve slope
Cl_alpha_w=Cl_alpha; %% Two-dimensional lift curve slope
c_w = 5.3;         %% Mean aerodynamic chord of the wing [ft]
D_p = 6.67;        %% Diameter of propeller [ft]
d = 5.5;           %% Average diameter of the fuselage [ft]
e = 0.82;          %% Oswald efficiency factor
eta_h = 0.85;      %% Horizontal Tail Efficiency Factor
eta_p = 0.85;      %% Propeller Efficiency
Gamma = 2*pi/180; %% Geometric dihedral angle, positive for dihedral, negative for anhedral
[rad]
Lambda=0;          %% Wing sweep angle [deg]
lambda = 0.7119;  %% Taper ratio of the wing
lambda_h = 0.7142; %% Horizontal tail taper ratio
lambda_w = lambda; %% Taper ratio of the wing
l_b = 28.15;       %% length of the fuselage [ft]
l_f = 12;          %% The horizontal length of the fuselage [ft]
l_h = 14;          %% Distance from c/4 of wing to c/4 of horizontal tail [ft]
l_v = 13;          %% Horizontal distance from the aircraft CG to the vertical tail aero
center [ft]
M = 0.2;           %% Mach number
q_bar = 1;         %% Dynamic pressure ratio (free stream)
q_bar_h = 1;       %% Dynamic pressure ratio at the tail
rho = 0.002015;   %% Air density at 6000ft [slugs/ft^3]
S_h = 48.9;        %% Area of the horizontal tail [ft^2]
S_w = 175;         %% Area of the wing [ft^2]
T = 30;           %% Temperature [F]
theta = -1.5;     %% This is the wing twist in degrees, negative for washout [deg]
theta_h = 0;      %% Horizontal tail twist between the root and tip stations, negative for
washout [deg]
two_r_one = 2;    %% Fuselage depth in region of vertical tail [ft] Ref.(2), Figure 7.5
U = 149.8;        %% Free Stream Velocity [ft/s]
U1 = 110.0;       %% Cruise flight speed [ft/s]
W = 3535.6;       %% Weight of Airplane [lbf]

AR_h = b_h^2/S_h;   %% Aspect Ratio of Horizontal Tail
AR_w = b_w^2/S_w;   %% Aspect Ratio of wing
beta = sqrt(1-M^2); %% Compressibility correction factor
kappa=Cl_alpha/(2*pi); %% Ratio of 2D lift coefficient to 2pi for the wing
kappa_h = Cl_alpha_h/(2*pi); %% Ratio of 2D lift coefficient to 2pi for the horiz. tail
V_h = (Xh*S_h)/(c_h*S_w); %% Horizontal Tail Volume Coefficient
Cd = Cd_0 + (CL^2/(pi*AR_w*e)); %% Drag Coefficient

```

```

% Constants
g=32.17405; % g, Acceleration of gravity, ft/(sec*sec)

% Lift Force
constant(28)=CL_0(S_w,S_h,M,tc_w,alpha_0,epsilon_t,i_w,i_h,epsilon_0_h,AR_w,Lambda_c4,Lambda_c2,l
ambda_w,kappa,beta,b_w,d,AR_h,eta_h); % CL0
constant(29)=CL_alpha(AR_w,AR_h,Lambda_c2,lambda_w,l_h,h_h,b_w,d,eta_h,S_h,S_w,kappa_h,Lambda_c2_
h,beta,kappa); % CLalpha
constant(30)=CL_de(S_w,S_h,AR_h,ce_ch,eta_oe,eta_ie,beta,kappa_h,lambda_h,Lambda_c2_h,tc_h,delta
e,Cl_alpha_h); % CLdeltaE
constant(31)=CL_alpha_dot(l_h, h_h, b_w, lambda, AR_w, AR_h, Lambda_c4, Lambda_c4_h, beta, kappa,
kappa_h, V_h, eta_h); % CLalphadot
constant(32)=CL_q(Xw,b_w,c_w,c_h,AR_w,Lambda_c4,Lambda_c2,Lambda_c2_h,Xh,S_h,S_w,eta_h,AR_h,beta,
V_h,b_h, kappa, kappa_h); % CLQ

% Trim conditions. These may or not be used by subsequent programs. Small
% variations in these trim flight conditions are OK.
constant(58)=U; % trim speed, Vt, ft/sec
constant(59)=5000; % Trim altitude, ft
constant(60)=0; % Trim alpha, >>>DEGREES<<<This is not used by CessnaLongSC

%Determine CL_0
function
[CL_0]=CL_0(S_w,S_h,M,tc_w,alpha_0,epsilon_t,i_w,i_h,epsilon_0_h,AR_w,Lambda_c4,Lambda_c2,lambda_
w,kappa,beta,b_w,d,AR_h,eta_h)
CLalpha_wing= 2*pi*(AR_w)/(2+sqrt((AR_w*beta/kappa)^2*(1+(tan(Lambda_c2))^2/beta^2)+4));
Kwb= (1-.25*(d/b_w)^2+.025*(d/b_w));
CLalpha_wing_b=Kwb*CLalpha_wing;
CL_alpha_h=2*pi*AR_h/(2+sqrt((AR_h*beta/kappa)^2*(1+(tan(Lambda_c2))^2/beta^2)+4));
CL_0_wf = (i_w - alpha_0_L_w)*CLalpha_wing_b;
epsilon_0_h = 0;
CL_0 = CL_0_wf + CL_alpha_h*eta_h*(S_h/S_w)*(i_h - epsilon_0_h);
return

%CL_alpha - wing+tail
function
[CL_alpha]=CL_alpha(AR_w,AR_h,Lambda_c2,lambda_w,l_h,h_h,b_w,d,eta_h,S_h,S_w,kappa_h,Lambda_c2_h,
beta,kappa)
CLalpha_wing= 2*pi*(AR_w)/(2+sqrt((AR_w*beta/kappa)^2*(1+(tan(Lambda_c2))^2/beta^2)+4));
Kwb= (1-.25*(d/b_w)^2+.025*(d/b_w));
CLalpha_wing_b=Kwb*CLalpha_wing;
CLalpha_horizontal=2*pi*AR_h/(2+sqrt((AR_h*beta/kappa_h)^2*(1+(tan(Lambda_c2_h))^2/beta^2)+4
));
K_AR=(1./AR_w)-(1./(1+(AR_w)^1.7));
CLalpha_wing_M_is_zero=2*pi*(AR_w)/(2+sqrt((AR_w*1/kappa)^2*(1+(tan(Lambda_c2))^2/1^2)+4));
K_H=(1-(h_h./b_w))/((2.*l_h./b_w)^(1./3));
K_lambda=(10-(3*lambda_w))./7;
d_epsilon_over_d_alpha_M_is_zero=4.44*(K_AR*K_lambda*K_H*sqrt(cos(Lambda_c2)))^1.19;
d_epsilon_over_d_alpha=d_epsilon_over_d_alpha_M_is_zero*CLalpha_wing./CLalpha_wing_M_is_zero;
CL_alpha = CLalpha_wing_b + CLalpha_horizontal*eta_h*(S_h/S_w)*(1-d_epsilon_over_d_alpha);
return

%CL_u - Change in lift coefficient due to change in forward speed
function [CL_u]=CL_u(U,gamma,r,T,M,CL_alpha)
M = U /sqrt(gamma*r*T);
CL_u=(M^2)./(1-M^2)*CL_alpha;
return

%CD_u - Change in Drag coefficient due to change in forward speed
function [CD_u]=CD_u(U,gamma,r,T,M,CL_alpha)
CD_u = 0;
return

%CT_u - Change in Thrust coefficient due to change in forward speed
CT_u = -Cd

%CD_alpha - Change in drag coefficient due to change in angle of attack
function [CD_Alpha] = CD_alpha(l_h, h_h, b_w, lambda, AR_w, AR_h, Lambda_c4, Lambda_c4_h, beta,
kappa, kappa_h, V_h, eta_h)
d_CD_o_dalpha = 0;

```

```

CL_alpha_w= 2*pi*AR_w/(2+sqrt((AR_w*beta/kappa)^2*(1+(tan(Lambda_c4))^2/beta^2)+4));
CD_alpha= 2*CL*(1/pi*AR_w*e)*CL_alpha
return

%%CZ_a_dot - Change of downward force with change of change in angle of attack
function [CL_alpha_dot] = CL_alpha_dot(l_h, h_h, b_w, lambda, AR_w, AR_h, Lambda_c4, Lambda_c4_h,
beta, kappa, kappa_h, V_h, eta_h)
K_H=(1-(h_h./b_w))/(((2.*l_h)/b_w)^(1./3));
K_lambda = (10-3*lambda)/7;
K_A = 1/AR_w - 1/(1+AR_w^1.7);
d_epsilon_over_dalpha_M_is_zero = 4.44*(K_A*K_lambda*K_H*sqrt(cos(Lambda_c4)))^1.19;
CZ_alpha_w= 2*pi*AR_w/(2+sqrt((AR_w*beta/kappa)^2*(1+(tan(Lambda_c4))^2/beta^2)+4));
CZ_alpha_w_M_is_zero= 2*pi*AR_w/(2+sqrt((AR_w*1/kappa)^2*(1+(tan(Lambda_c4))^2/1^2)+4));
d_epsilon_over_dalpha = d_epsilon_over_dalpha_M_is_zero*CL_alpha_w/CL_alpha_w_M_is_zero;
CZ_alpha_H = (2*pi*AR_h)/(2+sqrt(AR_h^2*beta^2/kappa_h^2*(1+(tan(Lambda_c4_h))^2/beta^2)+4));
CZ_alpha_H_dot = 2*CZ_alpha_H*eta_h*V_h*d_epsilon_over_dalpha; %eqn 6.3
return

%Determin CZ_q - Change in downward force with change in pitch
function
[CZ_q]=CL_q(Xw,b_w,c_w,c_h,AR_w,Lambda_c4,Lambda_c2,Lambda_c2_h,Xh,S_h,S_w,eta_h,AR_h,beta, V_h,
b_h, kappa, kappa_h)
CLa_w= 2*pi*(AR_w)/(2+sqrt((AR_w*beta/kappa)^2*(1+(tan(Lambda_c2))^2/beta^2)+4));
CLa_h=2*pi*AR_h/(2+sqrt((AR_h*beta/kappa_h)^2*(1+(tan(Lambda_c2_h))^2/beta^2)+4));
CZ_q_w_M0=(0.5+2*Xw/c_w)*CLa_w;
CZ_q_w_M=(AR_w+2*cos(Lambda_c4))/(AR_w*b_h+2*cos(Lambda_c4))*CL_q_w_M0;
CZ_q_w=CZ_q_w_M;
CZ_q_h=2*CLa_h*eta_h*V_h;
CZ_q=CZ_q_w+CZ_q_h;
return

%Change in Z-force due to change in forward speed
Zu=-(CLu+2*CL)*((qbar*S)/(mass*U)) % 1/sec
%Change in Z-force due to change in downward speed
Zw=-(CLalpha+CD)*((qbar*S)/(mass*U)) % ft/sec*sec
%Change in Z-force due to change in downward acceleration
Zwdot=-CZalphadot*cbar*((qbar*S)/(2*mass*U)) % ft/sec
%Change in Z-force due to change in pitch rate
Zq=-qbar*S*cbar*CLq/(2*mass*U1) % ft/sec
%Change in X-Force due to change in forward speed
Xu=-(CDu+2*CD)*((qbar*S)/(mass*U)) % 1/sec
%Change in X-Force due to change in downward speed
Xw=-(CDalpha-2CL)*((qbar*S)/(mass*U)) % ft/sec*sec

%Perturbation Calculation
for n = 1:length(mainData(x).time)+1
perturb_mainData(x).all(n) = mainData(x).all-(mainData(x).all+1)
del_u_dot(n) = -g*cos(mainData(x).pitch)*perturb_mainData(x).pitch +...
+Xu*perturb_mainData(x).Vx+...
+Xw*perturb_mainData(x).Vz;
del_w_dot(n) = (1./(1-Zwdot))*(-g*sin(mainData(x).pitch)*perturb_mainData(x).pitch(n) +...
+Zu*perturb_mainData(x).Vx(n)+...
+Zw*perturb_mainData(x).Vz(n)+
+(Zq-mainData(x).Vx)*perturb_mainData(x).pitchrate(n));
end

%Integration
U_ab=[];
W_ab=[];
for i = 1:length(mainData(x).time)-1
xtime_ab = [mainData(x).time(1:end-1);i]
U_ab = trapz(vel+mainData(x).time(1:i))
W_ab = trapz(vel+mainData(x).time(1:i))
end

%Angle of Attack Time History
aoa_NED = atand(W_ab./U_ab)+0.1; %Correction for DAS Rack difference
aoa_BODY = atand(mainData(x).Z_v_ellipse./mainData(x).X_v_ellipse);

figure;
hold on;

```

```
subplot(6,1,[1 3]),plot(test_time,aoa_NED,test_time,mainData(x).alpha_vanes_calibrated,  
test_time,mainData(x).alpha_vanes);  
title('Alpha Vane and Angle of Attack vs. Time - Trim Shot');  
xlabel('Time (s)');ylabel('Angle of Attack (degree)');legend('Calculated AOA','Calibrated Alpha  
Vane','Raw Alpha Vane');  
subplot(6,1,4),plot(test_time,-mainData(x).a_z_nav);  
xlabel('Time (s)');ylabel('Load Factor')  
subplot(6,1,5),plot(test_time,mainData(x).h);  
xlabel('Time (s)');ylabel('Altitude (ft)')  
subplot(6,1,6),plot(test_time,mainData(x).V_i);  
xlabel('Time (s)');ylabel('Indicated Airspeed (ft/s)')
```

Appendix B – UTSI Cessna 210 Aircraft Description

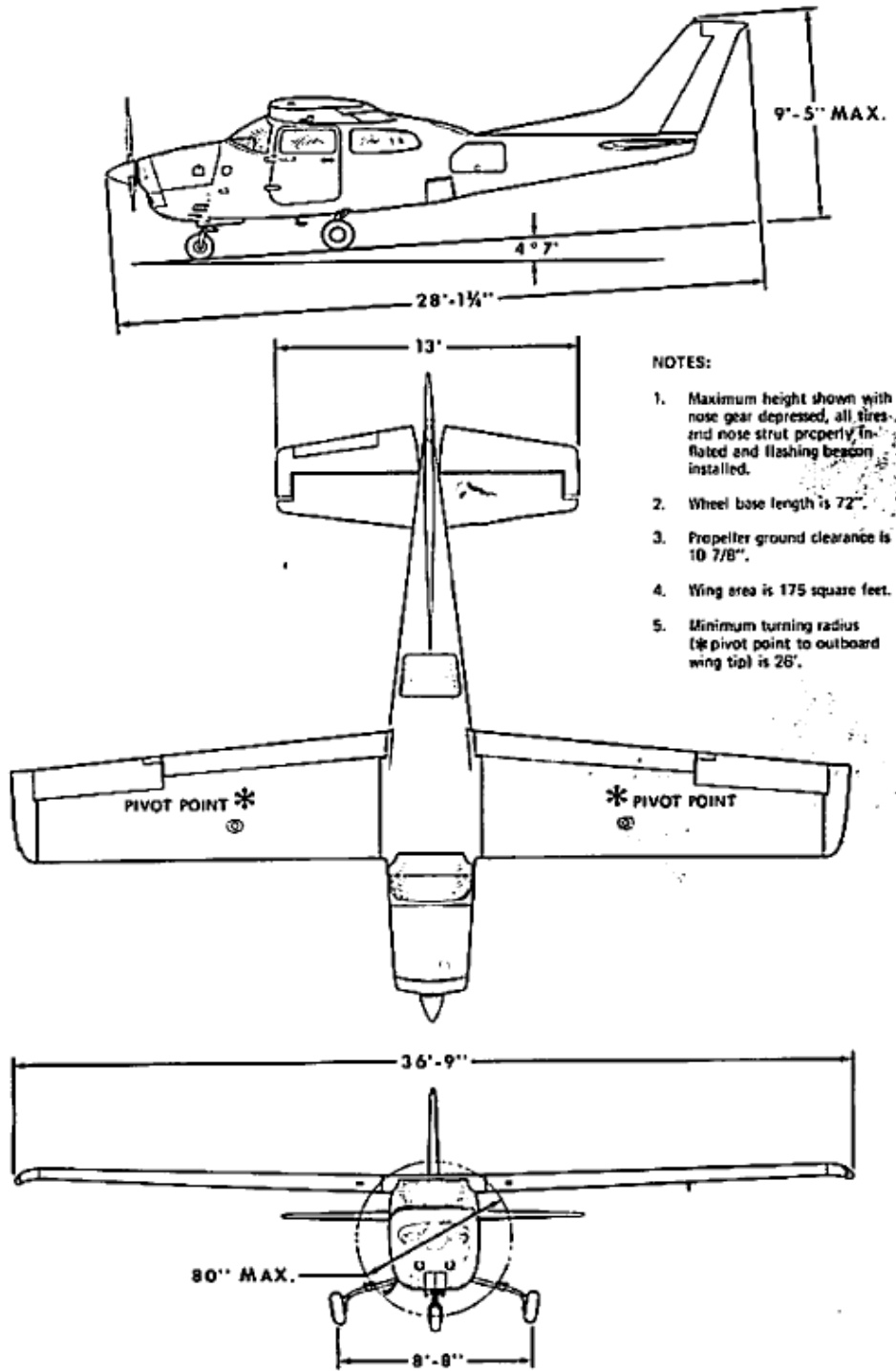


Figure 21: Cessna 210 Aircraft Three-View

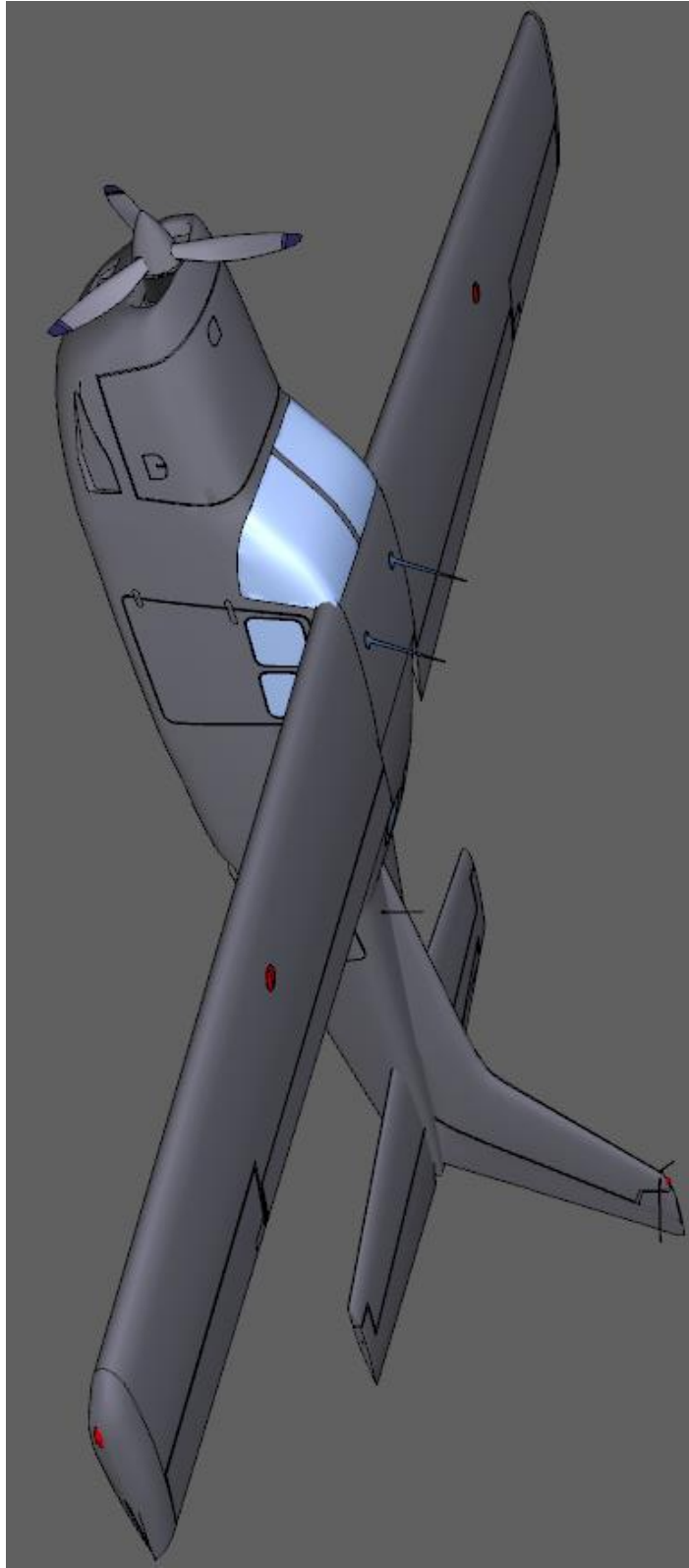


Figure 22: Cessna 210 Aircraft 3D Model

Table 4: Cessna 210 Aircraft Geometry and Data

Parameter	Symbol	Value	Units
<b>Wings</b>			
Wing Airfoil		NACA 64A215	
Wing Area	$S$	175	ft <sup>2</sup>
Wing Span	$b$	36.75	ft
Wing Aspect Ratio	$\mathcal{A}$	7.718	
Wing Root Chord	$c_r$	5.9	ft
Wing Tip Chord	$c_t$	4.2	ft
Wing Taper Ratio	$\lambda$	1.405	
Wing Sweep	$\Lambda$	0	degree
<b>Horizontal Tail</b>			
Tail Airfoil		NACA 64A412	
Horizontal Tail Area	$S_H$	48.90	ft <sup>2</sup>
Horizontal Tail Span	$b_H$	13.00	ft
Horizontal Tail Aspect Ratio	$\mathcal{A}_H$	3.456	
Horizontal Tail Tip Chord	$c_r$	3.00	ft
Horizontal Tail Root Chord	$c_t$	4.20	ft
Horizontal Tail Taper Ratio	$\lambda$	0.7142	
Horizontal Tail Sweep	$\Lambda$	0	
<b>Aircraft</b>			
Max Gross Weight	$W_{ref}$	3800	lbf
Empty Weight		2539	lbf
Max Fuel Capacity	$\mathcal{V}$	89	gal
Length		28.10	ft
Height		9.417	ft
Distance from Wing Quarter Chord to Horizontal Tail Quarter Chord	$x_H$	15.10	ft
<b>Engine</b>			
Manufacturer		Teledyne Continental	
Model Number		TSIO-520-H	
Power Rating		285	bhp

SEA LEVEL VS. ALTITUDE PERFORMANCE CURVE  
 TSIO-520-C & H

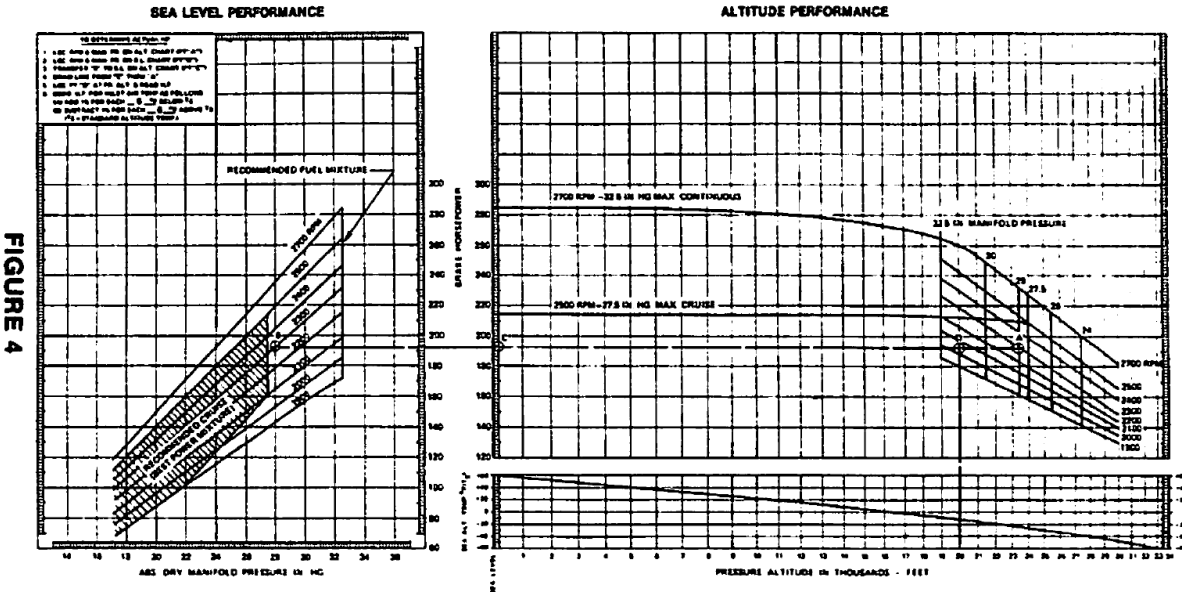


Figure 23: Cessna 210 Engine Power Chart (TSIO-520-H)

W&B Cessna T210L Centurion (N33UT)		23-Mar-17		
ITEM		WT	ARM	MOM/100
Empty Wt		2,539.00	41.23	1,046.83
Fit Test Boom	TBD	0.00		0.00
Pilot, Right Front	Kolwyck	208.00	37.00	76.96
Pilot, Left Front	Heatherly	204.00	37.00	75.48
Pax, Right Middle	(Empty)	0.00	71.00	0.00
Pax, Left Middle	Ly	150.00	71.00	106.50
Pax, Right Rear	(Empty)	0.00	101.00	0.00
Pax, Left Rear	(Empty)	0.00	101.00	0.00
Cargo, Aft		0.00	138.00	0.00
Zero Fuel Weight		3,101.00	42.11	1,305.77
T/O Fuel (gal)		534.00	42.70	228.02
89				
Takeoff Condition		3,635.00		1,533.79
			42.19	
Ldg Fuel (gal)		90.00	94.00	84.60
15				
Landing Condition		3,191.00		1,390.37
			43.57	
Remarks:				

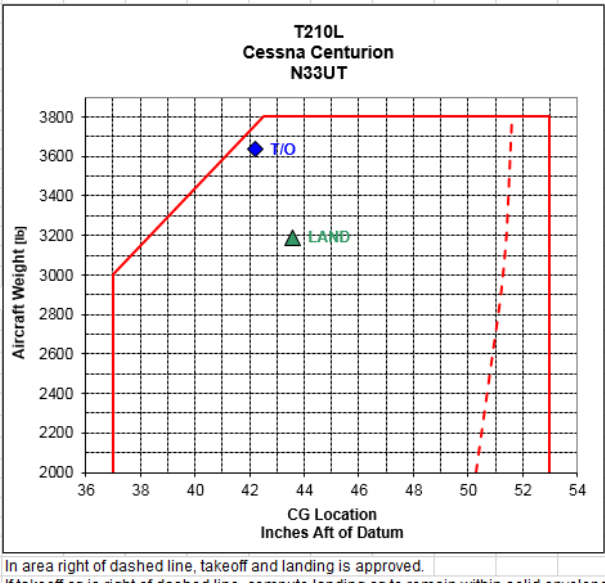


Figure 24: Sample Cessna 210 Weight and Balance CG Spreadsheet

## Appendix C – Air Data System Boom Description

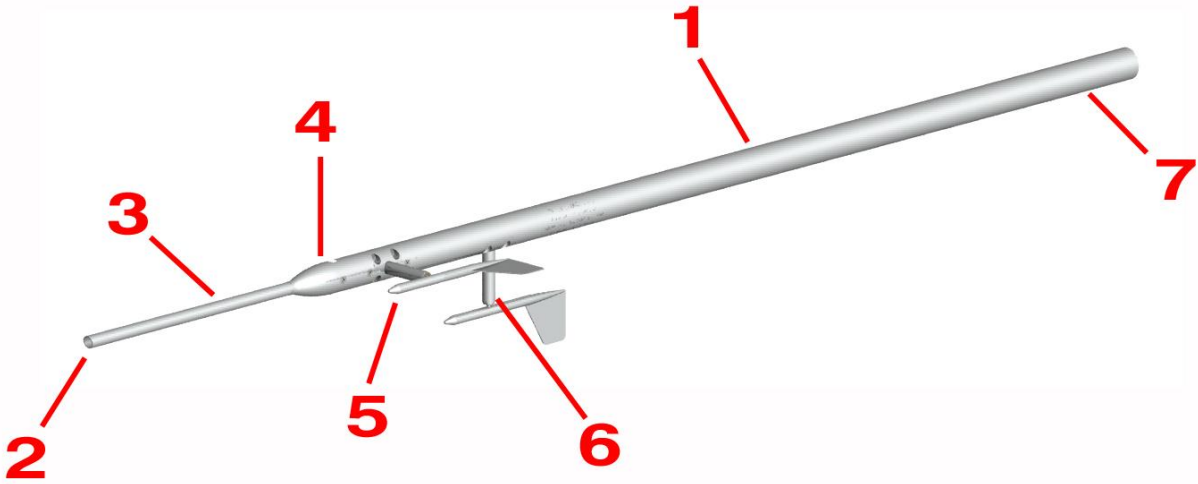


Figure 25: SpaceAge Control 100400 Mini Air Data Boom 3D model

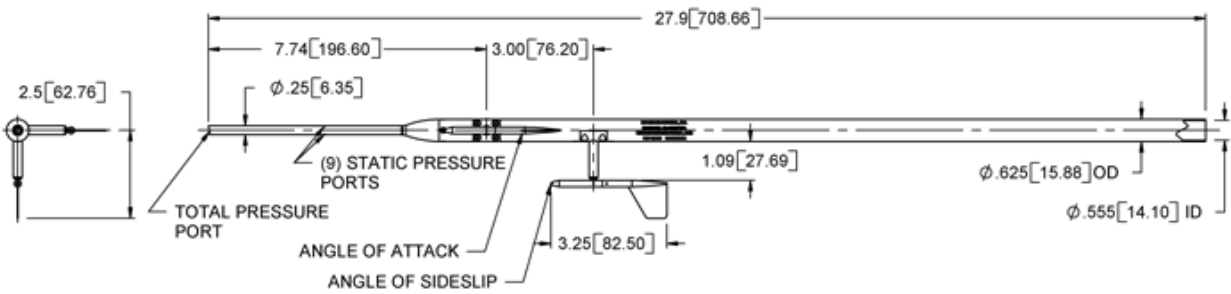


Figure 26: SpaceAge Control 100400 Mini Air Data Boom Drawings and Dimensions

Table 5: SpaceAge Control 100400 Mini Air Data Boom Specifications

<b>Item</b>	<b>Value</b>
Vane Sensor Type	conductive plastic, voltage divider (other options available)
Vane Sensor Resistance	1500 ohms $\pm$ 15%
Vane Sensor Independent Linearity	$\pm$ 5% max per VRCI-P-100A
Vane Sensor Electrical Travel	60° min (other options available)
Vane Sensor Mechanical Travel	360° continuous
Vane Sensor Power Rating at 70° C	0.5 Watt min
Vane Sensor Output Signal	analog signal from 0 to supply voltage
Vane Sensor Supply Current	12 mA max
Vane Sensor Supply Voltage	35 VDC max
Vane Sensor Output Smoothness	0.1% max
Vane Sensor Insulation Resistance	1 Gohms at 500 VAC min
Vane Sensor Dielectric Strength	1000 VDC min
Vane Sensor Resolution	infinite signal
Vane Sensor Electrical Connection	flying leads (3-conductor, 30 AWG Teflon-insulated, 48-in (1219-mm) min length from end of air data boom body, 0.08 (2.03) nominal diameter
Vane Sensor Electrical Cable Diameter, Material	0.10 in (2.5 mm) nominal diameter, Thermo-Fit shrink tube outer jacket, black color
Vane Sensor Temperature Coefficient	$\pm$ 400 ppm/°C max
Vane Sensor Mechanical Life	100 million shaft revolutions min
Total/Static (Pitot/Static) Type	non-deiced (unheated)
Total Pressure Tube Connection	0.090 in OD x 0.055 ID (2.29 mm OD x 1.40 mm ID) clear Nylon tube, 15 in (381 mm) min exposed from end of air data boom
Static Pressure Tube Connection	0.090 in OD x 0.055 ID (2.29 mm OD x 1.40 mm ID) clear Nylon tube, 15 in (381 mm) min exposed from end of air data boom
Operating Temperature	-65° to 257° F (-54° to 125° C)
Nominal Mass	6 oz (170 g)

## Appendix D – Ellipse-N Inertial Navigation System Unit



Figure 27: SBG Ellipse-N INS Unit

Table 6: Ellipse-N Data

<b>Mechanical</b>	
Size	1.34x1.34x0.51in
Weight	0.02lb
<b>Accuracy</b>	
Roll / Pitch	0.1 degree
Heading	<0.5 degree
Velocity	0.33 ft/s
Position	6.56 ft
<b>Range</b>	
Accelerometers	+ 16g
Gyroscopes	+ 450 degree/s
Magnetometers	+ 50 Gauss
<b>Interface</b>	
Output Rate	20 Hz
Main Serial Interface	USB 2.0
Input Voltage	5-36V

Table 7: Sensor Outputs

Parameter	Symbol	Units	Source
Pitch	$\theta$	degree	Ellipse-N INS
Roll	$\phi$	degree	Ellipse-N INS
Yaw (Heading)	$\psi$	degree	Ellipse-N INS
Roll Rate	$p$	degree/s	Ellipse-N INS
Pitch Rate	$q$	degree/s	Ellipse-N INS
Yaw Rate	$r$	degree/s	Ellipse-N INS
Acceleration – X direction	$a_x$	m/s <sup>2</sup>	Ellipse-N INS
Acceleration – Y direction	$a_y$	m/s <sup>2</sup>	Ellipse-N INS
Acceleration – z direction	$a_z$	m/s <sup>2</sup>	Ellipse-N INS
North Velocity	$V_N$	m/s	Ellipse-N INS
East Velocity	$V_E$	m/s	Ellipse-N INS
Down Velocity	$V_D$	m/s	Ellipse-N INS
Altitude - GPS	$h$	m	Ellipse-N INS
GPS Time		mm:ss.ms	Ellipse-N INS / DAS
Altitude - pressure	$h_i$	ft	DAS
Indicated Airspeed	$V_i$	ft/s	DAS
Outside Air Temperature	$T$	°F	Shipboard
RPM	RPM		Shipboard
MAP	MAP	inHg	Shipboard
Fuel	$\mathcal{F}$	gal	Shipboard
Angle of Attack (Alpha Vane)	$\alpha$	degree	DAS

Appendix E – Sample Calculations + Flow Chart to Determine

**Power-Speed (P<sub>iw</sub>-V<sub>iw</sub>) Method for determining Zero-Lift Drag Coefficient – Steady Trim Shots**

Parameter	Symbol	Value	Units
<b>Standard Values</b>			
Pressure – Standard Sea Level	$p_{SSL}$	2116	lbf/ft <sup>2</sup>
Air Density – Standard Sea Level	$\rho_{SSL}$	0.002377	slug/ft <sup>3</sup>
Temperature – Standard Sea Level	$T_{SSL}$	518.7	°R
Gravitational Acceleration - Standard	$g$	32.17	ft/s <sup>2</sup>
Ratio of Specific Heats – Air, Earth	$\gamma$	1.4	
Fuel Density	$\rho_{fuel}$	6.00	lbf/gal
Universal Gas Constant	$R$	1716	ft lbf/slug °R
Cessna 210 Zero-Lift Drag Coefficient	$C_{D_o}$	0.02778	
<b>Corrected Air Data - Trim Shot Data</b>			
Indicated Airspeed, Weight Corrected	$V_{i,w}$	154.9	KIAS
Density Ratio	$\sigma_{act}$	0.8246	
RPM		2500	
MAP		27.5	inHG
Shaft Horse Power from Engine Chart		212	
Reference Weight	$W_{ref}$	3800	lbf
Test Weight	$W$	3462.2	lbf

Power, Indicated, Weight Corrected

$$P_{iw} = \frac{(SHP)\sqrt{\sigma}}{\left(\frac{W_{ref}}{W}\right)^{3/2}} = \frac{(212)\sqrt{0.8246}}{\left(\frac{3800}{3462.2}\right)^{3/2}} = 167.42hp$$

Test to get lowest C<sub>D</sub> Value

Normalized Indicated Airspeed, Weight Corrected

$$V_{iwn} = 1000000000$$

$$P_{iwn} = \frac{\left(\frac{P_{iw} \times V_{iw}}{10^3}\right)_n \times 10^3}{V_{iwn}} = \frac{\left(\frac{167.42 \times 154.9}{10^3}\right)_n \times 10^3}{1000000000} = 42090000$$

$$C_D = \frac{2 * 550 * 42090000 * .85}{0.002377 * (1.687 * 1000000000)^3 * 175} = 0.027780486$$

$$C_L = \sqrt{\left(\frac{2 * 3800}{0.002377 * (1.687 * 1000000000)^2 * 175}\right)^2} = 0.0000006413 \quad ***$$

\*\*\*Essentially 0

PIW-VIW Data Reduction (5,000 ft)												
	$V_e$ (Kts)	$\theta$	$\delta$	$\sigma$	$V_e$ (Kts)	MAP (inHG)	SHP	$V_{in}$ (Kts)	$P_{in}$ (hp)	$P_{in} \times V_{in} / 10^3$	$V_{in}^4 / 10^7$	
MAX	153.02	0.9711	0.8007	0.8246	153.024	27.5	212	159.24	167.4203954	26.6605	64.3039	
110	107.99	0.9672	0.8018	0.8289	107.995	16.5	110	110.251792	86.51026752	9.5379	14.7755	
70	72.71	0.9653	0.7993	0.8281	72.7099	16	89	74.2346616	69.66520862	5.1716	3.0369	
PIW-VIW Data Reduction (10,000ft)												
	$V_e$ (Kts)	$\theta$	$\delta$	$\sigma$	$V_e$ (Kts)	MAP (inHG)	SHP	$V_{in}$ (Kts)	$P_{in}$ (hp)	$P_{in} \times V_{in} / 10^3$	$V_{in}^4 / 10^7$	
MAX	152.76	0.9576	0.6874	0.7179	152.764	27.5	212	157.003677	194.9997385	30.6157	60.7630	
110	111.23	0.9537	0.6848	0.7180	111.233	16	111	114.501581	102.5955111	11.7473	17.1888	
70	74.04	0.9537	0.6880	0.7214	74.0428	14.5	85	76.3264456	79.08126946	6.0360	3.3939	
update												
Normalized Data curvefit												
$V_{in}^4 \times 10^7$	$P_{in} \times V_{in} \times 10^3$	$V_{in}$ (Kts)	$P_{in}$ (hp)	$C_D$	$C_L^2$	$C_L$						
2	5.3088	66.87403	79.3851	0.175197246	2.05685	1.43417067						
4	6.1506	79.52707	77.3397	0.101488866	1.02842	1.0141118						
6	6.9924	88.01117	79.449	0.076919406	0.68562	0.82801882						
8	7.8342	94.57416	82.8366	0.064634676	0.51421	0.71708533						
10	8.676	100	86.76	0.057263838	0.41137	0.64138062						
12	9.5178	104.6635	90.9371	0.052349946	0.34281	0.58549772						
13.2611	10.04859699	107.3112	93.6398	0.050013447	0.31021	0.55696263						
14	10.3596	108.7757	95.2382	0.048840023	0.29384	0.54206556						
16	11.2014	112.4683	99.5961	0.046207581	0.25711	0.5070559						
1000000000	420900004.5	10000	4.2E+07	0.027780486	4.1E-09	6.4138E-05						
				0.02778								

Reference Figure 30 for graphical drag polar

Parameter	Symbol	Value	Units
<b>Trim Data – Point 1</b>			
<b>INS Observed Data</b>			
Angle of Attack (Alpha Vane)	$\alpha_m$	6.6119	degree
North Velocity	$V_N$	45.983	m/s
East Velocity	$V_E$	5.038	m/s
Down Velocity	$V_D$	-0.360	m/s
Roll Angle	$\phi$	4.581	degree
Pitch Angle	$\theta$	1.318	degree
Yaw Angle (Heading)	$\psi$	-2.039	degree
GPS Altitude	$h$	1898.4	m
<b>DAS Observed Data</b>			
Pressure Altitude	$h_i$	6030.8	ft
<b>Shipboard Observed Data</b>			
Outside Air Temperature	$T$	30.0	°F
Takeoff Weight	$W_{TO}$	3635.6	Lbf
Takeoff Fuel Volume	$\mathcal{V}_{TO}$	89	gal
Test point Fuel Remaining	$\mathcal{V}$	71.8	gal

## Angle of Attack (Alpha Vane) Calibration

Calibration Curve

$$\alpha_c = 0.8053\alpha_m - 0.8405 = 0.8053(6.6119) - 0.8405 = 4.3675 \text{ degree}$$

## Conversion from Inertial (North-East-Down) Velocity to Body-Fixed Velocity

Conversion from m/s to ft/s

$$V \left[ \frac{ft}{s} \right] = V \left[ \frac{m}{s} \right] \times 3.281$$

Parameter	Symbol	Value	Units
North Velocity	$V_N$	150.9	ft/s
East Velocity	$V_E$	16.53	ft/s
Down Velocity	$V_D$	-1.181	ft/s

$$\begin{bmatrix} \cos(4.581) \cos(-2.039) & \cos(4.581) \sin(-2.039) & -\sin(4.581) \\ \sin(1.318) \sin(4.581) \cos(-2.039) - \cos(1.318) \sin(-2.039) & \sin(1.318) \sin(4.581) \sin(-2.039) + \cos(1.318) \cos(-2.039) & \sin(1.318) \cos(4.581) \\ \cos(1.318) \sin(4.581) \cos(-2.039) + \sin(1.318) \sin(-2.039) & \cos(1.318) \sin(4.581) \sin(-2.039) - \sin(1.318) \cos(-2.039) & \cos(1.318) \cos(4.581) \end{bmatrix} \begin{bmatrix} 150.9 \\ 16.53 \\ -1.181 \end{bmatrix} \Rightarrow$$

$$\begin{bmatrix} u \\ v \\ w \end{bmatrix} = \begin{bmatrix} 149.8 \\ -9.321 \\ 11.44 \end{bmatrix}$$

True Velocity

$$V_t = \sqrt{u^2 + v^2 + w^2} = \sqrt{149.8^2 + (-9.321)^2 + 11.44^2} = 151.7 \text{ ft/s}$$

## Standard Atmosphere Ratios

\*Considerations – pressure altitude and GPS altitude are different. The intent is to use INS only, then pressure altitude is not known. GPS altitude is the geometric altitude measured above mean sea level. For low altitudes, the difference is not significant.

Conversion from meters to feet

$$h[ft] = h[m] \times 3.281 = 1898.4 \times 3.281 = 6228.7 \text{ ft}$$

Pressure Ratio

$$\delta_{act} = (1 - 6.8756 \times 10^{-6} \times h)^{5.2559} = (1 - 6.8756 \times 10^{-6} \times 6228.7)^{5.2559} = 0.80045$$

Temperature Ratio

$$\theta_{act} = \frac{T_{act}}{T_{SSL}} = \frac{30.0 + 459.67}{518.69} = 0.94405$$

Density Ratio

$$\sigma = \frac{\delta}{\theta} = \frac{0.80045}{0.94405} = 0.84788$$

## Aircraft State Data

### Dynamic Pressure

$$q = \frac{1}{2} \rho V_t^2 = \frac{1}{2} \sigma \rho_{ssl} V_t^2 = \frac{1}{2} (0.84788)(.002377)(151.7)^2 = 23.19 \frac{lbf}{ft^2}$$

### Test Weight and Mass

$$W = W_{TO} - ((\gamma_{to} - \gamma) * 6) = 3635.6 - ((89 - 71.8) * 6) = 3532.4lbf$$

### Conversion from Weight (lbf) to Mass (slug)

$$m[slug] = \frac{W \text{ [lbf]}}{g \text{ [32.17} \frac{ft}{s^2}]} = \frac{3532.4}{32.17} = 109.9slug$$

### Mach number

$$M = \frac{V_t}{a} = \frac{V_t}{\sqrt{\gamma RT}} = \frac{151.7}{\sqrt{(1.4)(1716)(30 + 459.67)}} = 0.1399$$

### Compressibility Correction Factor

$$B = \sqrt{1 - M^2} = \sqrt{1 - .1399^2} = 0.9902$$

### Steady-State Reference Lift Coefficient

$$C_L = \frac{W}{qS} = \frac{3532}{(23.19)(175)} = 0.8703$$

## Aircraft Geometry Data

Parameter	Symbol	Value	Units
Wing Area	$S$	175	ft <sup>2</sup>
Wing Span	$b$	36.75	ft
Aspect Ratio	$\mathcal{A}$	7.718	
Wing Sweep Angle	$\Lambda$	0.0	degree
Root Chord	$c_r$	5.90	ft
Tip Chord	$c_t$	4.20	ft

### Wing Aspect Ratio

$$\mathcal{A} = \frac{b^2}{s} = \frac{36.75^2}{175} = 7.718$$

### Wing Mean Aerodynamic Chord

\*Assumption: Rectangular straight taper wing

$$\lambda = \frac{c_t}{c_r} = \frac{4.20}{5.90} = 0.7119$$

$$\bar{c} = \frac{2}{3} c_r \frac{1+\lambda+\lambda^2}{1+\lambda} = \frac{2}{3} (5.9) \frac{1+0.7119+(0.7119)^2}{1+(0.7119)} = 5.097ft$$

### Wing Reynolds Number at 6000ft

$$Re = \frac{\rho V_t c}{\mu} = \frac{\sigma \rho_{ssl} V_t \bar{c}}{\mu} = \frac{(0.8479)(0.002377)(151.7)(5.097)}{3.659 \times 10^{-7}} = 4.3 \times 10^6$$

### Wing: NACA64A215 Airfoil (Figure 28)

$$\text{Lift curve slope } C_{l_\alpha} = \frac{0.7}{7} \frac{1}{\text{deg}} = 0.1 \frac{1}{\text{deg}} = 5.730 \frac{1}{\text{rad}}$$

### 2D Section Wing Lift ratio

$$\kappa = \frac{C_{l_\alpha}}{2\pi} = \frac{5.730}{2\pi} = 0.9119$$

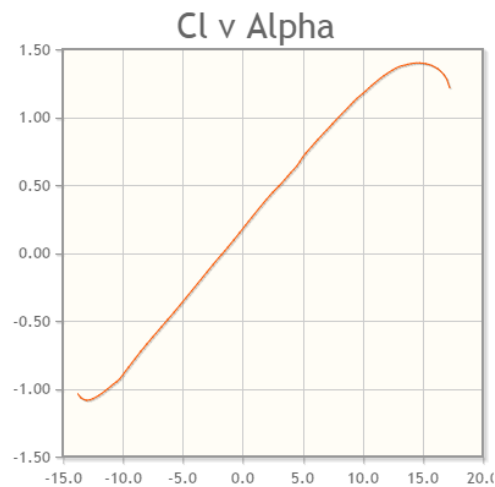


Figure 28: NACA64A215 Airfoil at  $Re=4.0 \times 10^6$  [23]

### Change in lift coefficient due to change in angle of attack - 3D Lift Curve Slope

$$\begin{aligned} C_{L_\alpha} &= \frac{2\pi \mathcal{A}}{2 + \sqrt{\frac{\mathcal{A}^2 \mathcal{B}^2}{\kappa^2} \left(1 + \frac{\tan^2 \Lambda}{\mathcal{B}^2}\right) + 4}} = \frac{2\pi(7.718)}{2 + \sqrt{\frac{(7.718)^2 (0.9902)^2}{(0.9119)^2} \left(1 + \frac{\tan^2(0)}{(0.9902)^2}\right) + 4}} \\ &= 4.568 \frac{1}{\text{rad}} \end{aligned}$$

### Horizontal Tail Aspect Ratio

$$\mathcal{A}_H = \frac{b_H^2}{S_H} = \frac{13.00^2}{48.90} = 3.456$$

### Horizontal Tail Mean Aerodynamic Chord

\*Assumption: Rectangular straight taper wing

$$\lambda = \frac{c_t}{c_r} = \frac{3.00}{4.20} = 0.7142$$

$$\bar{c} = \frac{2}{3} c_r \frac{1+\lambda+\lambda^2}{1+\lambda} = \frac{2}{3} (4.2) \frac{1+0.7142+(0.7142)^2}{1+(0.7142)} = 3.633 \text{ ft}$$

Tail Reynolds Number at 6000ft

$$Re = \frac{\rho V_t c}{\mu} = \frac{\sigma \rho_{ssl} V_t \bar{c}}{\mu} = \frac{(0.8479)0.002377(151.7)(3.633)}{3.659 \times 10^{-7}} = 3.0 \times 10^6$$

Tail: NACA64A412 Airfoil (Figure 29)

$$\text{Lift curve slope } C_{l_\alpha} = \frac{0.8}{7} \frac{1}{\text{deg}} = 0.1143 \frac{1}{\text{deg}} = 6.549 \frac{1}{\text{rad}}$$

2D Section Wing Lift ratio

$$\kappa = \frac{C_{l_\alpha}}{2\pi} = \frac{6.549}{2\pi} = 1.042$$

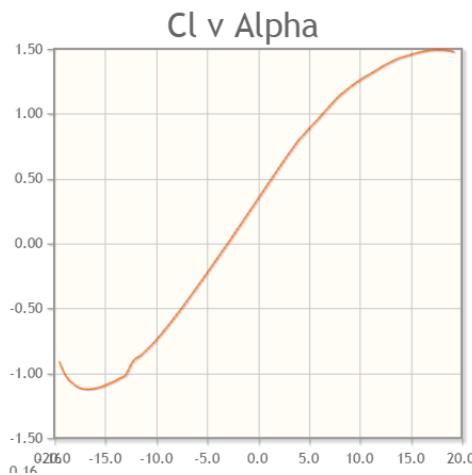


Figure 29: NACA64A412 Airfoil at  $Re=3.0 \times 10^6$

Change in lift coefficient due to change in angle of attack – 3D Lift Curve Slope

$$C_{L_{\alpha H}} = \frac{2\pi \mathcal{A}}{2 + \sqrt{\frac{\mathcal{A}^2 B^2}{\kappa^2} \left(1 + \frac{\tan^2 \Lambda}{B^2}\right) + 4}} = \frac{2\pi(3.456)}{2 + \sqrt{\frac{(3.456)^2 (0.9902)^2}{(1.042)^2} \left(1 + \frac{\tan^2(0)}{(0.9902)^2}\right) + 4}}$$

$$= 3.715 \frac{1}{\text{rad}}$$

Change in lift coefficient due to change in forward speed/Mach number

$$C_{L_u} = \frac{\partial C_L}{\partial M} = \frac{M^2}{1 - M^2} C_{L_\alpha} = \frac{(0.1399)^2}{1 - (0.1399)^2} (4.568) = 0.0912$$

Steady-State Reference Drag Coefficient

$e = 0.82$  for  $\mathcal{A} = 7.718$  from Figure 8

$$C_D = C_{D_o} + \frac{C_L^2}{\pi \mathcal{A} e} = 0.02778 + \frac{.8703^2}{\pi(7.718)(0.82)} = 0.0659$$

Change in drag coefficient due to change in forward speed

$$C_{D_u} = M \frac{\partial C_D}{\partial M} = (0.1399)0 = 0$$

Change in thrust coefficient due to change in forward speed

$$C_{T_u} = -C_D = -0.3159$$

Change in drag coefficient due to change in angle of attack

$$C_{D_\alpha} = \frac{\partial C_{D_e}}{\partial \alpha} + \frac{2C_L}{\pi A e} C_{L_\alpha} = 0 + \frac{2(0.8703)}{\pi(7.718)(0.82)} (4.568) = 0.3999$$

Change in downward force coefficient due to change in pitch rate

$$V_H = \frac{x_H S_H}{\bar{c} S} = \frac{(15.10)(48.90)}{(5.097)(175)} = 0.8278$$

$$\eta_H = 0.9$$

$$C_{Z_q} = C_{Z_{\dot{\alpha}}} = 1.1 \left( -2C_{L_{\alpha_H}} \eta_H V_H \right) = 1.1 \left( -2(3.715)(0.9)(0.8278) \right) = -6.089 \frac{1}{rad}$$

Change in downward force coefficient due to time rate of change of angle of attack

$$\frac{d\varepsilon}{d} = \frac{2C_{L_\alpha}}{\pi A} = \frac{2(4.568)}{\pi(7.718)} = 0.3768$$

$$C_{Z_{\dot{\alpha}}} = -2C_{L_{\alpha_H}} \eta_H V_H \frac{2C_{L_\alpha}}{\pi A} = -2(3.715)(0.9)(0.8278)(0.3768) = -2.086 \frac{1}{rad}$$

### **Stability Derivatives**

Change in Z-force due to change in forward speed

$$Z_u = \frac{\left( \frac{\partial Z}{\partial u} \right)}{m} = -(C_{L_u} + 2C_L) \frac{qS}{mu} = -((0.0020) + 2(0.8704)) \frac{(23.19)(175)}{(109.9)(149.8)} = -0.4296 \frac{1}{s}$$

Change in Z-force due to change in downward speed

$$Z_w = \frac{\left( \frac{\partial Z}{\partial w} \right)}{m} = -(C_{L_\alpha} + C_D) \frac{qS}{mu} = -(0.1005 + 0.3159) \frac{(23.19)(175)}{(109.9)(149.8)} = -0.1026 \frac{1}{s}$$

Change in Z-force due to change in pitch rate

$$Z_q = \frac{\left( \frac{\partial Z}{\partial q} \right)}{m} = -C_{Z_q} \frac{\bar{c} qS}{2 mu} = -(6.089) \frac{5.097}{2} \frac{(23.19)(175)}{(109.9)(149.8)} = -3.825 \frac{ft}{s}$$

Change in Z-force due to change in downward acceleration

$$Z_{\dot{w}} = \frac{\left(\frac{\partial Z}{\partial \dot{w}}\right)}{m} = -\left(C_{Z\dot{\alpha}} \frac{\bar{c}}{2u}\right) \frac{qS}{mu} = -\left((2.086) \frac{5.097}{2(149.8)}\right) \frac{(23.19)(175)}{(109.9)(149.8)} = 0.0087 \frac{ft}{s}$$

Change in X-force due to change in forward speed

$$X_u = \frac{\left(\frac{\partial X}{\partial u}\right)}{m} = -\left((C_{D_u} + 2C_D) + C_{T_u}\right) \frac{qS}{mu} = -\left((0 + 2(.3159)) + (-0.3159)\right) \frac{(23.19)(175)}{(109.9)(149.8)} \\ = -0.07787 \frac{1}{s}$$

Change in X-force due to change in downward speed

$$X_w = \frac{\left(\frac{\partial X}{\partial w}\right)}{m} = -(C_{D\alpha} + 2C_L) \frac{qS}{mu} = -((.0079) + 2(0.8704)) \frac{(23.19)(175)}{(109.9)(149.8)} = -0.4311 \frac{1}{s}$$

## Appendix F – Supporting Plots

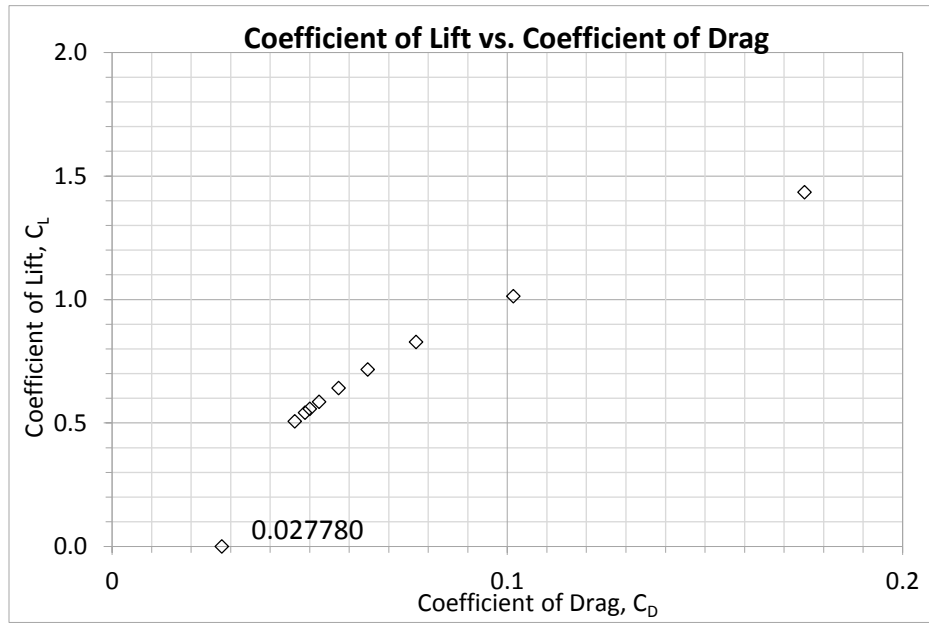


Figure 30: Drag Polar for Cessna 210 obtained through Power-Speed Flight Test Technique

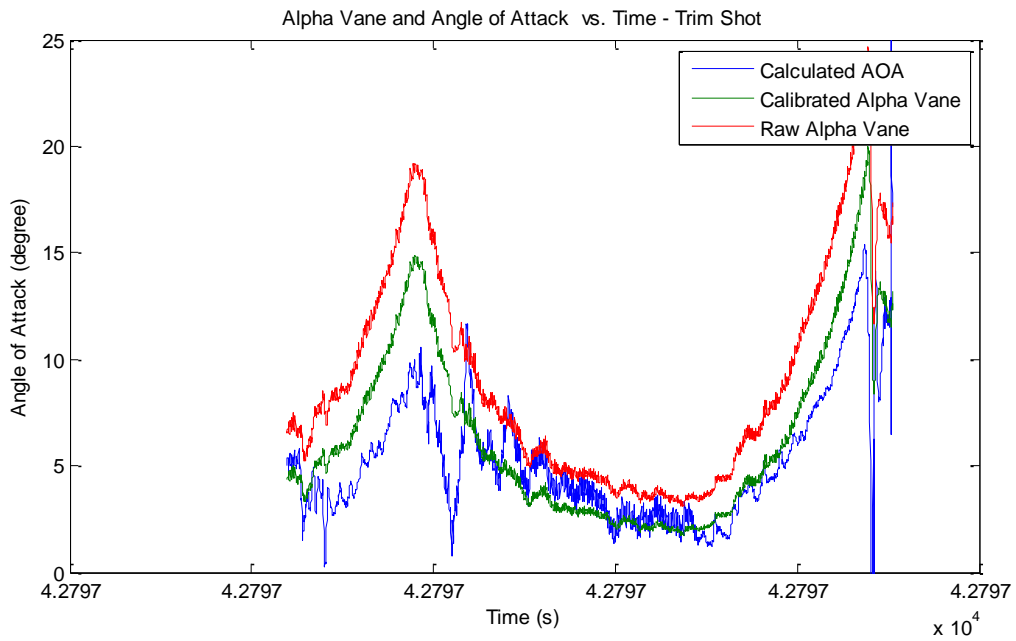


Figure 31: Time history of Angle of Attack Algorithm for Level Acceleration/Deceleration with Pitch Rate

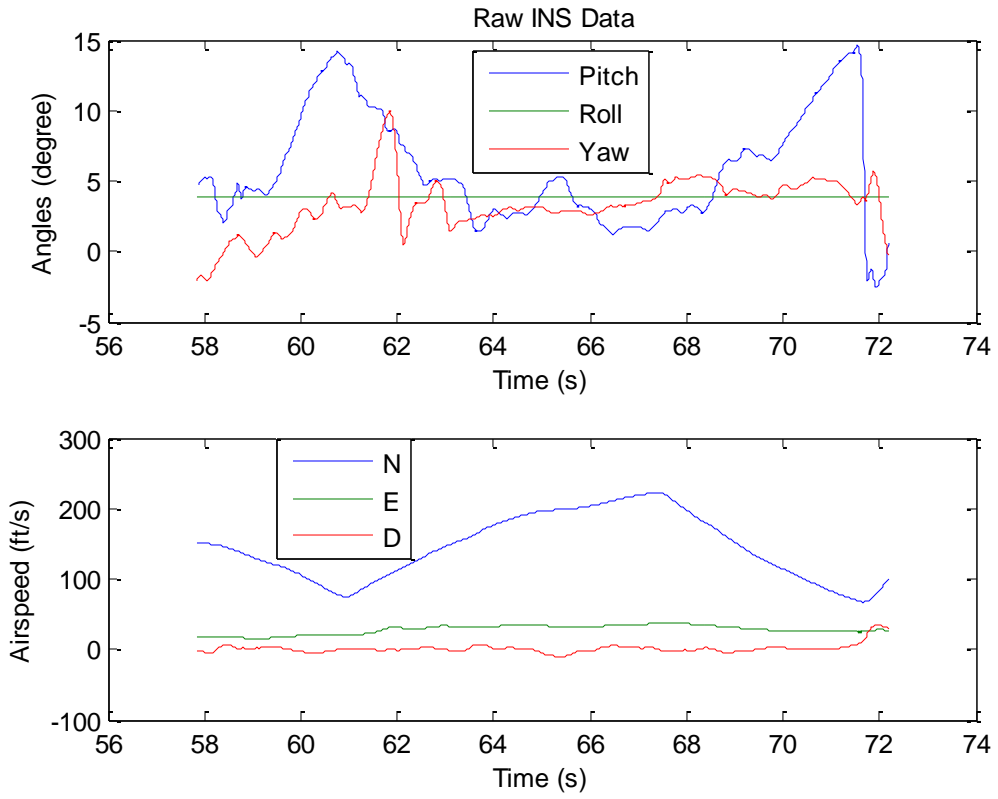


Figure 32: Level Acceleration and Deceleration: Inertial-to-Body Transformation Data Inputs

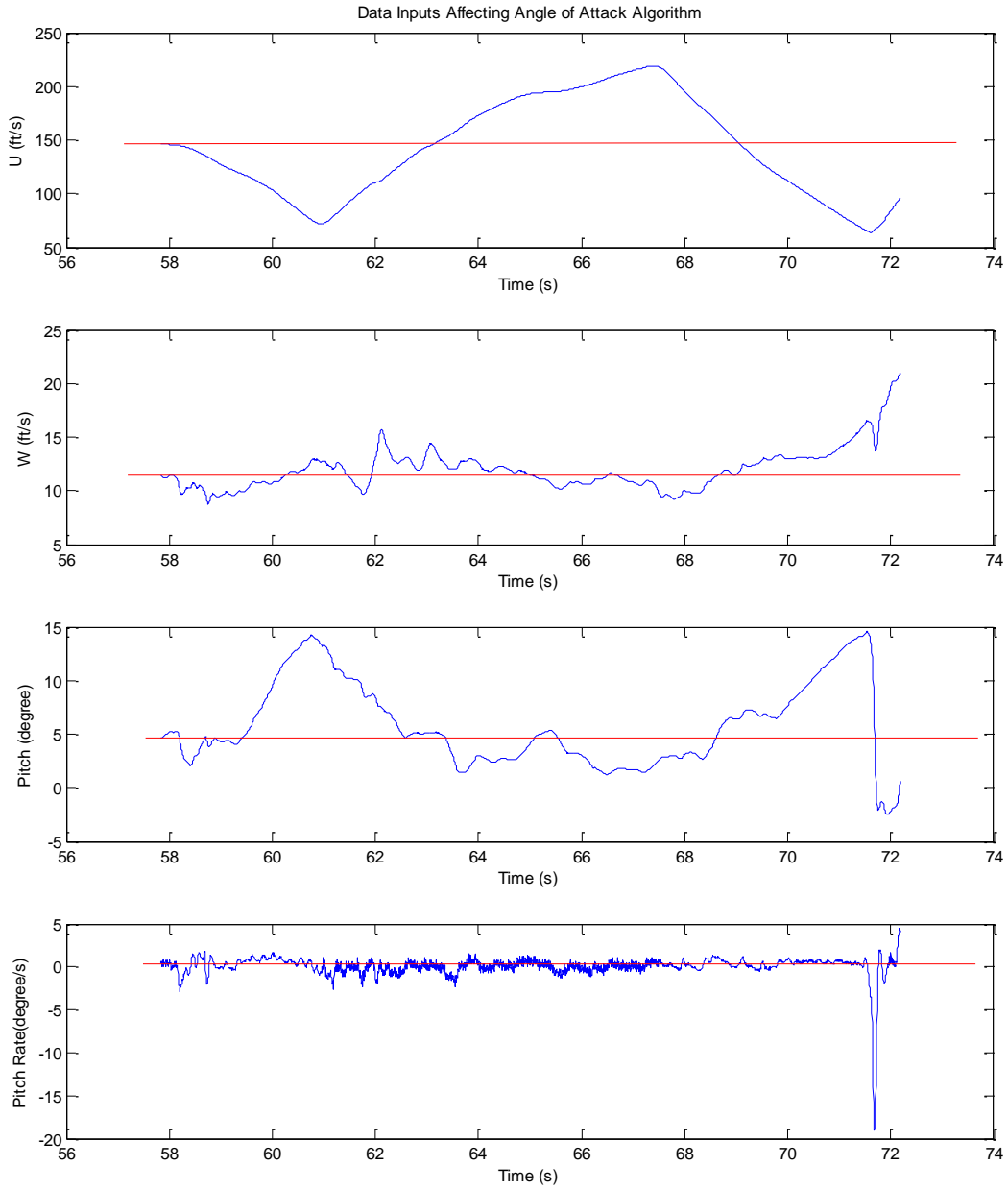


Figure 33: INS Data inputs ( $u, w, \theta, q$ ) utilized by Angle of Attack Algorithm - Level Accel/Decel

\*Note: the redline denotes the steady level trim value.

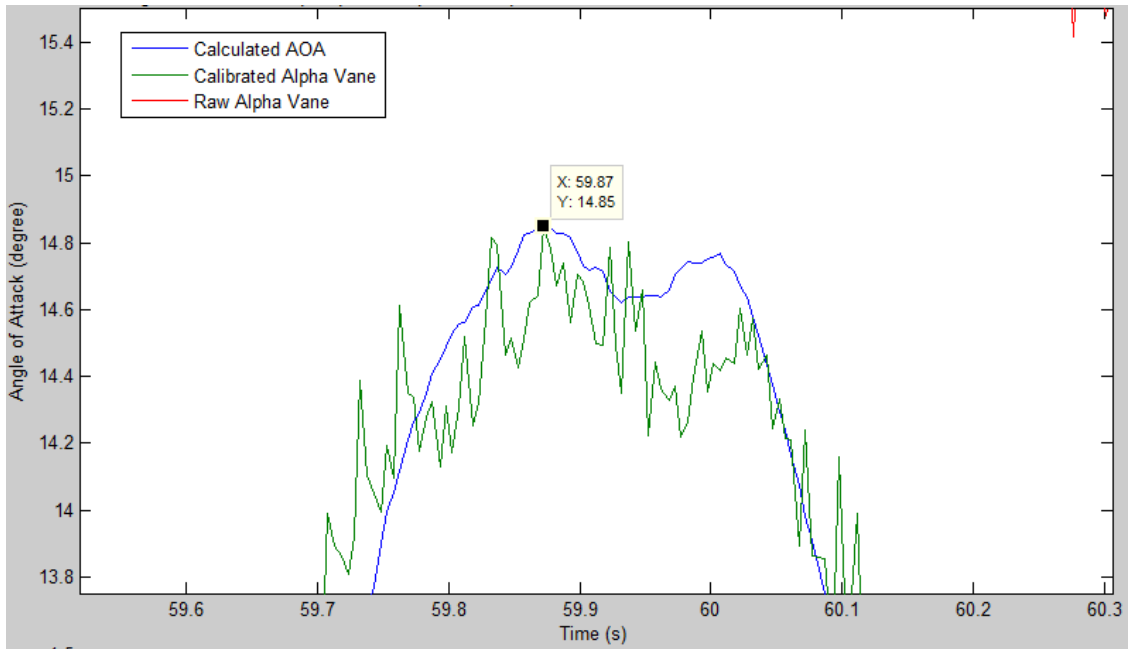


Figure 34: Peak Value for first Deceleration - Level Acceleration and Deceleration

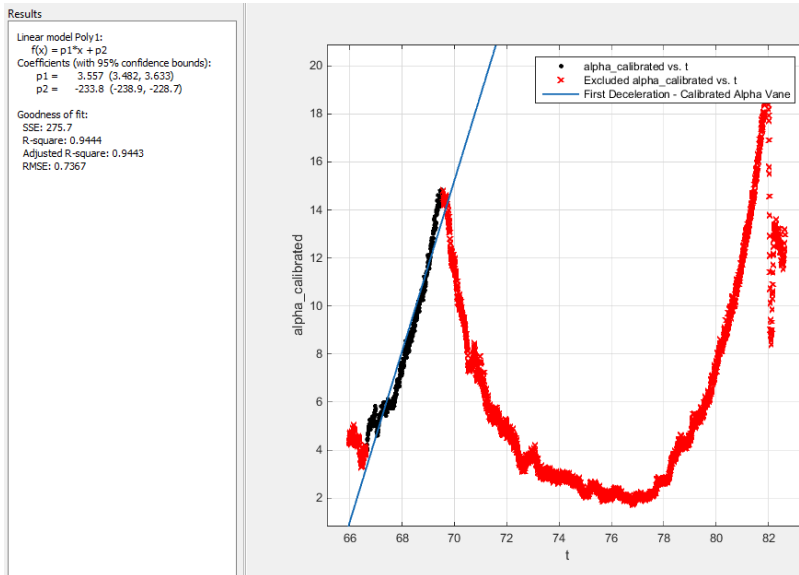


Figure 35: Calibrated Alpha Vane change in angle of attack - first deceleration

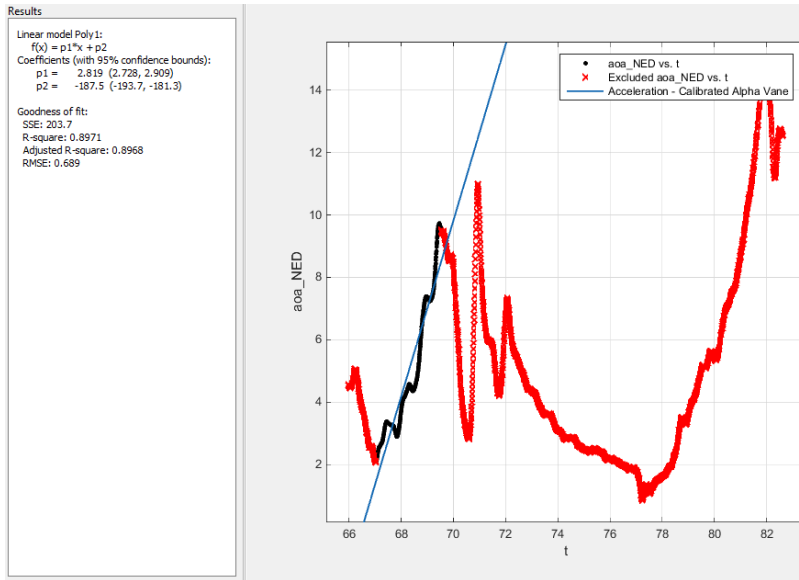


Figure 36: Calculated Angle of Attack change in angle of attack - first deceleration

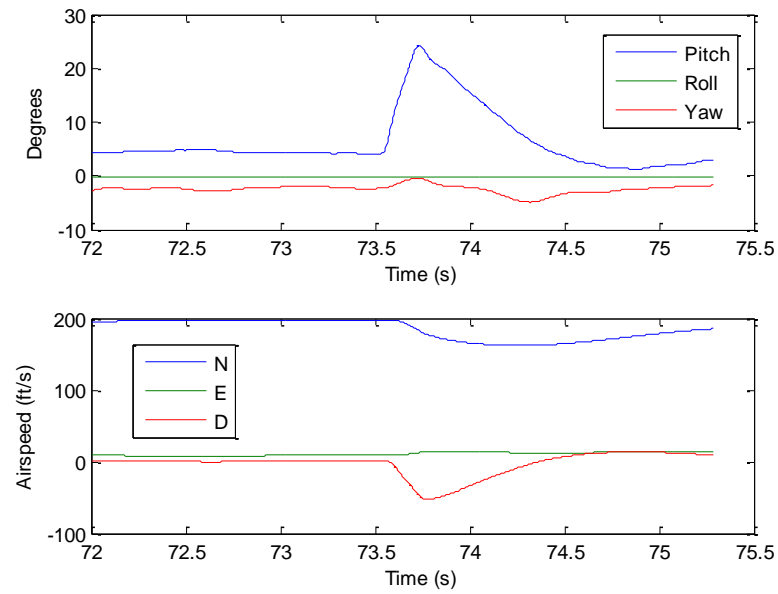


Figure 37: 2G Pull Up: Inertial-to-Body Transformation Data Inputs

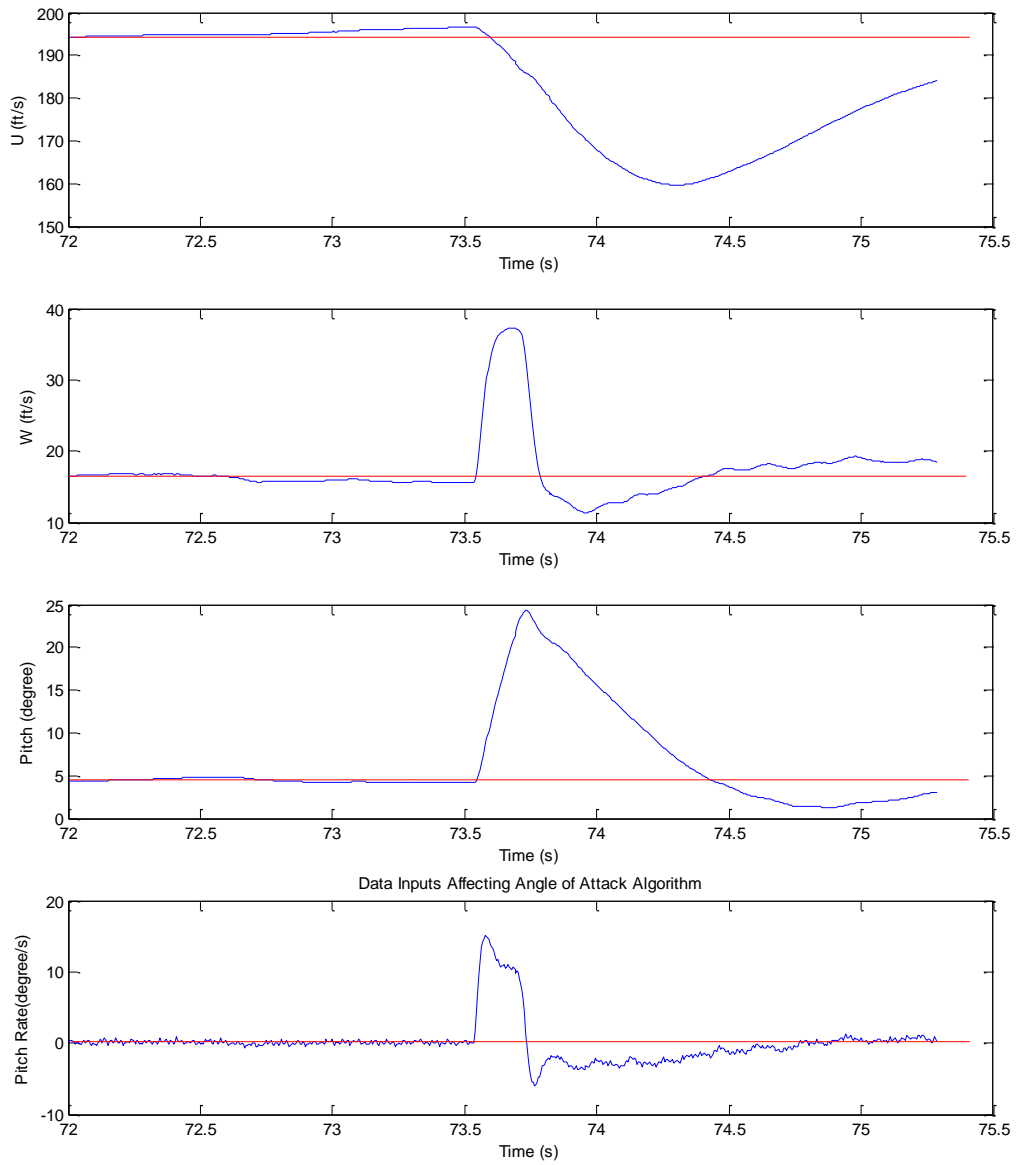


Figure 38: INS Data inputs ( $u, w, \vartheta, q$ ) utilized by Angle of Attack Algorithm - 2G Pull Up

## Appendix G - Windup Turn Maneuver Addendum

The results of the windup turn flight test are depicted in Figure 39. The maneuver as attempted but not successfully completed; the pilot was unable to attain a load factor of 2 while maintaining constant airspeed. Analysis on the data was attempted regardless. The windup turn started from a steady level trim airspeed of 110KIAS at 6000ft. The data are presented as three angle of attack time-histories. The first is the calculated angle of attack (blue) from the algorithm. The second is the calibrated alpha vane (green). The third is the raw alpha vane (red). Accompanying the angle of attack traces is load factor, altitude, and indicated airspeed data for the duration of the maneuver.

The results are mixed, as the calculated angle of attack is unable to follow the trace of the alpha vane at any point during the maneuver. The first oddity is that at trim, the alpha vane is not around 4.5degrees, as it was in the prior test portions. This means at trim, there was already a deviation between the two traces. This calls into question the validity of the test data. Further investigation is required.

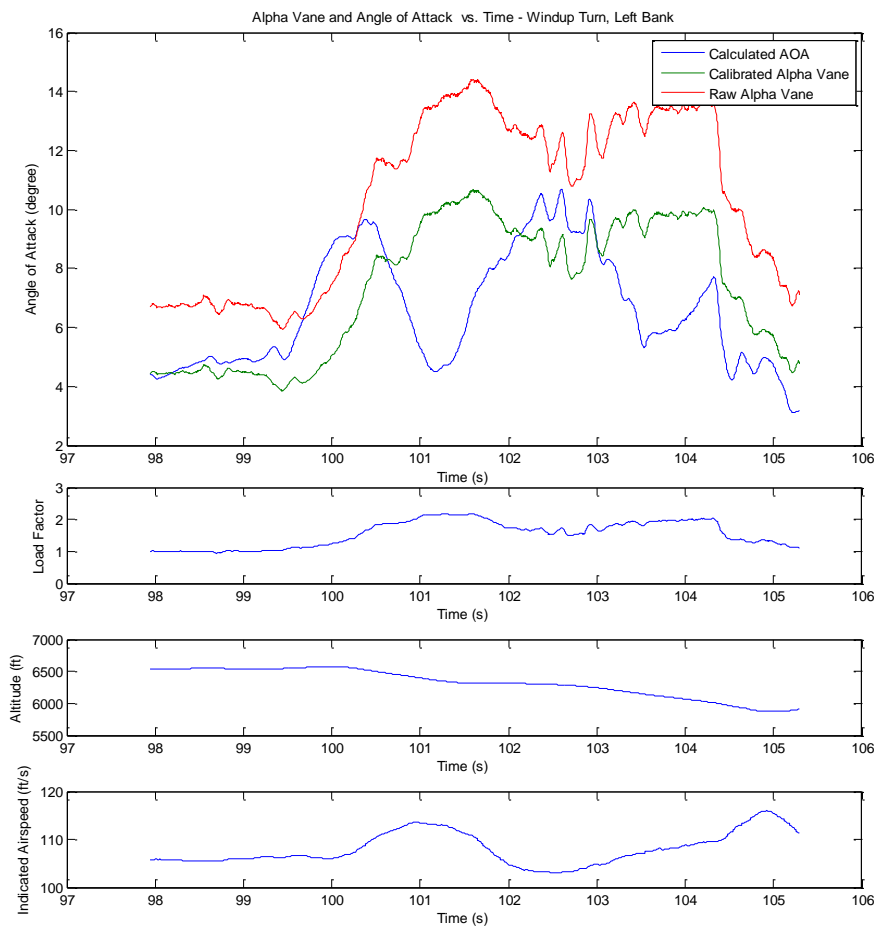


Figure 39: Angle of Attack vs. Time - Windup Turn, Left Bank

# Appendix H – Flight Test Cards

## INS Calibration Flight Test Cards

TAIL NO: N33UT		AOA/AOS		DATE: 3/2/17	
INS CALIBRATION AOA/AOS ALGORITHM DATA ACQUISITION FLIGHT					
FLT		CREW			
LF	PILOT	G. HEATHERLY			
LR	FTE #1	J. LY			
RF	FTE #2	J. KOLWYCK			
MISSION FREQ		V <sub>g</sub> - 75 KIAS			
PRI: 123.0		SEC: 123.45			
THA AWOS: 128.325		BINGO: 15			
GW: 3,048.0		JOKER: 20			
FUEL: 89		Hsv 300 @ 28 330 @ 29 MB			
C.G.: 42.032		BNA 340 @ 21 320 @ 23 MB			
NOTES:		3K 6K			
<b>TEST LIMITS</b> MIN TEST ALT 2,000 AGL (3,000 MSL) MIN/MAX TEST A/S STALL/168 KIAS MAX A/S LIMIT - ADS BOOM (186KIAS) 168 KIAS					
NEXT: FLIGHT PROFILE					1

TAIL NO: N33UT		AOA/AOS		DATE:	
FLIGHT PROFILE					
A	MAX POWER TAKEOFF CLIMB TO TEST ALTITUDE CLEARING TURNS				
B	FLIGHT TEST TECHNIQUE ELLIPSE CALIBRATION 5000 FT				
GPS 4-LEG- INS CHECK OUT 5000 FT - 110 KIAS					
LEVEL ACCEL/DECEL -INS/Time permitting 5000 FT - 110 KIAS TRIM					
C	RETURN VISUAL LDG				
NEXT: GROUND BLOCK					2

TAIL NO: N33UT		AOA/AOS		DATE:	
GROUND BLOCK					
A	CHANGE NAV440 SETTINGS				
B	ENGINE START				
C	INSTRUMENTS ON				
D	DAS ON				
E	COMM CHECK				
F	INSTRUMENT TEST				
V <sub>0</sub> 2.1 H <sub>0</sub> 755 OAT <sub>0</sub> 37 °F					
RPM 3100 MAP 15 Fuel 53.3					
FTE #1					
Ellipse-N					
Angles: Roll 0.32 Pitch 3.56 HDG 325					
α (AOA) 4.0					
FTE #2					
NAV440					
Angles: Roll 0.2 Pitch 5.4 HDG 5.6					
1.10 4.0 314.8					
NEXT: AWOS WEATHER					3

TAIL NO: N33UT		AOA/AOS		DATE:	
AWOS WEATHER					
THA AWOS (128.325 / 931-454-2052)					
TIME: 1430Z 1535Z					
WIND 320 @ 12 360 @ 11					
VIS: 10 10					
SKY: ↓ 12000 ↓ 12000					
T/DP: 3 1 - 2 0 1 - 3 1					
ALT 30.30 30.32					
D ALT					
REMARKS:					
NOTAMS:					
NEXT: TAXI / TAKEOFF / CLIMB					4

TAIL NO: N33UT		AOA/AOS		DATE:	
TAXI/ TAKEOFF/ CLIMB					
A	TAXI				
NAV440 GROUND CALIBRATION - 380DEG TURN VALIDATE HEADINGS - ground block					
B	PRE-TAKEOFF				
RUN-UP / SAFETY BRIEFING					
C	T/O TIME: 4.42				
D	T/O FUEL: 86.3 GALS				
E	T/O: MAX POWER				
F	SET ALT TO 29.92'				
G	CLIMB TO TEST ALT: 5K 6K				
H	AT TEST ALT: CLEARING TURNS				
NEXT: LEVEL PERF TRIM SHOTS					5

TAIL NO: N33UT		AOA/AOS		DATE:	
ELLIPSE CALIBRATION					
LIMITS: MIN TEST ALT 3,000 MSL / MIN TEST A/S 65 KIAS TOL: HOLD ALT +/- 100 FT; A/S +/- 1 KIAS; HDG +/- 5 DEG CONFIG: CLEAN; FLAPS UP, GEAR UP, COWL FLAPS CLOSED					
A	SET UP				
TRIM AT STEADY HEADING 270.5 205.5					
B	METHOD				
HIGH INCLINATION FIGURE 8'S					
OR					
60DEG LEFT TURN 60DEG RIGHT TURN NOSE UP - STALL HORN NOSE DOWN FULL RIGHT RUDDER FULL LEFT RUDDER					
D	DATA				
PILOT: FLY MANEUVER					
FTE #1: CALLOUT, RUN ELLIPSE/CALIBRATION					
FTE #2: VERIFY NAV440 HEADING, PITCH, YAW ANGLES					
NEXT: LEVEL PERF TRIM SHOTS					6

TAIL NO: N33UT	AOA/AOS	DATE:
<b>LEVEL PERF TRIM SHOTS</b>		
LIMITS: MIN TEST ALT 3,000 MSL / MIN TEST A/S 65 KIAS TOL: HOLD ALT +/- 100 FT; A/S +/- 1 KIAS; HDG +/- 5 DEG CONFIG: CLEAN: FLAPS UP, GEAR UP, COWL FLAPS CLOSED		
A	INS/TIME Permitting <b>SET UP</b> -SET POWER AND TRIM FOR 110KIAS (STEADY LEVEL) -SET HEADING AT 0°	
B	<b>METHOD</b> -MAINTAIN AIRSPEED, ALTITUDE, HEADING -RECORD DATA -CHANGE HEADING BY 90° -CHANGE HEADINGS 3X	
D	<b>DATA</b> PILOT: CALL RPM, MAP, STEADY HEADING FTE #1: CALLOUT, EVT, V <sub>0</sub> , α, TRK ELLIPSE HDG, PITCH, ROLL FTE #2: RPM, MAP, FUEL, OAT, H <sub>0</sub> GPS 6/5 NAV440 HDG, PITCH, ROLL	
NEXT: LEVEL PERF TRIM SHOTS		7/8

TAIL NO: N33UT	AOA/AOS	DATE:
<b>LEVEL PERF TRIM SHOTS</b>		
LIMITS: MIN TEST ALT 3,000 MSL / MIN TEST A/S 65 KIAS TOL: HOLD ALT +/- 100 FT; A/S +/- 1 KIAS; HDG +/- 5 DEG CONFIG: CLEAN: FLAPS UP, GEAR UP, COWL FLAPS CLOSED		
N	110 EVT HDG PITCH ROLL OAT FUEL RPM MAP 3 341° 6.0° 3.5° 30.5 76.3 25 17.5	
W	NAV 440 5 207° 5.7° 1.5° 30 75.4 25 17.5	
S	7 205° 6.8° 0.7° 30 74.9 25 17.5	
E	9 115.2° 6.2° 1.04° 30 74.1 35 17.5	
110 EVT HDG PITCH ROLL α V <sub>0</sub> H <sub>0</sub> TRK		
SBG	3 358 5.2 1.21 7.0 104 6000 014	
	5 267 5.0 0 7.0 105 6044 257	
	7 184 5.7 1.1 7.1 106 5992 154	
	9 93 5.01 0 7.0 106 6001 110	
NEXT: LEVEL TRIM SHOTS		8

TAIL NO: N33UT	AOA/AOS	DATE:
<b>LEVEL ACCEL / DECEL</b>		
LIMITS: MIN TEST ALT 3,000 MSL / MIN TEST A/S 65KIAS TOL: HOLD ALT ±50 FT CONFIG: CLEAN: FLAPS UP, GEAR UP, COWL FLAPS CLOSED		
A	<b>SET UP</b> -SET RPM AND MAP FOR 110 KIAS AND TRIM	
B	<b>METHOD</b> -HOLD ALTITUDE THROUGHOUT -REDUCE POWER TO IDLE AND SLOW TO 70KIAS -ADD FULL POWER (2750) AND ACCEL TO MAX LEVEL (160) -POWER TO IDLE AND SLOW TO FIRST INDICATION OF STALL (BUFFET)	
C	<b>DATA</b> PILOT: FLY MANEUVER, CALL STABLE WHEN TRIMMED FTE #1: CALLOUT, EVT, V <sub>0</sub> , α° FTE #2: RPM*, MAP*, FUEL*, OAT*, H <sub>0</sub> *, MONITOR H <sub>0</sub> * TRIM SHOT ONLY NAV Values θ, φ, ψ	
NEXT: LEVEL ACCEL/DECEL		9/10

TAIL NO: N33UT	AOA/AOS	DATE:
<b>LEVEL ACCEL / DECEL</b>		
LIMITS: MIN TEST ALT 3,000 MSL / MIN TEST A/S 65KIAS TOL: HOLD ALT ±50 FT CONFIG: CLEAN: FLAPS UP, GEAR UP, COWL FLAPS CLOSED		
TRIM	EVT V <sub>0</sub> α RPM MAP OAT <sub>0</sub> FUEL H <sub>0</sub> 13 105 7.1 25 17.5 30 71.8 6030	
END	$\theta$ 0 $\phi$ 0 $\psi$ 4 5.2 0.7 4.8 11 Elev doublet	
NEXT: DESCENT/LANDING		10/11

TAIL NO: N33UT	AOA/AOS	DATE:
<b>DESCENT AND LANDING</b>		
A	<b>SECURE CABIN, E.G. LAPTOP, CLIPBOARDS, ETC.</b>	
B	<b>DESCENT CHECKS</b> 180 285 171 260.6 257	
C	<b>AWOS</b>	
D	<b>LDG TIME:</b> 15:45	
E	<b>LDG FUEL:</b> 68.4 GALS	
F	<b>POST-FLT GROUND BLOCK</b>	
G	COMPASS ROSE CHECK	
NEXT: GROUND BLOCK		11/16

TAIL NO: N33UT	AOA/AOS	DATE:
<b>GROUND BLOCK</b>		
A	<b>INSTRUMENT TEST</b> V <sub>0</sub> 11.4 H <sub>0</sub> 682 OAT <sub>0</sub> 42.5 RPM 1000 MAP 10 Fuel 67.8 FTE #1 Ellipse-N Angles: Roll -0.7 Pitch 3.48 HDG 1° α (AOA) 4.0 FTE #2 NAV440 Angles: Roll -0.7 Pitch 3.3 HDG 357	
B	<b>DAS OFF</b>	
C	<b>INSTRUMENTS OFF</b>	
D	<b>ENGINE OFF</b>	
E	<b>EXIT PLANE</b>	
F	<del>WINDS A/OFF (REMINDER-POST-FLIGHT)</del>	
NEXT: COMMENTS		17/17



TAIL NO: N33UT	AOA	DATE: 3-9-17																																										
<b>LEVEL PERF TRIM SHOTS (PIW-VIIV)</b>																																												
LIMITS: MIN TEST ALT 3000 MSL / MIN TEST A/S 55 KIAS																																												
TOL: HOLD ALT +/- 50 FT; HOLD A/S +/- 2.5 KIAS; HDG +/- 5DEG																																												
CONFIG: CLEAN: FLAPS UP, GEAR UP, COWL FLAPS CLOSED																																												
5,000 FT 0.5 GAL BURN PER TRIM SHOT																																												
160 => FUEL FLOW = $\frac{5 \text{ GAL}}{\text{TIME}} \times 3600 \text{ SEC}$																																												
110,70 KIAS => FUEL FLOW = $\frac{3 \text{ GAL}}{\text{TIME}} \times 3600 \text{ SEC}$ 470																																												
<table border="1"> <thead> <tr> <th rowspan="2">EVT</th> <th colspan="2">FUEL</th> <th rowspan="2">OAT<sub>0</sub></th> <th rowspan="2">V<sub>0</sub></th> <th rowspan="2">H<sub>0</sub></th> <th rowspan="2">RPM</th> <th rowspan="2">MAP</th> </tr> <tr> <th>REM</th> <th>TIME</th> </tr> </thead> <tbody> <tr> <td>3</td> <td></td> <td></td> <td>43</td> <td>152</td> <td>5995</td> <td>25</td> <td>27.5</td> </tr> <tr> <td>7</td> <td></td> <td></td> <td>141</td> <td>105</td> <td>5957</td> <td>25</td> <td>16.5</td> </tr> <tr> <td>9</td> <td></td> <td></td> <td>141</td> <td>104</td> <td>5990</td> <td>25</td> <td>16</td> </tr> <tr> <td>9</td> <td></td> <td></td> <td>41</td> <td>70.6</td> <td>6052</td> <td>22</td> <td>16</td> </tr> </tbody> </table>			EVT	FUEL		OAT <sub>0</sub>	V <sub>0</sub>	H <sub>0</sub>	RPM	MAP	REM	TIME	3			43	152	5995	25	27.5	7			141	105	5957	25	16.5	9			141	104	5990	25	16	9			41	70.6	6052	22	16
EVT	FUEL			OAT <sub>0</sub>	V <sub>0</sub>						H <sub>0</sub>	RPM	MAP																															
	REM	TIME																																										
3			43	152	5995	25	27.5																																					
7			141	105	5957	25	16.5																																					
9			141	104	5990	25	16																																					
9			41	70.6	6052	22	16																																					
NEXT: LEVEL PERF TRIM SHOTS FUEL FLOW		7																																										

3.0 17  
4.9 7.0  
16.8 12.5  
fume  
cowl \*

TAIL NO: N33UT	AOA	DATE: 3-9-17																																		
<b>LEVEL PERF TRIM SHOTS (PIW-VIIV)</b>																																				
LIMITS: MIN TEST ALT 3000 MSL / MIN TEST A/S 55 KIAS																																				
TOL: HOLD ALT +/- 50 FT; HOLD A/S +/- 2.5 KIAS; HDG +/- 5DEG																																				
CONFIG: CLEAN: FLAPS UP, GEAR UP, COWL FLAPS CLOSED																																				
5,000 FT 0.5 GAL BURN PER TRIM SHOT																																				
160 => FUEL FLOW = $\frac{5 \text{ GAL}}{\text{TIME}} \times 3600 \text{ SEC}$																																				
110,70 KIAS => FUEL FLOW = $\frac{3 \text{ GAL}}{\text{TIME}} \times 3600 \text{ SEC}$																																				
<table border="1"> <thead> <tr> <th rowspan="2">EVT</th> <th colspan="2">FUEL</th> <th rowspan="2">OAT<sub>0</sub></th> <th rowspan="2">V<sub>0</sub></th> <th rowspan="2">H<sub>0</sub></th> <th rowspan="2">RPM</th> <th rowspan="2">MAP</th> </tr> <tr> <th>REM</th> <th>TIME</th> </tr> </thead> <tbody> <tr> <td>3</td> <td>00.1</td> <td>20.9</td> <td>20.9</td> <td></td> <td></td> <td>25</td> <td>27.5</td> </tr> <tr> <td>7</td> <td>57.8</td> <td>1.32</td> <td>11.7</td> <td>42°</td> <td></td> <td>25</td> <td>16</td> </tr> <tr> <td>9</td> <td>55.9</td> <td>1.16</td> <td>9.2</td> <td>41°</td> <td></td> <td>22</td> <td>14.5</td> </tr> </tbody> </table>			EVT	FUEL		OAT <sub>0</sub>	V <sub>0</sub>	H <sub>0</sub>	RPM	MAP	REM	TIME	3	00.1	20.9	20.9			25	27.5	7	57.8	1.32	11.7	42°		25	16	9	55.9	1.16	9.2	41°		22	14.5
EVT	FUEL			OAT <sub>0</sub>	V <sub>0</sub>						H <sub>0</sub>	RPM	MAP																							
	REM	TIME																																		
3	00.1	20.9	20.9			25	27.5																													
7	57.8	1.32	11.7	42°		25	16																													
9	55.9	1.16	9.2	41°		22	14.5																													
NEXT: LEVEL PERF TRIM SHOTS FUEL FLOW		7																																		

TAIL NO: N33UT	AOA	DATE:
<b>LEVEL PERF TRIM SHOTS (PIW-VIIV)</b>		
LIMITS: MIN TEST ALT 3000 MSL / MIN TEST A/S 55 KIAS		
TOL: HOLD ALT +/- 50 FT; HOLD A/S +/- 2.5 KIAS; HDG +/- 5DEG		
CONFIG: CLEAN: FLAPS UP, GEAR UP, COWL FLAPS CLOSED		
NEXT: TRIM SHOTS - PIW,VIIV - 10000FT		8

\* required alt elevator trim + pilot input to maintain at 70 KIAS  
- best glide 75

TAIL NO: N33UT	AOA	DATE:
<b>LEVEL PERF TRIM SHOTS (PIW-VIIV)</b>		
LIMITS: MIN TEST ALT 3000 MSL / MIN TEST A/S 55 KIAS		
TOL: HOLD ALT +/- 50 FT; HOLD A/S +/- 2.5 KIAS; HDG +/- 5DEG		
CONFIG: CLEAN: FLAPS UP, GEAR UP, COWL FLAPS CLOSED		
NEXT: TRIM SHOTS - PIW,VIIV - 10000FT		8

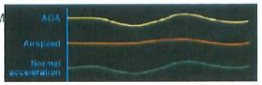
TAIL NO: N33UT	AOA	DATE: 3-9-17
<b>LEVEL PERF TRIM SHOTS (PIW-VIIV)</b>		
LIMITS: MIN TEST ALT 3000 MSL / MIN TEST A/S 55 KIAS		
TOL: HOLD ALT +/- 50 FT; HOLD A/S +/- 2.5 KIAS; HDG +/- 5DEG		
CONFIG: CLEAN: FLAPS UP, GEAR UP, COWL FLAPS CLOSED		
<p>A SET UP - 10000 FT</p> <ul style="list-style-type: none"> <li>-SET REQUIRED MAP AND 2500 RPM FOR 160KIAS</li> <li>-TRIM</li> <li>-KEEP BALL CENTERED</li> <li>-WINGS LEVEL</li> </ul> <p>B METHOD</p> <ul style="list-style-type: none"> <li>-RECORD DATA AT TRIM</li> <li>-HOLD FOR 0.5 GAL BURNED</li> </ul> <p>C REDUCE A/S (MAP AS REQ'D)</p> <ul style="list-style-type: none"> <li>-REPEAT TRIM SHOT AT 110, 70 KIAS</li> </ul> <p>D DATA</p> <p>PILOT: CALL RPM AND MAP WHEN STABLE</p> <p>FTE #1: CALLOUTS, EVENT, RPM, MAP, RECORD AND MONITOR V<sub>0</sub>, H<sub>0</sub>, HDG</p> <p>FTE #2: TIME, FUEL, CALCULATE FUEL FLOW, OAT<sub>0</sub></p>		
NEXT: LEVEL PERF TRIM SHOTS DATA		9

TAIL NO: N33UT	AOA	DATE:																																					
<b>LEVEL PERF TRIM SHOTS (PIW-VIIV)</b>																																							
LIMITS: MIN TEST ALT 3000 MSL / MIN TEST A/S 55 KIAS																																							
TOL: HOLD ALT +/- 50 FT; HOLD A/S +/- 2.5 KIAS; HDG +/- 5DEG																																							
CONFIG: CLEAN: FLAPS UP, GEAR UP, COWL FLAPS CLOSED																																							
10000 FT 0.5 GAL BURN PER TRIM SHOT																																							
MAX MAP => FUEL FLOW = $\frac{5 \text{ GAL}}{\text{TIME}} \times 3600 \text{ SEC}$																																							
110,70 KIAS => FUEL FLOW = $\frac{3 \text{ GAL}}{\text{TIME}} \times 3600 \text{ SEC}$																																							
<table border="1"> <thead> <tr> <th rowspan="2">EVT</th> <th colspan="2">FUEL</th> <th rowspan="2">OAT<sub>0</sub></th> <th rowspan="2">V<sub>0</sub></th> <th rowspan="2">H<sub>0</sub></th> <th rowspan="2">RPM</th> <th rowspan="2">MAP</th> </tr> <tr> <th>REM</th> <th>TIME</th> </tr> </thead> <tbody> <tr> <td>11</td> <td></td> <td></td> <td>14.7</td> <td>37</td> <td>147</td> <td>9976</td> <td>25</td> <td>27.5</td> </tr> <tr> <td>13</td> <td></td> <td></td> <td>11.22</td> <td>35</td> <td>105</td> <td>10070</td> <td>25</td> <td>16</td> </tr> <tr> <td>15</td> <td></td> <td></td> <td>11.24</td> <td>35</td> <td>69.8</td> <td>9874</td> <td>2550</td> <td>14.5</td> </tr> </tbody> </table>			EVT	FUEL		OAT <sub>0</sub>	V <sub>0</sub>	H <sub>0</sub>	RPM	MAP	REM	TIME	11			14.7	37	147	9976	25	27.5	13			11.22	35	105	10070	25	16	15			11.24	35	69.8	9874	2550	14.5
EVT	FUEL			OAT <sub>0</sub>	V <sub>0</sub>						H <sub>0</sub>	RPM	MAP																										
	REM	TIME																																					
11			14.7	37	147	9976	25	27.5																															
13			11.22	35	105	10070	25	16																															
15			11.24	35	69.8	9874	2550	14.5																															
NEXT: LEVEL PERF TRIM SHOTS FUEL FLOW		10																																					

TAIL NO:	AOA	DATE:						
N880J								
<b>LEVEL PERF TRIM SHOTS (PIW-VIW)</b>								
LIMITS: MIN TEST ALT 3000 MSL / MIN TEST A/S 55 KIAS TOL: HOLD ALT +/- 50 FT; HOLD A/S +/- 2.5 KIAS; HDG +/- 5 DEG CONFIG: CLEAN; FLAPS UP, GEAR UP, COWL FLAPS CLOSED								
10000 FT 0.5 GAL BURN PER TRIM SHOT								
MAX MAP => FUEL FLOW = $\frac{5GAL}{TIME} \times 3600 SEC$								
110,70 KIAS => FUEL FLOW = $\frac{3GAL}{TIME} \times 3600 SEC$								
EVT	FUEL REM	FUEL TIME	FUEL FLOW	OAT	V <sub>0</sub>	H <sub>0</sub>	RPM	MAP
11	51.1	1.35	19.5	30 F			2700	27.5
13	49.5	1.00	11.9	35 F			25	16.5
15	47.5	1.05	10.2	34 F			23	16
NEXT: LEVEL PERF TRIM SHOTS FUEL FLOW			10					

TAIL NO:	AOA	DATE:	
N33UT		3-9-17	
<b>LEVEL PERF TRIM SHOTS (PIW-VIW)</b>			
LIMITS: MIN TEST ALT 3000 MSL / MIN TEST A/S 55 KIAS TOL: HOLD ALT +/- 50 FT; HOLD A/S +/- 2.5 KIAS; HDG +/- 5 DEG CONFIG: CLEAN; FLAPS UP, GEAR UP, COWL FLAPS CLOSED			
Fuel Flow (GPH)			
Indicated Airspeed (KIAS)			
diff. in MAP and RPM.			
NEXT: PUSHOVER, PULL UP			11

TAIL NO:	AOA	DATE:	
N33UT		3-9-17	
<b>LEVEL PERF TRIM SHOTS (PIW-VIW)</b>			
LIMITS: MIN TEST ALT 3000 MSL / MIN TEST A/S 55 KIAS TOL: HOLD ALT +/- 50 FT; HOLD A/S +/- 2.5 KIAS; HDG +/- 5 DEG CONFIG: CLEAN; FLAPS UP, GEAR UP, COWL FLAPS CLOSED			
Fuel Flow (GPH)			
Indicated Airspeed (KIAS)			
NEXT: PUSHOVER, PULL UP			11

TAIL NO:	AOA	DATE:	
N33UT			
<b>PUSH OVER, PULL UP (POPU)</b>			
LIMITS: MIN TEST ALT 3000 MSL, MIN TEST A/S 65 KIAS, +2.5/-0.5g TOL: ALT +/- 500 FT; A/S +/- 2.5 KIAS (TRIM); HDG +/- 5 DEG CONFIG: CLEAN; FLAPS UP, GEAR UP, COWL FLAPS CLOSED			
A	SET UP - 6000 ft.		
	-SET RPM AT 2500 AND MAP FOR 110 KIAS AND TRIM		
B	<b>METHOD</b>		
	-CLIMB 500 FT - RESET TRIM POWER (DO NOT RETRIM)		
	-CONSTANT POWER (DO NOT RETRIM; DO NOT ADJUST POWER)		
	-PITCH TO ADJUST SPEED		
	-PITCH DOWN 110 - 100 - 53		
	-PITCH UP 110 - 100 -		
	-RECOVER TO 110 KIAS		
C	<b>DATA</b>		
	PILOT: CALL MAP AND RPM WHEN STABLE		
	FTE #1: CALLOUTS, EVENT, *a, *Nz MONITOR HDG, H <sub>0</sub> , a, Nz (Ellipse)		
	FTE #2: *OAT, *FUEL, *RPM, *MAP, *V <sub>0</sub> , *Nz MONITOR V <sub>0</sub> , Nz (DAS)		
	* TRIM 		
NEXT: PUSHOVER, PULL UP - DATA			12

TAIL NO:	AOA	DATE:					
N33UT		3-9-17					
<b>PUSH OVER, PULL UP (POPU)</b>							
LIMITS: MIN TEST ALT 3000 MSL, MIN TEST A/S 65 KIAS, +2.5/-0.5g TOL: ALT +/- 500 FT; A/S +/- 2.5 KIAS (TRIM); HDG +/- 5 DEG CONFIG: CLEAN; FLAPS UP, GEAR UP, COWL FLAPS CLOSED							
EVT	V <sub>0</sub>	RPM	MAP	OAT	FUEL	H <sub>0</sub>	HDG
TRIM	17	25	17		27.5	87	
	Nz				Nz		Ellipse
	(DAS)				(ELLIP)		
TRIM	17			6.9	1.0		
PO							
PU							
END							
ADA Estimates							
	Airspeed	Altitude	Factor	No Load Factor	Alpha		
	110	5500	1	7	-2.3	-21.582	
	150	4500-5500	0.5	3.1	-2.4	-23.544	
	70	4500-5500	2	19	-2.5	-24.525	
NEXT: WINDUP TURN			13				

TAIL NO:	AOA	DATE:					
N33UT		3-9-17					
<b>PUSH OVER, PULL UP (POPU)</b>							
LIMITS: MIN TEST ALT 3000 MSL, MIN TEST A/S 65 KIAS, +2.5/-0.5g TOL: ALT +/- 500 FT; A/S +/- 2.5 KIAS (TRIM); HDG +/- 5 DEG CONFIG: CLEAN; FLAPS UP, GEAR UP, COWL FLAPS CLOSED							
EVT	V <sub>0</sub>	RPM	MAP	OAT	FUEL	H <sub>0</sub>	HDG
TRIM	17	25	16.5	41 F	4.4		
	Nz				Nz		Ellipse
	(DAS)				(ELLIP)		
TRIM	17						
PO							
PU							
END							
ADA Estimates							
	Airspeed	Altitude	Factor	No Load Factor	Alpha		
	110	5500	1	7	-2.3	-21.582	
	150	4500-5500	0.5	3.1	-2.4	-23.544	
	70	4500-5500	2	19	-2.5	-24.525	
NEXT: WINDUP TURN			13				

TAIL NO: N33UT	AOA	DATE:
<b>WIND UP TURN</b>		
LIMITS: MIN ALT 3000MSL, MIN A/S 65KIAS, 60° BANK, +2.5/-0.5Nz		
TOL: ALT +/- 500 FT; A/S +/- 2.5 KIAS (TRIM); +/- 0.3Nz		
CONFIG: CLEAN: FLAPS UP, GEAR UP, COWL FLAPS CLOSED		
<b>A</b>	<b>SET UP</b>	
	-SET RPM AT 2500 AND MAP FOR <u>110 KIAS</u> AND TRIM	
<b>B</b>	<b>METHOD</b>	
	-CLIMB 500FT, RESET TRIM POWER (DO NOT RETRIM)	
	-CONSTANT POWER (DO NOT RETRIM, DO NOT ADJUST POWER)	
	-AT 110KIAS	
	MAINTAIN AIRSPEED	
	INCREASE BANK	
	INCREASE Nz	
	STABILIZE AT 60DEG BANK, (5 SECONDS)	
	RECOVER	
	"COMPLETE" AFTER RECOVERY	
	-REPEAT FOR OTHER BANK DIRECTION	
<b>C</b>	<b>DATA</b>	
	PILOT: FLY MANUEVER, CALL MAP AND RPM WHEN STABLE	
	FTE #1: CALLOUTS, EVENT, $\alpha$ , Nz, $\phi$ , $\alpha$ , $\phi$ , $\alpha$ , $\phi$	
	MONITOR $H_0$ , Nz(ELLIPSE)	
	FTE #2: *OAT, *FUEL, *RPM, *MAP, *V <sub>0</sub> , *% <sub>0</sub>	
	MONITOR V <sub>0</sub> , Nz(DAS)	
NEXT: WIND UP TURN - DATA		14

TAIL NO: N33UT	AOA	DATE: 3-9-17					
<b>WIND UP TURN</b>							
LIMITS: MIN ALT 3000MSL, MIN A/S 65KIAS, 60° BANK, +2.5/-0.5Nz							
TOL: ALT +/- 500 FT, A/S +/- 2.5 KIAS (TRIM); +/- 0.3 Nz							
CONFIG: CLEAN: FLAPS UP, GEAR UP, COWL FLAPS CLOSED							
	EVT	RPM	MAP	OAT	FUEL	H <sub>0</sub>	V <sub>0</sub>
	24					8049	
BANK	EVT	V <sub>0</sub>	Nz (DAS)	$\alpha$	Nz (ELLIP)		
						Nz	Ellipse
						m/s <sup>2</sup>	m/s <sup>2</sup>
TRIM	25		4.8	6.8	1	-0.5	-4.905
						-0.6	-5.886
						-0.7	-6.867
60°	26				2	-0.8	-7.848
						-0.9	-8.829
						-1	-9.81
	27				1	-1.1	-10.791
						-1.2	-11.772
						-1.4	-13.734
60°	28				1.9	-1.5	-14.715
						-1.6	-15.696
						-1.7	-16.677
	30					-1.8	-17.658
			1.74	Nz	$\phi$ (BANK)	-1.9	-18.639
					1	0	-2
					1.15	30	-2.1
					1.41	45	-2.2
					1.74	55	-2.4
					2	60	-2.5
NEXT: DESCENT AND LANDING		15					

TAIL NO: N33UT	AOA	DATE: 3-9-17					
<b>WIND UP TURN</b>							
LIMITS: MIN ALT 3000MSL, MIN A/S 65KIAS, 60° BANK, +2.5/-0.5Nz							
TOL: ALT +/- 500 FT; A/S +/- 2.5 KIAS (TRIM); +/- 0.3 Nz							
CONFIG: CLEAN: FLAPS UP, GEAR UP, COWL FLAPS CLOSED							
	EVT	RPM	MAP	OAT	FUEL	H <sub>0</sub>	V <sub>0</sub>
	24	25	17	41	42.5		105.8
BANK	EVT	V <sub>0</sub>	Nz (DAS)	$\alpha$	Nz (ELLIP)		
						Nz	Ellipse
						m/s <sup>2</sup>	m/s <sup>2</sup>
TRIM	24					-0.5	-4.905
						-0.6	-5.886
						-0.7	-6.867
60°	25		-1.98			-0.8	-7.848
						-0.9	-8.829
						-1	-9.81
END	26					-1.1	-10.791
						-1.2	-11.772
						-1.4	-13.734
						-1.5	-14.715
						-1.6	-15.696
						-1.7	-16.677
						-1.8	-17.658
						-1.9	-18.639
						1	0
						1.15	30
						1.41	45
						1.74	55
						2	60
NEXT: DESCENT AND LANDING		15					

TAIL NO: N33UT	AOA	DATE: 3-9-17					
<b>WIND UP TURN</b>							
LIMITS: MIN ALT 3000MSL, MIN A/S 65KIAS, 60° BANK, +2.5/-0.5Nz							
TOL: ALT +/- 500 FT; A/S +/- 2.5 KIAS (TRIM); +/- 0.3 Nz							
CONFIG: CLEAN: FLAPS UP, GEAR UP, COWL FLAPS CLOSED							
	EVT	RPM	MAP	OAT	FUEL	H <sub>0</sub>	V <sub>0</sub>
	27	25	17	41	42.5		104.7
BANK	EVT	V <sub>0</sub>	Nz (DAS)	$\alpha$	Nz (ELLIP)		
						Nz	Ellipse
						m/s <sup>2</sup>	m/s <sup>2</sup>
TRIM	27					-0.5	-4.905
						-0.6	-5.886
						-0.7	-6.867
60°	28		-1.96			-0.8	-7.848
						-0.9	-8.829
						-1	-9.81
						-1.1	-10.791
						-1.2	-11.772
						-1.4	-13.734
						-1.5	-14.715
						-1.6	-15.696
						-1.7	-16.677
						-1.8	-17.658
						-1.9	-18.639
						1	0
						1.15	30
						1.41	45
						1.74	55
						2	60
NEXT: EXTRA		NA					

TAIL NO: N33UT	AOA	DATE:
<b>DESCENT AND LANDING</b>		
<b>A</b>	SECURE CABIN, E.G. LAPTOP, CLIPBOARDS, ETC.	
<b>B</b>	DESCENT CHECKS	
<b>C</b>	AWOS	
<b>D</b>	LDG TIME: <u>10:39.6</u> <u>33</u>	
<b>E</b>	LDG FUEL: <u>57.1</u> GALS	
<b>F</b>	POST-FLT GROUND BLOCK	
NEXT: GROUND BLOCK		16

TAIL NO: N33UT	AOA	DATE: 3-9-17
<b>GROUND BLOCK</b>		
<b>A</b>	<b>INSTRUMENT TEST</b>	
	V <sub>0</sub> <u>6.6</u> H <sub>0</sub> <u>3110</u> OAT <sub>0</sub> <u>65</u>	
	RPM _____ MAP _____ FUEL <u>37</u>	
	Nz (DAS) <u>-1</u>	
	FTE #1	
	ELLIPSE:	
	Roll <u>-0</u> Pitch <u>3.6</u> Yaw <u>3</u>	
	$\alpha$ (AOA) <u>-32</u> Nz(Ellipse) <u>1</u> Nz (DAS) _____	
<b>B</b>	DAS OFF	
<b>C</b>	INSTRUMENTS OFF	
<b>D</b>	ENGINE OFF	
<b>E</b>	EXIT PLANE	
NEXT: COMMENTS		17

# Vita

---

Jack Kevin Ly was born and raised in Garden Grove, CA. His parents were immigrants from Vietnam and he has an older sister. He attended Bryant Elementary, Alamos Intermediate, and graduated from Rancho Alamos High School in 2007. He attended the University of California, San Diego (UCSD) and graduated with a Bachelor of Science in Aerospace Engineering in 2011. While at UCSD, he was the President of the Triton Engineering Student Council and studied abroad in Rome, Italy. After graduating in 2011, he remained in San Diego, CA and interned at, and then converted to a full time position with, Solar Turbines, Inc., a subsidiary of Caterpillar. At Solar Turbines, he worked as a Mechanical Project Design Engineer, of which he was a subject matter expert, and spearheaded their summer internship program. After three years, he returned to school in 2015 as a Graduate Research Assistant to pursue a Master of Science degree in Flight Test Engineering at the University of Tennessee, Space Institute (UTSI) under Dr. Steve Brooks. While at UTSI, he received the Society of Flight Test Engineer (SFTE) Academic Scholarship award when he attended the SFTE symposium in Lancaster, CA in 2015. In 2016, Jack took a sabbatical from school to co-op at the National Aeronautics and Space Administration (NASA) Armstrong Flight Research Center at Edwards Air Force Base, CA. Upon receiving his Master's Degree from UTSI in May 2017, Jack accepted a Federal Civil Servant position as a Flight Test Engineer with NASA Armstrong. He is happy to return to California to be with his family and girlfriend, Sonia Joshi. He hopes to continue his education with an MBA and will also continue to apply to the NASA astronaut corp.